Master's thesis

NTNU
Norwegian University of Science and Technology
Faculty of Natural Sciences
Department of Biotechnology and Food Science

Nadia Elise Helene Ørning

The role of Toll-like receptors 4 and 9 in multiple myeloma cell viability and drug sensitivity

Master's thesis in Chemical Engineering and Biotechnology
Supervisor: Therese Standal (IKOM), Berit Løkensgard Strand (IBT)
Co-supervisor: Synne Stokke Tryggestad (IKOM)
June 2023

NTNU
Norwegian University of
Science and Technology

Nadia Elise Helene Ørning

The role of Toll-like receptors 4 and 9 in multiple myeloma cell viability and drug sensitivity

Master's thesis in Chemical Engineering and Biotechnology
Supervisor: Therese Standal (IKOM), Berit Løkensgard Strand (IBT)
Co-supervisor: Synne Stokke Tryggestad (IKOM)
June 2023

Norwegian University of Science and Technology
Faculty of Natural Sciences
Department of Biotechnology and Food Science

Abstract

Multiple myeloma is an incurable disease characterized by the presence of cancerous plasma cells in the bone marrow, resulting in the production of monoclonal immunoglobulins and loss of antibody variation. Toll-like receptors (TLRs) are pattern-recognition receptors that recognize microbial structures, and TLRs may be expressed by myeloma cells. In this study, the impact of TLR activation on the cell viability and drug sensitivity of multiple myeloma cells was investigated.

TLR4 and TLR9 mRNA expression was examined in various myeloma cell lines using RT-qPCR, along with their response to TLR4 and TLR9 agonists lipopolysaccharide (LPS) and CpG oligodeoxynucleotides (CpG), respectively. CellTiter Glo assay was used to assess the effects of these agonists on cell viability. Western blot analyses were used to validate the upregulation of pro-survival genes and to evaluate changes in histone modifications upon stimulation. Flow cytometry was used to evaluate the influence of TLR stimulation on myeloma cell sensitivity to bortezomib and to evaluate their cell surface expression of plasma cell markers.

The study revealed low TLR4 and TLR9 mRNA expression in some myeloma cell lines, with a lack of response to TLR ligands. The RPMI8226 cell line, on the other hand, responded to TLR-signaling. When RPMI8226 cells were stimulated with the TLR9 agonist CpG, cell viability was increased. This effect was dependent on TLR9, since CpG treatment had no effect on RPMI8226 cells that were depleted of TLR9. Further, CpG-stimulated RPMI8226 cells displayed reduced sensitivity to bortezomib, also mediated by TLR9-signaling. Moreover, stimulation with TLR4 and TLR9 agonists upregulated pro-survival proteins in RPMI8226 cells, which may explain the increase in cell viability and the reduced drug sensitivity. CpG-stimulated RPMI8226 cells showed TLR9-dependent downregulation of plasma cell markers and histone modifications, in support of a change of the stimulated cells towards a more immature plasma cell phenotype.

In summary, this study provides insights into the viability and drug resistance of LPS- and CpG-stimulated multiple myeloma cells, contributing to the identification of potential therapeutic targets for further investigation.

Sammendrag

Myelomatose er en uhelbredelig sykdom karakterisert av tilstedeværelsen av maligne plasmaceller i benmargen, noe som fører til produksjon av monoklonale immunoglobuliner og tap av antistoffvariasjon. Toll-liknende reseptorer (TLRer) er mønstergjenkjenningsreseptorer som gjenkjenner mikrobielle strukturer, og TLRer kan bli uttrykt på myelomceller. Denne studien undersøkte effekten av TLR4- og TLR9-aktivering på viabilitet og medikamentsensitivitet i ulike myelomcellelinjer.

TLR4 og TLR9 mRNA uttrykk ble undersøkt i ulike myelomcellelinjer ved hjelp av RT-qPCR, sammen med deres respons på TLR4- og TLR9-agonister lipopolysakkarid (LPS) og CpG oligodeoksynukleotider (CpG) henholdsvis. CellTiter Glo-analyse vurderte effektene av disse agonistene på celleviabilitet. Western blot analyse bekreftet oppregulering av pro-overlevelsesgener og endringer i histonmodifikasjoner ved stimulering. Flowcytometri evaluerte effekten av prestimulering på myelomcellers sensitivitet mot bortezomib og evaluerte deres overflateuttrykk av plasmacellemarkører.

Studien viste lavt uttrykk av TLR4 og TLR9 mRNA i noen myelomcellelinjer, med manglende respons til TLR-ligander. RPMI8226-cellelinjen derimot reagerte på TLR-signalering. Når RPMI8226-celler ble stimulert med TLR9-agonist CpG så økte celleoverlevelsen. Denne effekten var TLR9-avhengig, siden CpG behandling ikke hadde noen effekt på RPMI8226-celler med lite uttrykk av TLR9. Videre viste CpG-stimulerte RPMI8226-celler redusert sensitivitet for bortezomib, også mediert av TLR9-signalering. Dessuten oppregulerte stimulering med TLR4- og TLR9-agonister pro-overlevelsesproteiner i RPMI8226-celler, noe som kan forklare økningen i celleoverlevelse og den reduserte medikamentsensitiviteten. CpG-stimulerte RPMI8226-celler viste TLR9-avhengig nedregulering av plasmacellemarkører og histonmodifikasjoner, som støtter en endring av de stimulerte cellene mot en mer umoden plasmacellefenotype.

Oppsummert gir denne studien innsikt i viabilitet og medikamentresistens hos LPS- og CpG-stimulerte myelomceller, og bidrar til forståelsen av potensielle terapeutiske mål for videre undersøkelser.

Acknowledgements

This master's thesis is a part of the master's degree program Industrial Chemistry and Biotechnology at the Norwegian University of Science and Technology. It is the result of laboratory work carried out at the Department of Clinical and Molecular Medicine during the spring semester of 2023.

The master's thesis is a continuation of the Specialization project "*The cell survival and proliferation of multiple myeloma cell line ANBL-6 increase in a Toll-Like Receptor 4 dependent manner in response to LPS*", which was completed during the fall semester of 2022. Consequently, certain sections, such as **Section 1.1** and **Section 1.4.1** about Multiple Myeloma and TLR4, and **Section 3.3** and **Section 3.4** covering the CTG assay and Western Blot method, respectively, share similarities with the aforementioned project.

First and foremost I would like to express my sincere gratitude to my co-supervisor, Synne S. Tryggestad, for her exceptional guidance and unwavering support throughout this project when she already had her hands full with her PhD. Her advice and encouragement were instrumental in making this project a reality. Secondly, I would like to thank Professor Therese Standal, my supervisor, for her guidance and valuable insights into the thesis. In addition, I would like to thank Professor Berit L. Strand for being my supervisor at the Department of Biotechnology. I would also very much like to thank the rest of the Bone group for being so welcoming and helpful.

Sofie, Marianne, and Viveka; without you I would have gone insane during this stressful year as a master's student. Thank you for all your unwavering support and for reminding me to take breaks and have fun as well.

Finally, I would like to thank my family for all the endless love and support you have given me.

Table of Contents

List of Figures

List of Tables

List of Abbreviations

AP-1 – Activating protein 1
APC - Antigen-presenting cell
ATP - Adenosine-5'-triphosphate
Bcl-2 - B-cell lymphoma 2
Bcl-xL - B-cell lymphoma - extra large
BCMA - B cell maturation antigen
BIM - Bcl-2 interacting mediator of cell death
BM – Bone marrow
CD - Cluster of differentiation
c-Myc - Cellular-Myelocytomatosis
CpG – Deoxycytidyl deoxyguanosine
CREB - cAMP Response Element-Binding Protein
CTG - CellTiter Glo
DAMPs – Danger-associated molecular patterns
DMSO – Dimethyl Sulfoxide
DTT - Dithiothreitol
ER - Endoplasmic reticulum
ERK - Extracellular signal-regulated kinase
GAPDH - Glyceraldehyde 3-phosphate dehydrogenase
IFN - Interferon
Ig – Immunoglobulin
IKK – IκB kinase complex
IL – Interleukin
IL-6 – Interleukin 6
IRAK – IL-1 receptor-associated kinases
IRF - Interferon regulatory factor
JNG - Jun N-terminal kinase
LPS – Lipopolysaccharide
LRR – Leucine-rich repeats
MAPK – Mitogen-Activated Protein Kinase
Mcl-1 - Myeloid cell leukemia factor 1
MGUS - Monoclonal gammopathy of undetermined significance
MM – Multiple myeloma
MyD88 – Myeloid differentiation factor 88
NEMO - NF-κB essential modulator
NF-κB – Nuclear factor kappa-light-chain-enhancer of activated B cells
PAMP – Pathogen-associated molecular pattern
PC - Plasma cell
PRR – Pattern recognition receptor
Rh IL-6 – Recombinant human IL-6
SDS-PAGE - Sodium Dodecyl Sulfate-Polyacrylamide Gel Electrophoresis
SMM - Smoldering multiple myeloma
TAB – TAK-1 binding protein
TANK - TRAF family member-associated NF-κB activator
TAK1 – Transforming growth factor-b-activated kinase-1
TBK-1 - TANK-binding kinase 1
TBST - Tween-Tris buffered saline
TIR – Toll-interleukin 1 (IL-1) receptor
TIRAP – TIR-domain-containing adaptor protein
TLR – Toll-like receptor
TNF - Tumor necrosis factor
TNFR - TNF receptor
TRAF - TNF receptor-associated factor
TRAM – TRIF-related adaptor molecule
TRIF – TIR-domain containing adaptor inducing IFNβ

1 Introduction

1.1 Multiple Myeloma

Multiple myeloma (MM) is an incurable cancer where abnormal plasma cells in the bone marrow start to divide uncontrollably. Plasma cells are antibody-producing white blood cells that are important for the adaptive immune system. They can produce all the five heavy chains IgA, IgD, IgE, IgG, and IgM, and the two light chains κ and λ needed to produce a large variety of antibodies [1]. The abnormal plasma cells in myeloma crowd and outcompete the healthy plasma cells. These abnormal cells do not produce the variation of immunoglobulins needed by the adaptive immune system to protect the body against infection, but rather monoclonal immunoglobulins (M proteins), such as only IgA kappa, or IgG lambda, which causes complications [1]. There is not one major causing factor for the cancer, but rather multiple factors *e.g.* genetic components, lifestyle, and exposure to external factors [1]. In Norway, a total of 474 people in 2021 were diagnosed with multiple myeloma, and the median age of the diagnosed was 72 years old. Multiple myeloma diagnosis has increased since 2002. However, the 5-year relative survival has increased from 37% to 62.5% in the same period [2].

1.1.1 Development of MM

MM is the final stage of a multi-step transformation of plasma cells [3]. In the early stage, several primary genetic mutations such as chromosomal abnormalities and heavy chain Ig (IgH) translocations can accumulate in bone marrow (BM) plasma cells. These mutations lead to increased proliferation of the plasma cells. This step, where increased proliferation begins is called Monoclonal gammopathy of undetermined significance (MGUS), and only 1% of MGUS patients develop MM [3]. The next step of the progression is called Smoldering multiple myeloma (SMM), where abnormal amounts of plasma cells with high levels of Ig proteins are observed. These steps are non-symptomatic. The final step, where the increased amount of abnormal plasma cells become symptomatic, such as anemia and bone lesions, is called multiple myeloma [3]. The development is illustrated in **Figure 1.1**.

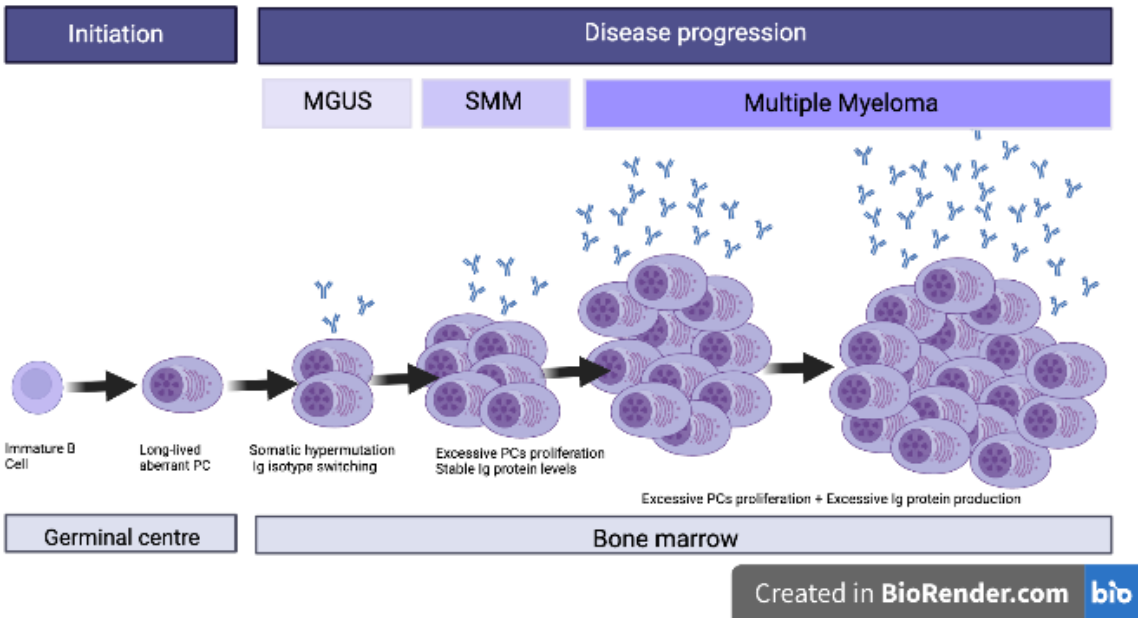

Figure 1.1: Multiple Myeloma development and progression. Multiple Myeloma is the end stage of several transformations of the plasma cells (PCs). Several genetic mutations that affect the proliferation, such as the translocation of IgH and chromosomal abnormalities, can occur in long-lived plasma cells. In the first stage, monoclonal gammopathy of undetermined significance (MGUS), proliferation of plasma cells is still quite low, while in the second stage, smoldering multiple myeloma (SMM), the proliferation and level of Ig are abnormally high. However, these two stages are asymptomatic. With the increased amount of abnormal plasma cells, symptoms will emerge. This stage is called multiple myeloma. The figure is created with BioRender and modified from Pinto *et al.* [3].

1.1.2 Infection in MM patients

Infection is one of the main causes of the high morbidity and mortality rates of MM patients. This is mainly a result of the humoral immunity defect in MM patients. Gram-positive bacteria, such as *Streptococcus pneumoniae*, primarily infect untreated MM patients, while Gram-negative bacteria primarily infect MM patients after chemotherapy [4]. With an increase in hospitalization and chemotherapy, an increasing trend of Gram-negative infections has been observed. However, Gram-positive bacterial infections in MM patients still cause major problems. According to a population-based study done in Sweden with 9253 myeloma patients between 1988 and 2004, the risk of bacterial and viral infection was 7 and 10 times higher for myeloma patients compared to their matched controls, respectively [5]. Nevertheless, the outcome of MM patients has improved with the increased use of anti-myeloma agents such as bortezomib, thalidomide, and carfilzomib, and stem cell transplantation. The cancer has been transformed into a chronic condition thanks to these therapies. However, this may increase the risk of infections. Bortezomib has been noted to increase reactivation of herpes simplex and

herpes zoster viruses, and infections caused by *Clostridium difficile* have also increased due to these therapies [6].

1.1.3 Treatment

Multiple myeloma has a high level of molecular heterogeneity, which makes it difficult to treat with precision medicine. Stem cell transplantation is currently the most effective treatment for MM [7]. However, the transplantation has several limits. The high-dose chemotherapy before the transplantation usually does not kill all abnormal plasma cells, thus there is a chance of relapse. There is also a high risk of serious infection in this treatment [7]. As a result, stem cell transplantation is not generally offered to patients over 65 years. Therefore, there is a need for new and improved therapies. Immunomodulatory drugs and proteasome inhibitors have emerged in the past decade, with positive effects [8].

Myeloma cells produce M proteins constantly. Proteasomes are needed to break down proteins in cells and are active in myeloma cells due to their excessive protein expression. Proteasome inhibitors have thus yielded good results [8]. Bortezomib and carfilzomib are both proteasome inhibitors that target the 26S proteasome complex [8]. This results in the apoptosis of the MM cells.

1.2 Plasma cell markers, and their expression in MM

Several of the new immune therapeutic drugs target surface proteins on the myeloma cells. Mature plasma cells express many surface receptors, such as B cell maturation antigen (BCMA), and cluster of differentiation (CD) 38 and CD138 [9]. The expression of CD38, a multifunctional ectoenzyme involved in cell adhesion and signal transduction, is high in B-lymphoid precursors [10]. CD38 expression becomes downregulated during B-cell maturation, and is not expressed in naïve B-cells. However, CD38 becomes highly upregulated again during plasma cell differentiation, and normal plasma cells express CD38 more highly compared to CD38-positive hematopoietic cells [10]. Therefore, CD38 is critical for the identification of plasma cells. CD138 is also a good marker for plasma cells. CD138 expression is identified more in fully differentiated, mature plasma cells [11]. BCMA is almost exclusively expressed on plasmablasts and plasma cells. A study found that lack of BCMA on plasma cells impaired long-term survival, but not survival of short-lived plasma cells. Therefore, BCMA is possibly required to enhance the survival of long-term plasma cells [12].

CD38 is a good MM biomarker, due to its' expression being even higher in MM cells compared

to normal plasma cells [13]. Therefore, many therapeutics already exist that target CD38. One of these drugs is Daratumumab, which is a monoclonal antibody that binds CD38, resulting in the destruction of that MM cell [13]. CD138 is a traditional MM biomarker, highly specific to terminally differentiated plasma cells [14]. However, several studies have discovered a decreased expression of CD138 in MM [15, 16]. They found that relapsed and progressive patients had a higher increase in CD138-negative MM cells compared to newly diagnosed patients, and that CD138-negative MM cells are more immature. These immature cells have a significantly higher proliferative potential [16]. BCMA has been found to be expressed in 80-100% of the MM cell lines, and is expressed more highly compared to normal plasma cells [12]. The level of expression also varies depending on the MM progression, increasing from normal to MGUS to SMM to MM. Therefore, BCMA is a very good marker for the prognosis of MM, and several BCMA-targeted therapies are in development [17].

1.3 Epigenetic modifications

The degree of differentiation in a cell is regulated by epigenetic modifications. Epigenetics refers to the scientific investigation of how environmental factors and an individual's behavior can influence the functioning of their genes. Epigenetic alterations are post-transcriptional changes that do not alter the DNA sequence itself, but rather impact how the DNA sequence is interpreted and utilized [18]. These epigenetic modifications can be classified into three main categories: DNA methylation, histone modifications, and non-coding RNA. DNA methylation involves the addition of methyl groups at specific locations on the DNA sequence, resulting in the suppression of gene activity. The DNA strand coils around proteins known as histones, and the extent of wrapping determines whether the gene is expressed or not. Chemical groups like methyl groups play a crucial role in regulating this process. The addition of a methyl group increases the tightness of the DNA strand around the histone, while its removal loosens the strand, thereby influencing the suppression or activation of genes. This phenomenon is referred to as histone modifications. Another significant epigenetic modification involves the participation of non-coding RNA, such as microRNA. Non-coding RNA molecules can bind to coding RNA leading to degradation, consequently preventing the corresponding RNA sequence from synthesizing proteins. Additionally, non-coding RNA can recruit other proteins to modify histones, thereby exerting control over their activity [18]. Dysregulation of epigenetic modifications is often associated with the development of cancer.

1.3.1 Histone modifications

The histone complex comprises four histones: H2A, H2B, H3, and H4, and modifications can occur on these. These modifications include acetylation, methylation, ubiquitination, phosphorylation, and sumoylation. They can take place on for example conserved lysine or serine residues located on the histone tail, as depicted in **Figure 1.2** [19].

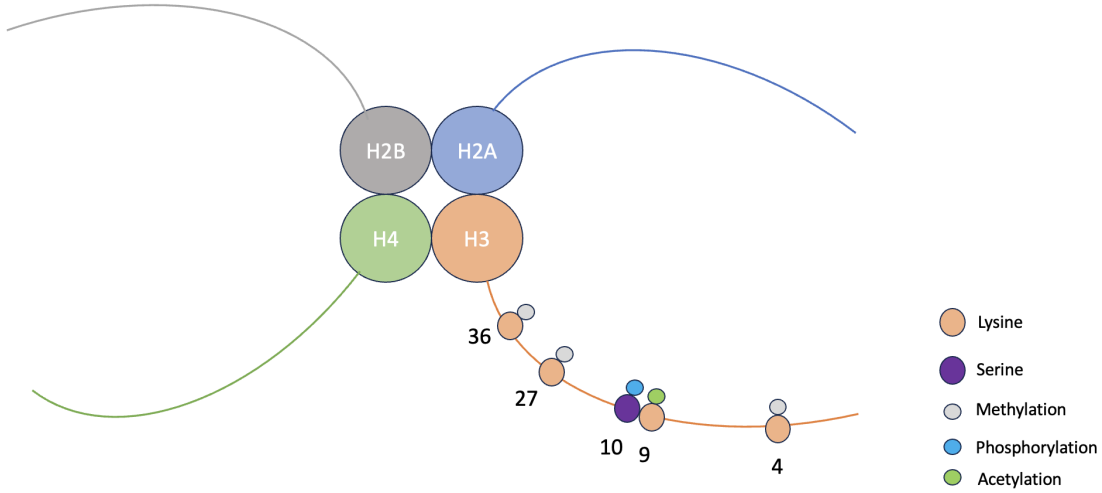

Figure 1.2: Histone modifications including acetylation, methylation, ubiquitination, phosphorylation, and sumoylation. Figure depicting the different histone modifications, and which groups are frequently targeted. For example, methylation occurs commonly on lysine 4, 27, and 36 on histone H3, while acetylation occurs commonly on lysine 9 on histone H3. The figure is modified from Zhang, Lu, and Chang [19].

Histone methylation is most frequently observed on the lysine (K) residue of histones H3 and H4, wherein methyl groups are added, leading to mono-, di-, and trimethylation states [20]. Specific lysine residues, such as H3K4, H3K36, and H3K79, are generally associated with active gene expression, while H3K9, H3K27, and H4K20 are linked to repressive gene expression. This indicates that active marks activate gene transcription, whereas repressive marks suppress gene transcription [20].

Histone acetylation involves the reduction of positive charge on lysine residues, resulting in an inability of the negatively charged DNA sequence to bind to the histone tails. Acetylation is thus commonly regarded as an active mark of gene expression, as it uncoils the DNA strand from the histones [20]. Numerous lysine residues can undergo acetylation, including H3K4, H3K9, and H3K27.

1.4 Toll-like Receptors (TLRs)

Toll-like receptors (TLRs) are a type of pattern recognition receptor (PRR) that are present in mammals and insects [21]. PRRs are capable of distinguishing microbes by recognizing pathogen-associated molecular patterns (PAMPs), which are conserved parts of a pathogen such as lipids, proteins, and nucleic acids. Additionally, PRRs can detect endogenous molecules called damage-associated molecular patterns (DAMPs) from dying or injured cells. Once PRRs recognize PAMPs or DAMPs, they initiate a cascade that leads to inflammatory responses [22].

TLRs are primarily found in antigen-presenting cells (APCs) such as dendritic cells and macrophages, but can also be present in non-immune cells such as fibroblast and endothelial cells [23]. At present, 10 TLRs have been described in humans. They are located on the cell membrane as well as intracellular vesicular membranes and consist of an intracellular, transmembrane, and extracellular domain [24]. The intracellular domain contains a conserved Toll-interleukin 1 receptor (TIR), while the extracellular domain has a leucine-rich repeat (LRR) that binds to specific ligands. For example, TLR1 can recognize lipoproteins, TLR3 recognizes viral double-stranded RNA, TLR4 recognizes lipopolysaccharide (LPS) found in the membrane of Gram-negative bacteria, and TLR9 recognizes unmethylated CpG DNA - a viral and bacterial motif rarely found in mammalian cells [23]. TLR1-2 and TLR4-6 are bound to the cell membrane, while TLR3 and TLR7-9 are bound to the intracellular vesicular membrane. TLR4 can also be endocytosed. **Figure 1.3** illustrates the location of TLR1-TLR9 in the cell, and which ligands activate them.

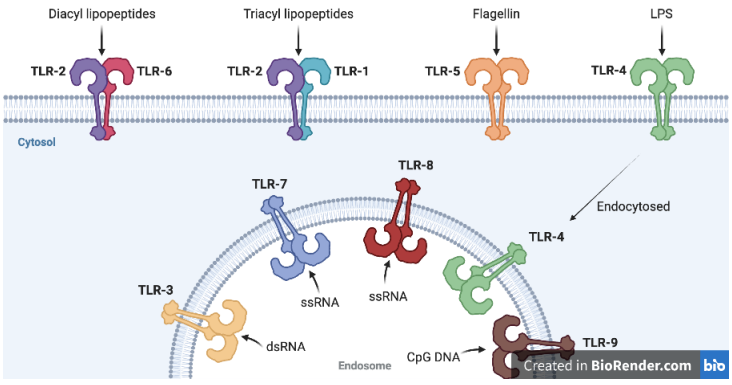

Figure 1.3: TLR1-9 location in the cell, and their ligands. Toll-like receptors (TLRs) 1-9 are primarily found in antigen-presenting cells, with TLRs 1-2 and 4-6 localized on the cell membrane, and TLRs 3 and 7-9 situated on intracellular vesicular membranes. Each TLR has a unique ligand-binding specificity; TLR3 recognizes double-stranded RNA, TLR7-8 single-stranded RNA, and TLR9 CpG DNA. TLR4 can undergo endocytosis upon stimulation by its ligand, lipopolysaccharide (LPS). TLR1 and TLR2 bind to triacyl lipopeptides, TLR2 and TLR6 recognize diacyl lipopeptides, while TLR5 specifically binds to flagellin. The figure is created with BioRender and modified from Akesolo *et al.* [24].

1.4.1 The TLR4 signaling pathway

When LPS binds to TLR4, it recruits an adaptor protein, either TIR domain-containing adaptor protein (TIRAP) or TIR domain-containing adapter-inducing interferon β (TRIF)-related adaptor molecule (TRAM) (**Figure 1.4**). TIRAP directs adaptor Myeloid differentiation primary response 88 (MyD88) to the receptor, while TRAM is involved in the interaction between adaptor TRIF and the receptor. This initiates a cascade of signals. As shown in **Figure 1.4**, MyD88 binds to Interleukin-1 receptor-associated kinases (IRAK) 1, 2, and 4, leading to the activation of the IRAK complex and the phosphorylation of TNF receptor-associated factor 6 (TRAF6). Activated TRAF6 then leads to the activation of either Mitogen-activated protein kinase (MAPK) or the IκB kinase (IKK)-complex containing IKKα, IKKβ, and IKKγ. The activation of MAPK and the IKK-complex leads to the activation of either AP-1 or CREB, or NF-κB, respectively. Activated AP-1, CREB, and NF-κB can translocate into the nucleus and induce gene expression of pro-inflammatory cytokines such as Tumor necrosis factor (TNF-α) and Interleukin 6 (IL-6) [25].

As illustrated in **Figure 1.4**, the interaction between TRIF and TRAM triggers the activation of Interferon regulatory factor 3 (IRF3), which subsequently translocates into the nucleus. In the nucleus, IRF3 promotes the expression of Type I interferon genes.

1.4.2 The TLR9 signaling pathway

TLR9 is an endosomal receptor that recognizes unmethylated CpG motifs in bacterial and viral DNA and plays a crucial role in the recognition of intracellular pathogens by the innate immune system [26].

Upon CpG DNA recognition, TLR9 triggers the MyD88-dependent pathway [27] (**Figure 1.4**). In the MyD88-dependent pathway, TLR9 activates MyD88, which further recruits IRAK4, IRAK1, and IRAK2, leading to the activation of TRAF6 and the downstream activation of MAPK and NF-κB. These transcription factors then translocate into the nucleus, leading to the induction of pro-inflammatory cytokines. IRAK1 and IRAK2 can also activate TRAF3, leading to the activation of IKKα and subsequently IRF7 and the induction of type I interferons [26].

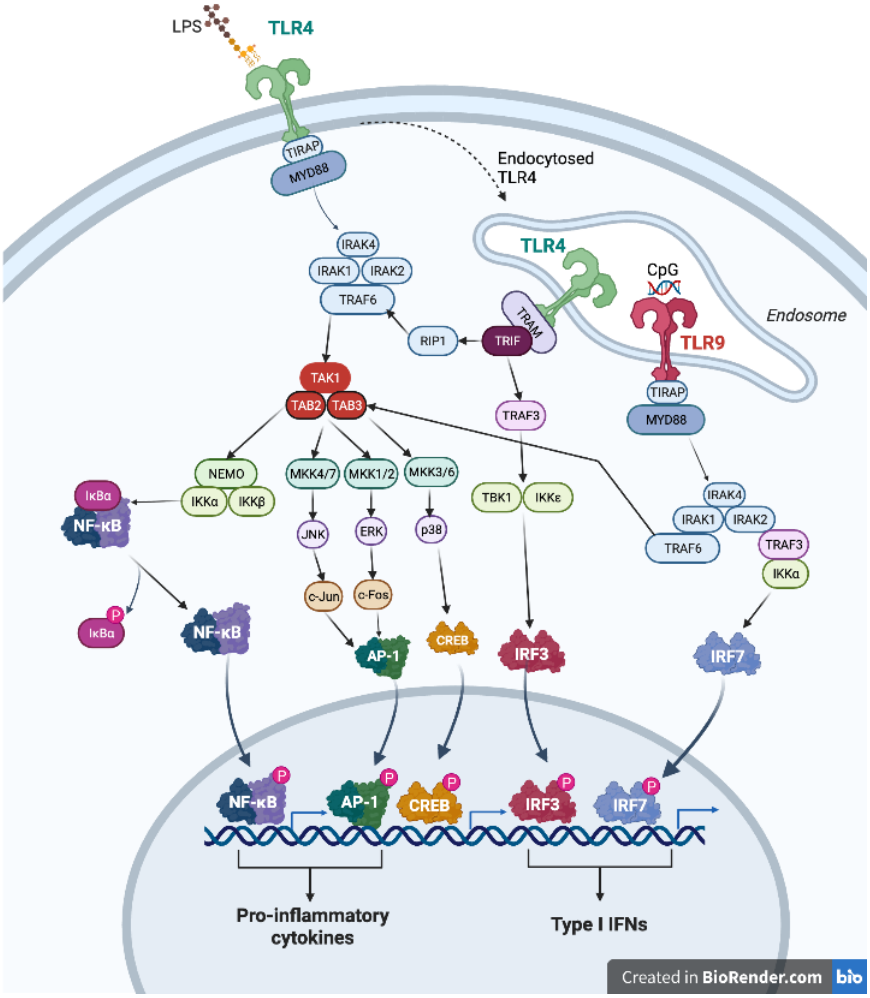

Figure 1.4: Overview of the major TLR4 and TLR9 signaling pathways. TLR4 can signal through two distinct pathways, the MyD88-dependent and TRIF-dependent pathways, while TLR9 signals through only the MyD88-dependent pathway. When LPS activates TLR4, MyD88 interacts with members of the IL-1 receptor-associated kinases (IRAK) family, activating IRAK4, followed by IRAK1 and IRAK2. This results in the dissociation of IRAK members from MyD88 and activation of TRAF6. Activated TRAF6 further activates TAK1, which activates both MAPK and the IKK-complex, including IKKα, IKKβ, and IKKγ. The IKK-complex activates NFκB, while MAPK activates AP-1 and CREB. Subsequently, NFκB, AP-1, and CREB translocate into the nucleus and induce gene expression of pro-inflammatory cytokines.
In addition to the MyD88-dependent pathway, LPS-activated TLR4 can recruit TRIF through the TRIF-dependent pathway when endocytosed. Recruited TRIF can activate TRAF3, leading to the activation of both TBK-1 and IKKε. These kinases can phosphorylate and activate IRF3, which then translocates to the nucleus and induces gene expression of Type I interferon.
TLR9 can signal through the MyD88-dependent pathway. When TLR9 is activated by CpG DNA, MyD88 activates IRAK4, followed by IRAK1 and IRAK 2, resulting in the activation of TRAF6. This pathway is similar to the MyD88-dependent cascade for TLR4. However, also TRAF3 can become activated through IRAK1 and IRAK2. TRAF3 subsequently activates IKKα which then phosphorylates IRF7. IRF7 can then translocate into the nucleus and induce gene expression of type I IFNs. The figure is created with BioRender and modified from Duan *et al.* [28], Kawasaki and Kawai [23], and O'Neill, Golenbock, and Bowie [27].

1.5 The MAPK/ERK pathway

One of the common downstream signaling pathways of TLR4 and TLR9 is the MAPK pathway. The MAPK pathway is one of the most conserved signal transduction pathways that regulate cell proliferation, differentiation, apoptosis, metastasis, and drug resistance [29]. Seven MAPK groups have been recognized in mammalian cells: The extracellular signal-regulated kinase (ERK) 1/2, ERK5, Jun N-terminal kinase (JNK) 1/2/3, p38 $\alpha/\beta/\gamma/\delta$, ERK3/4, ERK7, and Nemo like Kinase (NLK) [29].

The MAPK/ERK pathway involves the MAPKK proteins, MAPK kinase (MKK) 1/2 (**Figure 1.4**). They phosphorylate ERK1 (p44 MAPK) and ERK2 (p42 MAPK) at their threonine (T) and tyrosine (Y) residues (T202/Y204 for ERK1, T183/Y185 for ERK2) [30]. ERK1/2 becomes activated which in turn activates important genes involved in cell proliferation. Furthermore, ERK1/2 can inhibit the proapoptotic protein B-cell lymphoma 2 (Bcl-2) Interacting Mediator of cell death (BIM) by phosphorylation. Phosphorylated BIM can then disassociate from the anti-apoptotic factors Myeloid cell leukemia factor 1 (Mcl-1) and B-cell lymphoma-extra large (Bcl-xL), proteins belonging to the Bcl-2 family [30]. Free phosphorylated BIM becomes degraded by the proteasome. ERK1/2 also phosphorylate Mcl-1 to prevent it from becoming degraded. These actions lead to cell survival [30].

1.6 The role of Toll-like receptors in Multiple Myeloma

Studies have reported the expression of TLRs 1-10 in MM cells, with TLR1, TLR4, TLR7, and TLR9 exhibiting the highest expression levels compared to healthy plasma cells where TLR1 is the most prevalent [24, 31]. MM cells display notably elevated levels of specific downstream signaling targets of TLRs, including TRAF6, in contrast to healthy plasma cells [24]. Ligands binding to TLR4 and TLR9 have been reported to promote MM cell growth, evasion of immune responses, and protection against apoptosis [32, 33].

In a study conducted by Xu *et al.*, significantly higher expression of TLR4 and TLR9 mRNA was observed in cancer cells from MM patients compared to healthy donors' plasma cells [32]. Additionally, stimulation of the MM cell line RPMI8226 with LPS and CpG resulted in enhanced cell growth. This increase in proliferation was partially attributed to an autocrine loop of IL-6. The inhibitory effect of an IL-6 neutralizing antibody on LPS- and CpG-induced RPMI8226 proliferation supported this finding. Previous studies have also demonstrated that LPS-activated TLR4 induces proliferation in MM cells, including the ANBL-6 MM cell line, and that TLR4 inhibits endoplasmic reticulum (ER) stress-induced apoptosis [24, 31]. Further-

more, these studies unveiled the suppression of ER stress-induced apoptotic signals by TLR4, and that this suppression suggested a potential mechanism with drug resistance to bortezomib [24].

Both activated TLR4 and TLR9 have been identified as triggering the activation of the NFκB pathway, with TLR4 also activating the MAPK pathway [24, 32]. The aforementioned study by Xu *et al.* demonstrated that MM cells treated with IκBα, an NFκB inhibitor, exhibited decreased proliferation. Moreover, this decrease was still observed even with LPS and CpG stimulation, indicating a significant role of the NFκB pathway in the increased cell growth of MM cells mediated by TLR ligands.

1.7 Background data

This master's thesis is a continuation of the specialization project "*The cell survival and proliferation of multiple myeloma cell line ANBL-6 increase in a Toll-Like Receptor 4 dependent manner in response to LPS*" written in the fall semester of 2022 [34]. Here, it was discovered that TLR4 agonist LPS promotes survival of the MM cell line ANBL-6 through NFκB signaling, and that the pro-survival factor c-Myc increased with LPS stimulation.

Additionally, according to unpublished data by Tryggestad *et al.*, it has been shown that primary myeloma cells express a broad repertoire of TLRs, and TLR4 and TLR9 are among the most highly expressed receptors [35]. Further, Tryggestad *et al.* has shown that the viability of the MM cell line RPMI8226 was increased following stimulation with TLR4 agonist LPS and TLR9 agonist CpG (**Figure 1.5**).

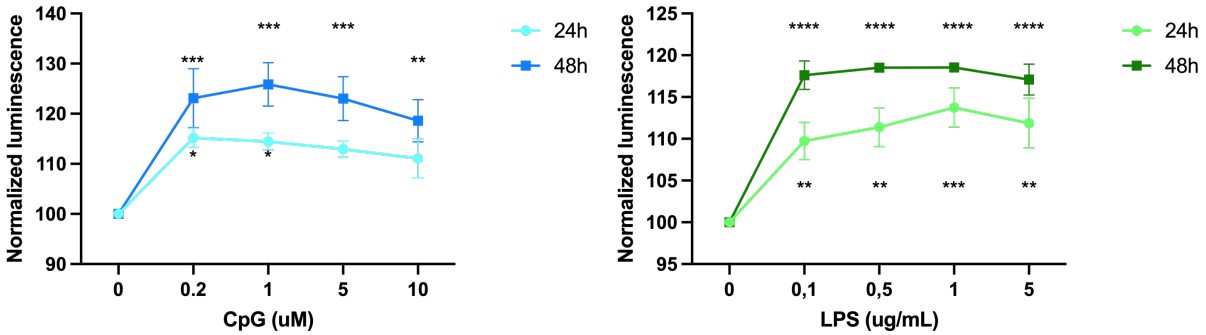

(a) RPMI8226 stimulated with CpG.

(b) RPMI8226 stimulated with LPS.

Figure 1.5: CTG assay of RPMI8226 stimulated with TLR4 and TLR9 agonists LPS and CpG. Figures **(a)** and **(b)** illustrate the cell viability of RPMI8226 as a function of CpG and LPS concentrations, respectively, over 24 and 48 hours. The viability was measured in the samples: 0, 0.2, 1, 5, and 10 µM CpG and 0, 0.1, 0.5, 1, and 5 µg/ml LPS. The mean and SEM for 3 biological replications were calculated. * p <0.05, ** p <0.01, *** p <0.001, **** p <0.0001 by two-way ANOVA, Šídák's and Tukey's multiple comparisons test. The data is obtained from an unpublished study done by Tryggestad *et al.* [35].

A gene expression analysis (Nanostring) was performed to understand which genes were upregulated by LPS stimulation in the RPMI8226 cells (**Figure 1.6**). It was found that several of the upregulated genes had a pro-survival function *e.g.* MYC and IRF4, and an anti-apoptotic function *e.g.* Bcl-2 and Bcl-xL.

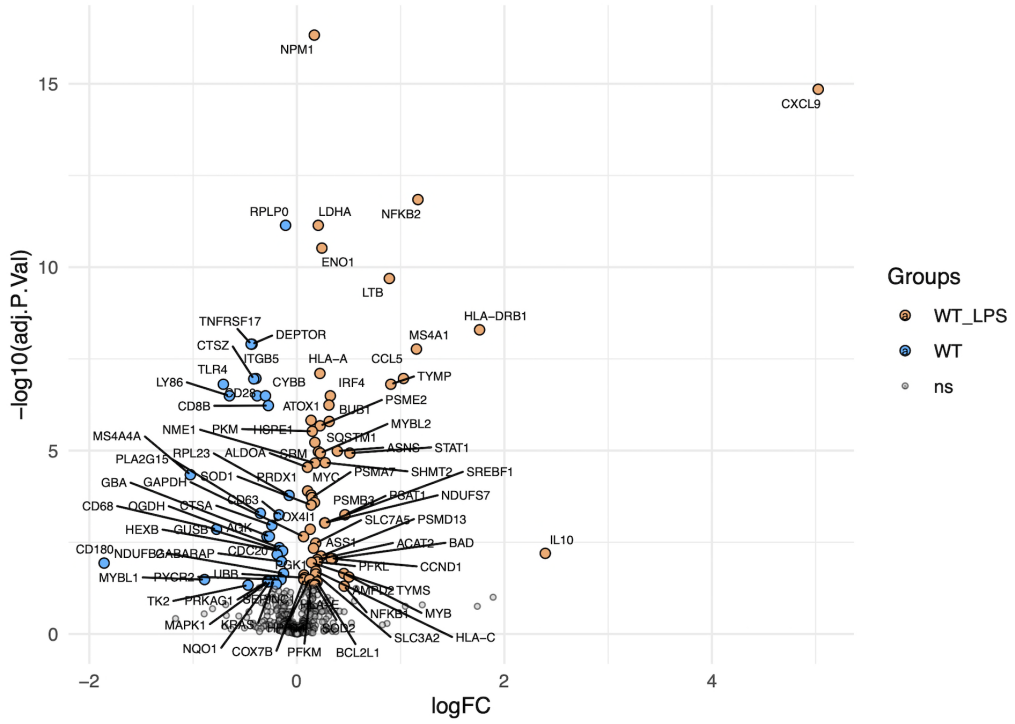

Figure 1.6: Gene Expression Profile of MM cell line RPMI8226 stimulated with LPS. A NanoString analysis was performed in MM cell line RPMI8226 stimulated with LPS. The orange dots represent upregulated genes, while the blue dots represent downregulated genes. The figure is taken from an unpublished study done by Tryggestad *et al.* (2022).

2 Aim

The overall aim of this master's thesis was to determine if and how activation of TLRs on myeloma cell lines AMO-1, MM.1S, H929, and RPMI8226 could promote cell viability and drug resistance. In particular, it was investigated if LPS-activated TLR4 and CpG-activated TLR9 increased the viability of multiple myeloma cells. Further, it was investigated if TLR9 activation could promote viability and drug resistance of RPMI8226 cells, and whether TLR stimulation increased expression of pro-survival and anti-apoptotic proteins p-ERK1/2, Mcl-1, and Bcl2-xL. Lastly, it was investigated if TLR activation could affect expression of plasma cell surface markers, and possible changes in histone modifications were evaluated.

The project had the following objectives:

- Characterize gene expression of TLR4 and TLR9 in different myeloma cell lines, and determine if TLR4 and TLR9 activation could promote viability of these cells.
- Determine if TLR9 activation could promote viability and drug resistance in MM cell line RPMI8226.
- Investigate at a molecular level how TLR activation could promote RPMI8226 viability.
- Examine if TLR activation could affect the expression of different plasma cell markers on MM cell lines, and evaluate possible changes in histone modifications.

3 Materials and Methods

All the kits and reagents used in this project are listed in Appendix II, Table II.1.

3.1 Maintaining of MM cell lines

In this study, the multiple myeloma cell lines ANBL-6 (a gift from Dr. D. Jelinek, Mayo Clinic, Rochester, MN, USA), RPMI8226 and H929 (American Type Culture Collection, Rockville, MD, USA), MM.1S (Max Delbruck Center for Molecular Medicine, Campus Berlin-Buch GmbH, Berlin, Germany), and AMO-1 (a gift from Dr. L. Besse and Dr. C. Driessen, Kantonsspital St Gallen, St Gallen, Switzerland) were used. RPMI8226 TLR9 knockout (KO) and wildtype (WT) were also used. These two cell lines were generated by using the CRISPR/Cas9 technology followed by single cell cloning, as described in *"IL-32 is induced by activation of toll-like receptors in multiple myeloma cells"* [36].

3.1.1 Cell media

RPMI-1640 medium (RPMI) was supplemented with 100 µg/ml of L-glutamine. RPMI and L-glutamine were obtained from Sigma Aldrich, fetal calf serum (FCS) from Invitrogen, and 2-mercaptoethanol (B-Me) and sodium pyruvate (NaPyr) from Thermo Fisher Scientific. The FCS was heat-inactivated in the lab before use. **Table 3.1** shows the cell culture media used for each multiple myeloma cell line.

Table 3.1: The different cell culture media for each of the multiple myeloma cell lines.

MM cell lines	Cell culture media	Experimental media
RPMI8226	20% FCS in RPMI	10% FCS in RPMI
AMO-1	10% FCS in RPMI	5% FCS in RPMI
H929	10% FCS in RPMI with 0.05 mM B-Me	-
MM.1S	10% FCS in RPMI with 1.0 mM NaPyr	-
RPMI8226 TLR9 knockout (KO)	20% FCS in RPMI	10% FCS in RPMI
RPMI8226 wildtype (WT)	20% FCS in RPMI	10% FCS in RPMI
ANBL-6	10% FCS in RPMI with rh IL-6 (1 ng/ml)	5% FCS in RPMI with rh IL-6 (0.5 ng/ml)

3.1.2 Conditions

All multiple myeloma cells were cultured at 37 °C, with 5% CO_2. The cell lines were split twice a week. Unless otherwise stated, the media presented in **Table 3.1** were used in the experiments.

3.2 Stimulation of MM cells with TLR agonists and anti-cancer drug bortezomib

In order to determine whether the TLR activation can affect myeloma cell viability and drug resistance, MM cell lines were stimulated with the TLR4 agonist LPS and the TLR9 agonist CpG. Subsequently, different cellular parameters including ATP levels were evaluated using CellTiter Glo assay, intracellular protein expression by western blotting, gene expression by RT-qPCR, and surface protein expression by flow cytometry. To assess the effect of TLR activation on drug resistance, the MM cell line RPMI8226 was treated with TLR agonist CpG together with the anti-myeloma drug bortezomib, and cell viability was measured using flow cytometry.

3.2.1 Reagents

LPS-EB Ultrapure (*Escherichia coli* 0111:B4) and CpG ODN 2006 were purchased from Invivogen (San Diego, CA, USA) and TIBMolBiol (Berlin, Germany), respectively.
Bortezomib was purchased from Selleck Chemicals (Houston, USA).

3.2.2 Procedure

The cells were centrifuged at 448 rcf for 5 minutes at 20°C, followed by the supernatant being discarded and fresh culture media added to resuspend the cells. The resuspended cells were seeded into culture plates, with the cell density being dependent on each cell line's growth rate and incubation time. The MM.1S cell line was added at 250,000 cells/ml and stimulated for up to 48 hours. Cells were counted using the instrument Beckman Coulter Counter (Brea, CA, USA). The H929, RPMI8226, TLR9 KO, WT, and ANBL-6 cells were added at 200,000 cells/ml and stimulated for up to 48 hours. 80,000 cells/ml of the fast-growing AMO-1 cell line was added for up to 48 hours. Depending on how many cells that were needed for each experiment, 6-, 12-, and 96-well culture plates were used with a maximum added volume of 3 ml, 2 ml, and 100 µl, respectively.

The different LPS, CpG, and bortezomib concentrations the cell lines were stimulated with, and the incubation time, in each experiment are stated in **Table 3.2**.

Table 3.2: Overview of the LPS, CpG, and bortezomib concentrations the MM cell lines were stimulated with in each experiment.

Experiments	Stimulation			Incubation time (hours)
	LPS concentrations (μg/ml)	CpG concentrations (μM)	Bortezomib (nM)	
MM.1S, AMO-1, and H929 (RT-qPCR experiment)	0 and 0.1	0 and 1.0	-	24
MM.1S and H929 (CTG experiment)	0, 0.01, 0.1, and 1.0	0, 0.01, 0.1, and 1.0	-	24 and 48
AMO-1 (CTG experiment)	0, 0.005, 0.01, 0.05, and 0.1	0, 0.005, 0.01, 0.05, and 0.1	-	24 and 48
TLR9 KO and WT (CTG experiment)	-	0, 0.2, and 1.0	-	24 and 48
RPMI8226 (western blot experiment)	0 and 0.1	0 and 1.0	-	4 and 24
RPMI8226, TLR9 KO and WT (histone western blot experiment)	0 and 0.1	0 and 1.0	-	48
TLR9 KO and WT (Flow cytometry - AnnexinV PI experiment)	-	0 and 1.0	0, 4, 6, 8, and 12 (16)	48
RPMI8226, TLR9 KO and WT, ANBL-6 (Flow cytometry experiment)	0 and 0.1 (1.0 for ANBL-6)	0 and 1.0	-	24 and 48

After the treatments, the cell cultures were either measured using CellTiter Glo assay or flow cytometry, or harvested for the western blot or RT-qPCR experiments.

An example of calculations done for stimulation of MM cells can be found in Appendix I.

3.3 CellTiter Glo (CTG assay)

To measure the viability of multiple myeloma cell lines in response to TLR activation, RPMI8226 TLR9 KO, WT, AMO-1, H929, and MM.1S were treated with TLR agonists and the levels of ATP in the cell cultures were measured using the CellTiter-Glo® Luminescent Cell Viability Assay from Promega.

3.3.1 Principle of CTG assay

The CellTiter-Glo® Luminescent Cell Viability Assay measures the metabolic activity of cells by assessing their ATP levels. This assay utilizes a luciferase enzyme that catalyzes the conversion of luciferin to oxyluciferin, which generates luminescence in the presence of oxygen, Mg^{2+}, and ATP, as shown in **Figure 3.1** [37]. The intensity of the luminescence produced by the assay is directly proportional to the amount of ATP present in the cells, providing a measure of their metabolic activity.

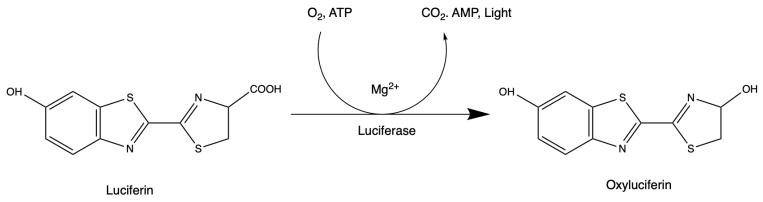

Figure 3.1: Luciferase reaction in CTG assay. The oxidative enzyme Luciferase catalyzes the monooxygenation of Luciferin into Oxyluciferin in the presence of oxygen, Mg^{2+}, and ATP. A luminescent signal is released in the process [37].

The luminescent signal has a linear relationship with the number of cells in the range of 0 to 50,000 cells per well. Consequently, it is crucial to control the number of cells added to each well during plate preparation to ensure accurate measurement of metabolic activity and to prevent exceeding the optimal range.

3.3.2 Reagents

CellTiter-Glo® Luminescent Cell Viability Assay was produced by Promega (Madison, Wisconsin, USA). The CellTiter-Glo® reagent was made by mixing the CellTiter-Glo® Buffer with the CellTiter-Glo® Substrate.

3.3.3 Procedure

Following the incubation of the culture plates with LPS or CpG for 24 or 48 hours as described in **Section 3.2**, 50 µl of CellTiter-Glo® reagent was added to each well, and the plates were shaken for 2 minutes on a shaker, covered, to facilitate cell lysis. After this, the plates were incubated for an additional 10 minutes at room temperature to allow for stabilization of the luminescent signal. To avoid light exposure, the plates were covered with aluminum foil during the whole procedure. The luminescent signal was then measured using the Victor 1420 Multilabel counter instrument and analyzed with the Wallac Software (Perkin Elmer Inc., Waltham, MA, USA).

3.4 Western Blot

Western blotting was used to measure the levels of intracellular proteins phospho-ERK1/2, Mcl-1, and Bcl-xL following the stimulation of cells with LPS and CpG. Furthermore, western blotting was used to evaluate changes in histone modification in TLR4- and TLR9-activated RPMI8226 cells.

3.4.1 Principle of western blot

Western blotting is a powerful technique used to identify and quantify proteins of interest in mixtures containing several proteins, extracted from the cell. This method allows for the detection of specific proteins based on their size. It involves separating the proteins using Sodium Dodecyl Sulfate-Polyacrylamide Gel Electrophoresis (SDS-PAGE) and transferring them onto

a solid membrane. The membrane is then blocked to prevent non-specific binding of the antibodies. A primary antibody that specifically targets the protein of interest is then applied to the membrane, followed by a secondary antibody conjugated to horseradish peroxidase (HRP) that recognizes and binds to the primary antibody. Finally, the detected protein bands are developed [38, 39].

To extract proteins from cells, a detergent-based cell lysis method is used to solubilize the cell membranes and release the proteins. The protein concentration in each sample can be determined by using the Bradford reagent. This method is based on the formation of blue color, occurring when the Coomassie Blue G dye binds to a protein. The protein is quantified by measuring the absorbance at 595 nm and compared with a protein standard [40].

The SDS-PAGE technique is based on the theory that smaller proteins separated by gel electrophoresis migrate faster than larger proteins do, due to less resistance. SDS is a negatively charged surfactant that has a strong denaturing effect, and by adding a reducing agent that can cleave the disulfide bonds, the protein unfolds into a linear chain. The chains have a negative charge and will migrate to the positively charged electrode [39]. In this study, the samples were treated with Lithium dodecyl sulfate (LDS) to denature the proteins and add a negative charge. Dithiothreitol (DTT) was used to disrupt the disulfide bonds in the tertiary and quaternary structure of the protein. After the proteins had been separated by SDS-PAGE, they were transferred to a solid membrane, which has a high affinity for proteins. The transfer of proteins from the gel to the membrane is achieved using an electric field, similar to the SDS-PAGE separation.

3.4.2 Reagents

The reagents used were prepared by:

- **Lysis buffer:** Mixed 1% IGEPAL® CA-630, 150 mM NaCl, 10% glycerol, 50 mM Tris-HCl, and Complete protease inhibitor to distilled water to make a total of 500 µl lysis buffer. 5 µl of $NaVO_4$ and 50 µl of NaF were added to the 500 µl of lysis buffer before use.
- **RIPA buffer:** Mixed 150 mM NaCl, 1% NP-40, 0.5% sodium deoxycholate, 0.1% SDS, and mM Tris-HCl with pH 8.0.
- **Sample buffer:** Diluted 100 µl of 1 M dithiothreitol (DTT) in 900 µl of 4X NuPAGE® LDS Sample buffer.
- **Protein standards:** SeeBluePlus2 Pre-stained Protein Standard and MagicMark^{TM} XP standard (Invitrogen).

- **NuPAGE ® MES SDS Running Buffer:** Diluted 50 ml of 20X MES in 950 ml distilled water.
- **Tween-Tris buffered saline (TBST):** Mixed together 500 ml of 1 M Tris HCl with pH 7.5, 300 ml of 5 M NaCl, and 100 ml of 10% Tween 20, and then filled with distilled water up to 10 L.
- **Blocking buffer:** 5% Bovine serium albumin (BSA) in 0.1% TBST.
- **Super Signal West Femto Maximum Sensitivity:** Mixing equal volumes of Stable Peroxide Solution and Luminol/Enhancer solution.

Antibodies Anti-ERK1/2 (#4695s), Anti-p-ERK1/2 (#4370), Anti-Bcl-xL (#2762), Anti-3M-H3-K27 (#9733), Anti-3M-H3-K36 (#4909), Anti-3M-H3-K4 (#9751), Anti-acetyl-H3-K9 (#9649), and Anti-acetyl-H3-K27 (#8173) are from cell signaling technology (Danvers, MA, USA), Anti-Mcl-1 (#A0815) from Santa Cruz Biotechnology (Dallas, TX, USA), Anti-β-actin (#A2066) from Sigma Aldrich (St. Louise, MO, USA), and Anti-GAPDH (#ab8245) and Anti-LaminB (#ab133741) from Abcam (Cambridge, UK). They were diluted 1:1000 in blocking buffer (5% BSA in 0.1% TBST). Polyclonal Goat Anti-Rabbit Immunoglobulins/HRP (#E0432) from Dako (Glostrup, Denmark) was diluted 1:3000 in TBST.

3.4.3 Procedure

After incubation with LPS and CpG (described in **Section 3.2**), the supernatant in each sample was discarded, and the cell pellets washed with 1 ml cold phosphate-buffered saline (PBS) before being centrifuged again. The cell pellets were stored at -80°C until analyzed.

Proteins were extracted from cells using a lysis buffer of 40 µl per $1x10^6$ cells. A standard lysis buffer was used for the experiments assessing expression of p-ERK, Mcl-1, and Bcl-xL, while the more efficient RIPA lysis buffer was used to assess histone modifications, as lysis of the nuclear membrane was necessary. The mixture was pipetted and vortexed, before incubated on ice for 25 minutes. Subsequently, the cell mixture was centrifuged at 15 700 rcf for 15 minutes at 4 °C. The supernatant, which contained the proteins of interest, was saved, and the cell pellet was discarded.

The protein concentration of each sample was determined using the Bradford reagent. A standard curve was constructed by mixing BSA in Bradford reagent. Further, lysates were mixed with Bradford reagent, and the protein concentration was determined by interpolation from the standard curve using iMark^{TM} Microplate Absorbance Reader (BioRad, California, USA).

The protein samples were then adjusted to equal concentrations using lysis buffer. The protein samples were diluted 1:4 in sample buffer, vortexed, heated at 70 °C for 10 minutes, and spun down. Next, the protein samples were loaded onto a NuPAGE^{TM} 4-12% Bis-Tris Midi Gel, along with 3.0 µl SeeBlyePlus2 Pre-stained Protein Standard and 1.0 µl MagicMark^{TM} XP standard as a gel migration monitor and molecular weight standard, respectively. The gel was run using the PowerEase® 300 W instrument at 80 V for 30 minutes, at 150 V for 30 minutes, and finally at 180 V for 1 hour with NuPAGE ® MES SDS Running Buffer.

The iBlot2 Dry Blotting System (Invitrogen, Carlsbad, California, USA) was used to transfer the proteins from the gel to a nitrocellulose membrane using 20 V for 1 minute, 23 V for 4 minutes, and 25 V for 2 minutes. After blotting, the membrane was blocked with a blocking buffer (5% BSA in 0.1% TBST) for 1 hour at room temperature on a shaker. Next, the membrane was incubated with the primary antibody for 24 to 72 hours at 4 °C on a shaker. Afterwards, the membrane was washed with TBST for 3x5 minutes and incubated with a secondary antibody for 1 hour at room temperature on a shaker, followed by washing for 5x5 minutes in TBST. The membrane was lastly developed with Super Signal West Femto Maximum Sensitivity substrate for 4 minutes before being imaged using LI-COR Odyssey FC imager and Image Studio^{TM} Software (LI-COR Biosciences, Lincoln, Nebraska, USA).

To correct for differences in sample loading, β-actin, GAPDH, and Lamin B were used as loading controls.

3.5 Quantitative reverse transcription PCR (RT-qPCR)

Quantitative reverse transcription PCR (RT-qPCR) was used in this study to measure the mRNA levels of TLR4 and TLR9 in MM cell lines AMO-1, MM.1S, and H-929. The TaqMan RT-qPCR method was used.

3.5.1 Principle of RT-qPCR

Polymerase chain reaction (PCR) is a powerful method that uses specific oligonucleotides, heat-stable DNA polymerases, and thermal cycling to amplify specific DNA sequences [41]. In traditional PCR, detection and quantification of specific sequences occur at the end of the last PCR cycle and require post-PCR analysis [41]. In contrast, RT-qPCR measures the amount of target sequence in ”real-time” after each PCR cycle using fluorescent dyes or probes, allowing determination of the initial sequence amount [41, 42]. To perform RT-qPCR, RNA is first converted to complementary DNA (cDNA) using reverse transcriptase enzymes, and the cDNA

is used as a template for the RT-qPCR reaction. Each PCR cycle consists of three steps: Denaturation, Annealing, and Extension, theoretically doubling the amount of PCR product per cycle. In addition to the three steps of each PCR cycle, RT-qPCR has three distinct phases: the exponential phase, in which the PCR product doubles per cycle due to the availability of fresh reagents; the linear phase, in which the amount of available reagents decreases, leading to the end of product doubling per cycle; and the plateau phase, in which the reaction product is no longer produced [42].

RT-qPCR allows for both absolute and relative quantification. Absolute quantification requires a set of standards with known quantities. In contrast, relative quantification compares the gene of interest between samples and expresses it as increased or decreased fold change (RQ). Relative quantification requires normalization with an endogenous control to account for variations in the amount of RNA added to the PCR reaction. The expression of the endogenous control should be consistent in all samples, and housekeeping genes are commonly used as endogenous controls [41]. In this project, the comparative Ct method was used for relative quantification of all RT-qPCR data. The Ct (threshold cycle) value is determined by the cycle number in the PCR at which the detected fluorescent signal exceeds the threshold value. This threshold is the value at which the relevant signal can be significantly distinguished from the background signal [41]. The Ct value measures the point at which the target sequence is amplified above the threshold. When more target sequence is present, the amplicon amount reaches a significant level sooner, resulting in a lower Ct value [42].

To calculate the fold change ($2^{-\Delta\Delta Ct}$) for expression of a gene of interest in the test sample compared to expression in the control (unstimulated sample), the following equations were used [41]:

$$\mathrm{Ct}^{\mathrm{s}}_{\text{Gene of interest}} - \mathrm{Ct}^{\mathrm{s}}_{\text{Endogenous control}} = \Delta\mathrm{Ct}_{\text{Sample}}$$

$$\mathrm{Ct}^{\mathrm{c}}_{\text{Gene of interest}} - \mathrm{Ct}^{\mathrm{c}}_{\text{Endogenous control}} = \Delta\mathrm{Ct}_{\text{Control}}$$

$$\Delta\mathrm{Ct}_{\text{Sample}} - \Delta\mathrm{Ct}_{\text{Control}} = \Delta\Delta\mathrm{Ct}$$

$$\mathrm{RQ} = \text{Fold change} = 2^{-\Delta\Delta\mathrm{Ct}}$$

TaqMan assay

The most commonly used RT-qPCR technique is the 5' nuclease assay, such as the TaqMan® assay. In addition to the gene-specific forward and reverse PCR primers, this assay uses an oligonucleotide probe with a fluorescent reporter dye at the 5' end and a quencher (a non-fluorescent

dye) at the 3' end [41]. The fluorescence emitted by the reporter dye is reduced by fluorescence resonance energy transfer (FRET) through space while the dye is near the quencher [42]. Once constructed, the probe binds to the target sequence along with the primers. The probe anneals between the primer sites and is cleaved by the 5'-nuclease-active Taq DNA polymerase during primer extension. This causes the reporter dye to separate from the quencher and increases the fluorescence emitted by the reporter dye. Reporter dyes are cleaved repeatedly at each cycle, so the increase in fluorescence intensity is proportional to the amount of amplicon produced [42]. **Figure 3.2** illustrates the steps of the TaqMan® assay.

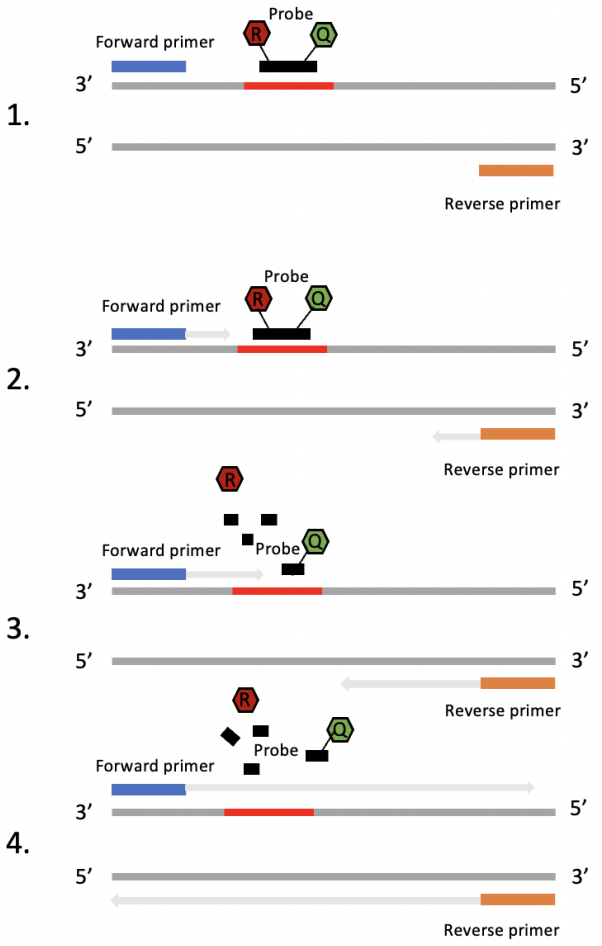

Figure 3.2: The steps of TaqMan® Assay. 1. A fluorescent reporter dye (R) and a quencher (Q) are attached to the 5' and 3' ends of the TaqMan® probe. Due to the fluorescence resonance energy transfer (FRET) the fluorescence emitted from the reporter dye is reduced when in proximity to the quencher. **2.** The probe is annealed to the target sequence between the forward and reverse PCR primers. The Taq DNA polymerase begins extending the primers. **3.** The Taq DNA polymerase cleaves the reporter dye from the probe resulting in the increase of fluorescence emitted from the reporter dye. **4.** The Taq DNA polymerase keeps extending the primers. The figure is modified from [41, 42].

3.5.2 Procedure of RT-qPCR

To perform RT-qPCR, RNA was first extracted and cDNA synthesized.

Reagents

RNA was isolated using the RNeasy® Mini Kit from Qiagen (Hilden, Germany), and cDNA synthesized using the High Capacity RNA-to-cDNA kit from Applied Biosystems (Foster City, CA, USA). TaqMan^{TM} Universal PCR Master Mix (Thermo Fisher Scientific, Waltham, MA, USA) was used for RT-qPCR analysis. TaqMan gene expression assays (probes) were purchased from Applied Biosystems: TLR4 (Hs00152939_m1), TLR9 (Hs00152973_m1), and TBP (Hs00427620_m1).

RNA isolation

For RNA isolation from MM cell lines, the RNeasy® Mini Kit was used according to the protocol "*RNeasy® Mini Handbook: Purification of Total RNA from Animal Cells Using Spin Technology*" with Appendix E [43]. RNA isolation was performed using the QIAcube instrument (QIAGEN, Hilden, Germany). After RNA extraction, samples were kept on ice and RNA concentration was measured using a NanoDrop® ND -1000 spectrophotometer (Thermo Fisher Scientific, Waltham, MA, USA). Finally, the RNA samples were stored at -80 °C until they were collected for reverse transcription.

cDNA synthesis

For cDNA synthesis, the High-capacity RNA-to-cDNA kit from Applied Biosystems was used. To ensure equal amounts of RNA in a total volume of 9.0 µl, RNA samples were diluted with RNase-free water based on the measured RNA concentrations. The RT reaction mixture was prepared by mixing RT buffer mixture and RT enzyme mixture according to the volumes indicated in **Table 3.3**, and then added to the PCR tubes containing the diluted RNA samples. After a brief spin, the RT reaction was run on a C1000^{TM} thermal cycler (Bio-Rad, Hercules, CA, USA) under the following conditions: 37 °C for 60 minutes, followed by 95 °C for 5 minutes and a 4 °C hold. After synthesis, the cDNA was diluted with sterile-filtered MilliQ water to a concentration of 1 ng/µL.

Table 3.3: Overview of components and their volumes used in cDNA synthesis reaction

Component	Volumes per reaction +RT (µl)	Volume per reaction -RT (µl)
2X RT Buffer mix	10	11
20X RT Enzyme mix	1	-
Isolated total RNA in RNase free water	9	9
Total per sample	**20**	**20**

TaqMan gene expression assays

To prepare the RT-qPCR, a reaction mix was created for each target gene by combining the TaqMan Universal PCR Master Mix and TaqMan probe volumes as indicated in **Table 3.4**. Then, the RT-qPCR reaction mix (11 µl) was transferred to each well of a MicroAmp Fast Optical 96-well Reaction Plate and 5 ng of cDNA was added to each well. The cDNA had previously been diluted with sterile ultrapure water (SIW) to a total volume of 9.0 µl. To avoid air bubbles and ensure good mixing, the plates were sealed with adhesive film and centrifuged at 448 rcf for 5 minutes at 20 °C. The StepOnePlus real-time PCR machine (Applied Biosystems) was used to analyze the plates under the following conditions: initial denaturation at 95 °C for 10 minutes, followed by 40 cycles at 95 °C for 15 seconds and 60 °C for 1 minute. TATA-binding protein (TBP) was used as an endogenous control and StepOne software^{TM} version 2.1 was used to determine the relative target amount in the samples using the comparative Ct method ($2^{-\Delta\Delta Ct}$).

Table 3.4: Reagents and their volumes used in the TaqMan fast real-time RT-qPCR assay.

Component	Volumes per reaction (µl)
TaqMan^{TM} Universal PCR Master Mix	10
TaqMan probe	1
cDNA + SIW	9
Total per sample	**20**

3.6 Flow Cytometry

To assess whether TLR9 activation can affect MM cell sensitivity to the anti-myeloma drug bortezomib, RPMI8226 TLR9 KO and WT cells were treated with CpG in combination with different doses of bortezomib. Using Annexin V and propidium iodide (PI) as apoptotic and necrotic markers, respectively, the percentage of live cells was quantified through flow cytometry.

Additionally, flow cytometry was employed to analyze the expression of surface receptors CD38, CD138, and BCMA in LPS- and CpG-stimulated RPMI8226 cells.

3.6.1 Principle of flow cytometry

Flow cytometry is a technique used to rapidly analyze and quantify the properties of individual cells in a heterogeneous mixture. The principle of flow cytometry involves passing each cell through a laser beam and analyzing its light scatter and fluorescent signals. The light scattering can be measured in a forward and a side direction, which provides information on cell size and granularity, respectively [44, 45]. Fluorescent signals are detected from cells stained with fluorescent dyes or fluorescently-conjugated antibodies, which become excited when the cells pass through the laser beam [44, 45]. This technique has a broad range of applications. It can be used to identify cell populations, characterize immune responses, and discover biomarkers [44].

3.6.2 Reagents

Apotest Annexin-A5-FITC kit (Nexins research), eBioscience^{TM} Fixable Viability Dye eFluor^{TM} 450, and OneComp eBeads all from Invitrogen (Carlsbad, USA), CD38 - PE-Cy7, CD138 - FITC from BD Biosciences (New Jersey, USA), BCMA - APC from BioLegend (San Diego, CA, USA), and Bortezomib from Selleck Chemicals (Houston, TX, USA) were utilized for flow cytometry analysis.

3.6.3 Procedure

AnnexinV PI experiment

AnnexinV PI was used to evaluate the effect of TLR9 activation on drug resistance of RPMI8226 cells towards bortezomib. Following stimulation, the RPMI8226 TLR9 KO and WT cells were harvested and washed once with PBS. Further, the cells were centrifuged at 448 rcf for 5 minutes at 4°C, before the supernatant was discarded, and the cell pellet was resuspended in AnnexinV dye (300 µl per sample). AnnexinV was prepared by mixing stock solution (0.25 µl) with 1X binding buffer (300 µl). The samples were incubated on ice for 1 hour covered with aluminum foil. Next, propidium iodide (2 µl in 50 µl binding buffer) was added and samples were incubated for additional 5 minutes. Cell viability was assessed using fluorescence, with AnnexinV (FITC) exciting at 488 nm and PI exciting at 552 nm, on an LSRII flow cytometer (BD Bioscience, New Jersey, USA), and the data were analyzed using FlowJo v10 software.

BCMA/CD38/CD138 experiment

Expression levels of surface receptors CD38, CD138, and BCMA on MM cell lines RPMI8226, TLR9 KO, WT, and ANBL-6 in response to TLR activation was assessed using flow cytometry. After 24 and 48 hours of incubation, 400,000 cells per sample were harvested for staining, while 200,000 cells per sample were harvested for unstained controls. One of the medium control samples of each cell line was used as a live/dead compensation control, where half of the cells were heated for 4 minutes at 70 °C and then combined with the live cells.

Samples were centrifuged at 448 rcf for 5 minutes at 4 °C, the supernatant was discarded, and cell pellets were washed with PBS. The samples were centrifuged again, the supernatant was discarded, and the cell pellet was stained with live/dead stain (eFlour^{TM} 450, 1 ml). The live/dead stain was prepared by mixing the stock solution (1 µl) with PBS (1 ml). After vortexing the samples, they were incubated on ice for 30 minutes, covered with aluminum foil. Following incubation, the samples were washed with flow buffer (0.1% BSA in PBS) before they were stained with antibody mix (1 ml). The antibody mix was prepared by combining CD38 - PE-Cy7 (2.5 µl), CD138 - FITC (10 µl), and BCMA - APC (2.0 µl) in flow buffer (1 ml). Further, the stained samples were vortexed and incubated on ice for 30 minutes, covered with aluminum foil.

For each cell line, Fluorescence minus one (FMO) controls were prepared by adding two of the three antibodies in the panel, as specified in **Table 3.5** which indicates the stains added to each sample. Compensation bead samples were prepared by washing the beads (1 drop per sample)

with flow buffer and adding BCMA-APC (1 µl), CD138-FITC (5 µl), and CD38-PE-Cy7 (1 µl) separately to the three samples. The samples were then incubated for 10 minutes on ice covered with aluminum foil.

All the samples were finally washed twice with flow buffer and resuspended in 300 µl flow buffer. The amount of expressed surface receptors was then determined by measuring the fluorescence emission peak at 660 nm (APC), 525 nm (FITC), and 780 nm (PE-Cy7) using an LSRII flow cytometer, and the data were analyzed using FlowJo v10 software.

Table 3.5: Overview of which stains were added for flow cytometry experiment

Samples	Antibodies added (stained)	Unstained samples
Ctrl 24 hours	Live/dead stain + BCMA-APC + CD138-FITC + CD38-PE-Cy7	Live/dead stain
Ctrl 48 hours	Live/dead stain + BCMA-APC + CD138-FITC + CD38-PE-Cy7	Live/dead stain
LPS 24 hours	Live/dead stain + BCMA-APC + CD138-FITC + CD38-PE-Cy7	Live/dead stain
LPS 48 hours	Live/dead stain + BCMA-APC + CD138-FITC + CD38-PE-Cy7	Live/dead stain
CpG 24 hours	Live/dead stain + BCMA-APC + CD138-FITC + CD38-PE-Cy7	Live/dead stain
CpG 48 hours	Live/dead stain + BCMA-APC + CD138-FITC + CD38-PE-Cy7	Live/dead stain
FMO - BCMA-APC	Live/dead stain + CD138-FITC + CD38-PE-Cy7	-
FMO - CD138-FITC	Live/dead stain + BCMA-APC + CD38-PE-Cy7	-
FMO - CD38-PE-Cy7	Live/dead stain + BCMA-APC + CD138-FITC	-
Beads - BCMA-APC	BCMA-APC	-
Beads - CD138-FITC	CD138-FITC	-
Beads - CD38-PE-Cy7	CD38-PE-Cy7	-

3.7 Statistical analysis

The statistical analyses were performed using GraphPad Prism 9. The statistical analysis and the replicate numbers used are stated in the figure legends. For experiments with two or more replicates, the mean and standard deviation (SD) were calculated. When several, independent experiments were combined, the standard error of the mean (SEM) was calculated. Unpaired T-test was used for comparisons of two unmatched groups. For treatments within groups, one-way ANOVA with Dunnett's multiple comparisons test was used. Two-way ANOVA with Tukey's multiple comparisons test was used to compare more than two groups over time. The statistical level of significance was set at a 5% level.

4 Results

Previous research has shown that activation of TLRs can increase the viability of multiple myeloma cell lines and promote resistance to anti-cancer drugs. This study examines the effect of TLR activation on viability of different MM cell lines, investigates if and how TLR activation can affect MM cell resistance against the anti-myeloma drug bortezomib, and examines if TLR4 and TLR9 activation can affect the expression of plasma cell markers and histone modifications in MM cell lines.

4.1 The expression of TLR4 and TLR9 in MM cell lines MM.1S, AMO-1, and H929

Previous studies have reported that TLR activation can enhance the viability of MM cells, and unpublished data (Tryggestad *et al.*, 2022) has shown that myeloma cells from patients express a range of TLRs, and that TLR4 and TLR9 were among the highest [35]. Therefore, this study aimed to investigate the effect of treatment with TLR4 agonist LPS and TLR9 agonist CpG on the viability of MM cell lines MM.1S, AMO-1, and H929. First, the cell lines were screened for expression of TLR4 and TLR9 using RT-qPCR, both at basal conditions and upon stimulation.

The results revealed that all the cell lines examined exhibited low or absent expression of both TLR4 and TLR9 (Ct-values between 30-36), as presented in **Table 4.1**. Additionally, no significant changes in the expression of TLR4 or TLR9 were observed between the control and stimulated cells, as depicted in **Figure 4.1**. The fold change (RQ) value of the stimulated cells did not differ significantly from the RQ value of the control at 1, indicating that the gene expression level in the stimulated samples was similar to that of the control. However, minor differences were noted among the cell lines. For instance, the AMO-1 cells stimulated with CpG exhibited an RQ value less than 1 for TLR4, indicating lower mRNA expression, while the H929 cells stimulated with both LPS and CpG showed an RQ value greater than 1 for TLR9, indicating higher mRNA expression.

Table 4.1: Mean Ct-values for MM cell lines of TLR4 and TLR9 mRNA. Mean Ct-values for MM cell lines MM.1S, AMO-1, and H929 stimulated with either LPS or CpG, TLR4 and TLR9 agonists, from performing RT-qPCR. Means were calculated from 3 technical replicates.

MM cell line	Mean Ct-values					
	Ctrl		LPS		CpG	
	TLR 4	TLR 9	TLR 4	TLR 9	TLR 4	TLR 9
MM.1S	30	35	31	36	30	35
AMO-1	36	31	36	31	36	31
H929	34	35	34	34	33	34

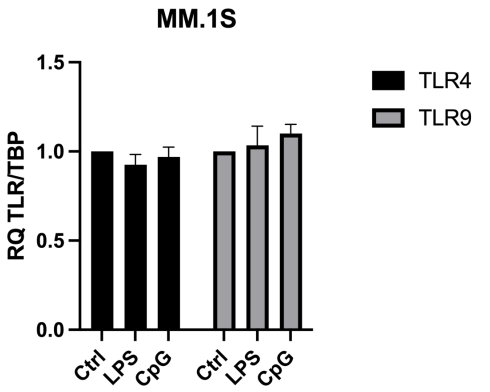

(a) TLR4 and TLR9 mRNA expression in MM.1S.

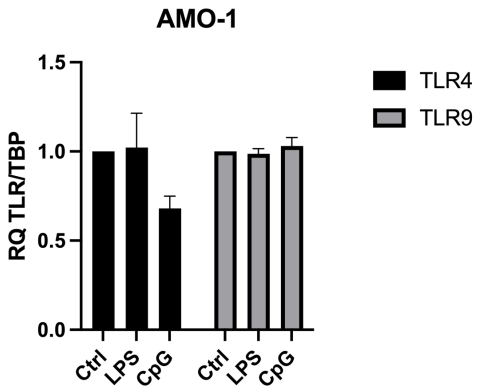

(b) TLR4 and TLR9 mRNA expression in AMO-1.

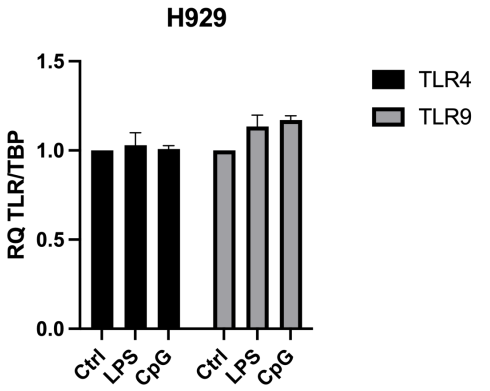

(c) TLR4 and TLR9 mRNA expression in H929.

Figure 4.1: RT-qPCR results for MM cell lines MM.1S, AMO-1, and H929 stimulated with TLR4 and TLR9 agonists LPS and CpG. Figures **(a)**, **(b)**, and **(c)** illustrate the relative quantity of TLR4 and TLR9 in cell lines MM.1S, AMO-1, and H929, respectively. The bars represent mRNA expression in treated cells relative to mRNA expression in unstimulated cells, which was set to 1. Gene expression of target genes were normalized to the endogenous control TBP in each sample. The RQ-values were calculated from the samples stimulated with medium, LPS (0.1 µg/ml), and CpG (1.0 µM) using the Ct method, and calculated from 1 biological and 3 technical replication. No statistically significant difference by two-way ANOVA, Tukey's multiple comparisons test.

4.2 The viability of cell lines MM.1S, AMO-1, and H929 in response to TLR4 and TLR9 activation

Despite the low expression of TLR4 and TLR9 in the MM.1S, AMO-1, and H929 cell lines, the potential effect of TLR activation on viability was examined. The cell lines were stimulated with varying concentrations of LPS and CpG for 24 and 48 hours, and viability was measured using the CTG assay. The results are shown in **Figure 4.2** (MM.1S), **Figure 4.3** (AMO-1), and **Figure 4.4** (H929). For MM.1S, there was no statistically significant difference between the control and stimulated samples.

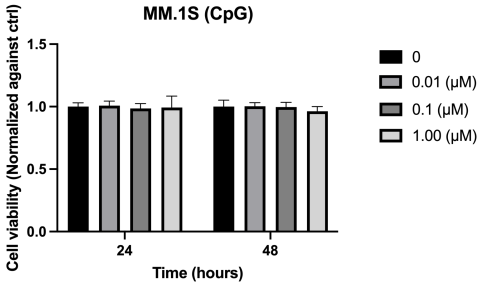

(a) CpG-stimulated MM.1S.

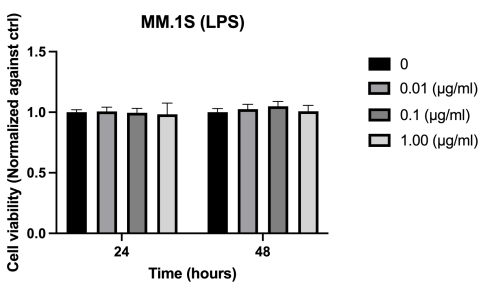

(b) LPS-stimulated MM.1S.

Figure 4.2: CTG results for MM cell line MM.1S stimulated with TLR4 and TLR9 agonists LPS and CpG. Figures **(a)** and **(b)** illustrate the viability of MM.1S as a function of CpG and LPS concentrations, respectively, over 24 and 48 hours. The viability was measured in the samples: 0, 0.01, 0.1, and 1.0 μM CpG and μg/ml LPS. The mean and SD for 3 biological and 5 technical replications were calculated. A two-way ANOVA, Tukey's multiple comparisons test was performed. However, there was no statistically significant difference between the concentrations.

For AMO-1, an increase in viability was observed, specifically at a concentration of 0.01 μM CpG after 48 hours. This finding could suggest an optimal concentration for this specific cell line. However, no significant difference was observed in the LPS-stimulated cells. Further work is required to determine the reason for the significant increase in viability at 0.01 μM CpG, but as no significant differences for concentrations lower or higher than 0.01 μM were observed, no further analysis was pursued.

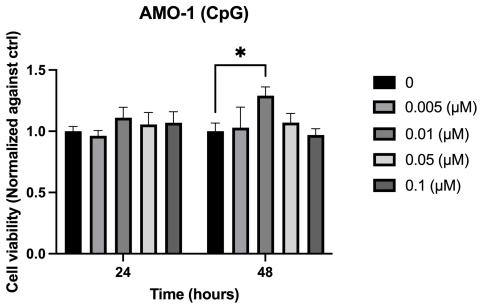

(a) CpG-stimulated AMO-1.

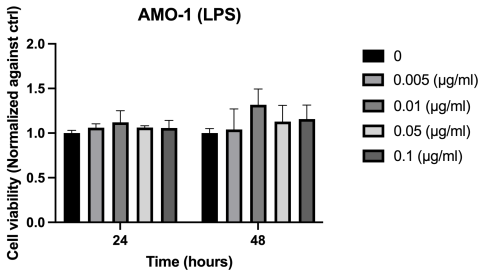

(b) LPS-stimulated AMO-1.

Figure 4.3: CTG results for MM cell line AMO-1 stimulated with TLR4 and TLR9 agonists LPS and CpG. Figures **(a)** and **(b)** illustrate the viability of AMO-1 as a function of CpG and LPS concentrations, respectively, over 24 and 48 hours. The viability was measured in the samples: 0, 0.01, 0.1, and 1.0 μM CpG and μg/ml LPS. The mean and SD for 3 biological and 5 technical replications were calculated. * p <0.05 by two-way ANOVA, Tukey's multiple comparisons test.

No significant difference was found in the viability of CpG-stimulated H929 cells. However, there was a significant decrease in the viability of LPS-stimulated H929 cells after 24 hours, which was not observed after 48 hours.

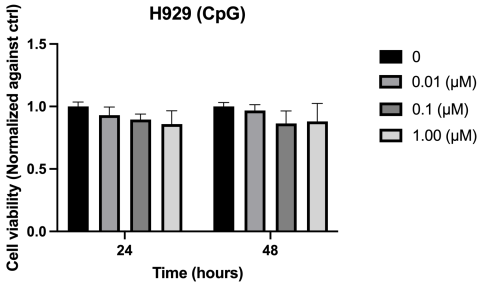

(a) CpG-stimulated H929.

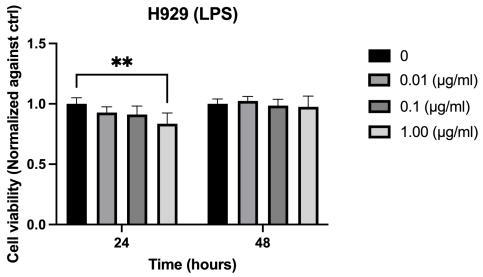

(b) LPS-stimulated H929.

Figure 4.4: CTG results for MM cell line H929 stimulated with TLR4 and TLR9 agonists LPS and CpG. Figures **(a)** and **(b)** illustrate the viability of H929 as a function of CpG and LPS concentrations, respectively, over 24 and 48 hours. The viability was measured in the samples: 0, 0.01, 0.1, and 1.0 μM CpG and μg/ml LPS. The mean and SD for 2 biological and 5 technical replications were calculated. ** p <0.01 by two-way ANOVA, Tukey's multiple comparisons test.

The stimulation with LPS and CpG did not substantially affect the viability of the MM.1S, AMO-1, or H929 cell lines. As a result, no additional analysis was performed on these particular cell lines.

4.3 Increased viability of RPMI8226 cell line in response to TLR9 activation

It was decided to further focus the study on the MM cell line RPMI8226, which has previously been shown by studies conducted by Tryggestad *et al.* (unpublished data, 2022) to increase in viability upon LPS and CpG stimulation (**Figure 1.5**) [35]. Whether the CpG-induced increase in viability of RPMI8226 was mediated by TLR9 signaling was investigated. To achieve this, the viability of CpG-stimulated RPMI8226 TLR9 KO and WT cells were measured over 24 and 48 hours using CTG, as shown in **Figure 4.5a** and **Figure 4.5b**, respectively. There was a significant increase in the viability of the WT cells stimulated with increasing CpG concentrations. In contrast, no significant increase was observed in viability for the TLR9 KO cell line. The viability rather decreased for the TLR9 KO cell line. This shows that the observed increase in viability of RPMI8226 upon CpG treatment is TLR9-dependent.

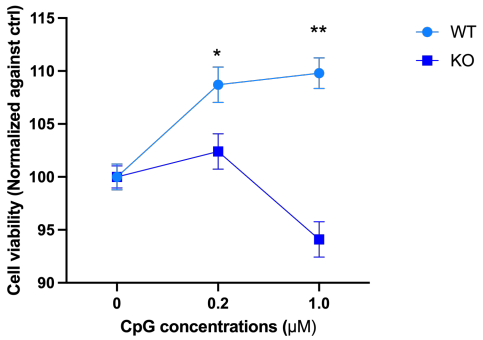

(a) RPMI8226 TLR9 KO and WT, 24 hours.

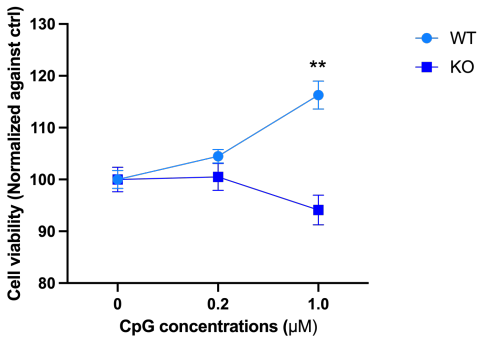

(b) RPMI8226 TLR9 KO and WT, 48 hours.

Figure 4.5: CTG results for MM cell lines RPMI8225 TLR9 KO and WT stimulated with TLR9 agonist CpG. Figures **(a)** and **(b)** illustrate the viability of TLR9 KO and WT as a function of CpG concentrations, over 24 and 48 hours, respectively. The viability was measured in the samples: 0, 0.2, and 1.0 µM CpG. The mean and SD for 3 biological and 3 technical replications were calculated. * $p < 0.05$, ** $p < 0.01$ by two-way ANOVA, Tukey's multiple comparisons test.

4.4 Increased expression of pro-survival/anti-apoptotic factors

Given the TLR-dependent increase in viability of RPMI8226 cells, this study aimed to investigate the potential upregulation of well-known pro-survival/anti-apoptotic factors upon TLR stimulation. Furthermore, the study sought to examine the activation of ERK signaling in response to TLR stimulation, considering its significant role as a downstream pathway for both TLR4 and TLR9. Thus, RPMI8226 cells were stimulated with CpG and LPS for 4 and 24 hours, and the protein expression of phospho-ERK1/2, and the pro-survival and anti-apoptotic factors Bcl-xL and Mcl-1 were measured using western blot. The results, depicted in **Figure**

4.6, showed a statistically significant increase in both p-ERK1 and p-ERK2 expression in LPS- and CpG-stimulated RPMI8226 cells when compared to controls, both at 4- and 24-hour treatment. Additionally, there was a significant increase in the expression of Bcl-xL and Mcl-1 after 4 hours. At 24 hours there was no significant difference between the control and stimulated samples.

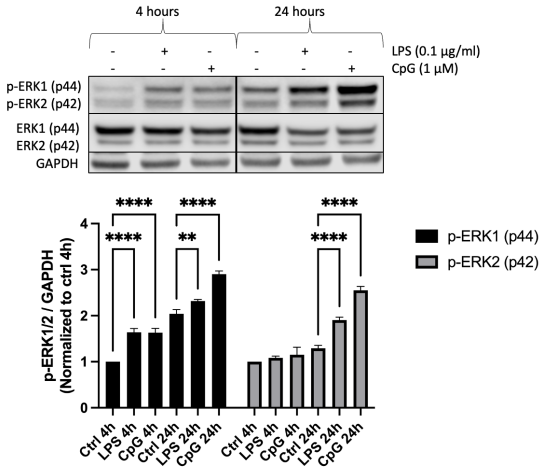

(a) The protein expression of p-ERK1/2 relative to GAPDH, 4 and 24 hours.

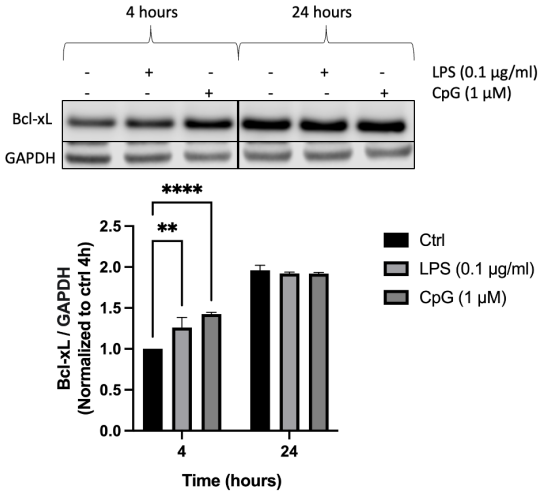

(b) The protein expression of Bcl-xL relative to GAPDH, 4 and 24 hours.

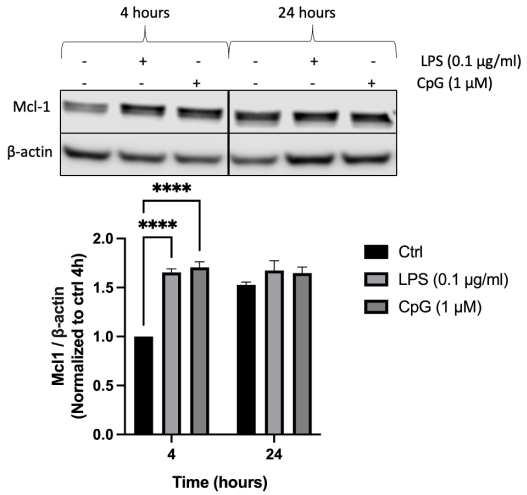

(c) The protein expression of Mcl-1 relative to β-actin, 4 and 24 hours.

Figure 4.6: Western blot results for MM cell line RPMI8226 stimulated with TLR4 and TLR9 agonists LPS and CpG, looking at the protein expression of phosphorylated ERK1/2 (p-ERK1/2), Bcl-xL, and Mcl-1. Figures **(a)**, **(b)**, and **(c)** illustrate the protein expression of pro-survival and anti-apoptotic factors phospho-ERK1/2, Bcl-xL, and Mcl-1, respectively, over 4 and 24 hours, relative to GAPDH and β-actin, and normalized to the control at 4 hours. The samples measured for each protein were: medium-control, 0.1 µg/ml LPS, and 1.0 µM CpG. The western blot bands for each protein, from one of the experiments, are also shown in each figure as a representative. The mean and SD with 3 biological and 1 technical replication were calculated. ** p <0.01, **** p <0.0001 by two-way ANOVA, Tukey's multiple comparisons test.

4.5 Reduced drug sensitivity of CpG-stimulated RPMI8226 cells towards proteasome inhibitor bortezomib

Considering the TLR9-dependent increase in viability of CpG-stimulated RPMI8226 cells, as well as the increased expression of pro-survival/anti-apoptotic factors upon TLR stimulation, this study further aimed to investigate the potential effect of TLR9 stimulation on the drug sensitivity of this cell line. The cells were thus pre-stimulated with CpG followed by treatment with different concentrations of the common anti-myeloma drug bortezomib. The viability of both TLR9 KO and WT cells was measured using the flow cytometry - AnnexinV PI assay. **Figure 4.7** shows results from a representative experiment, and shows how the living cells were gated. Living cells are negative for both AnnexinV - FITC and PI (lower left population), apoptotic cells are positive for AnnexinV (lower right population), and necrotic cells are positive for both dyes (upper right population).

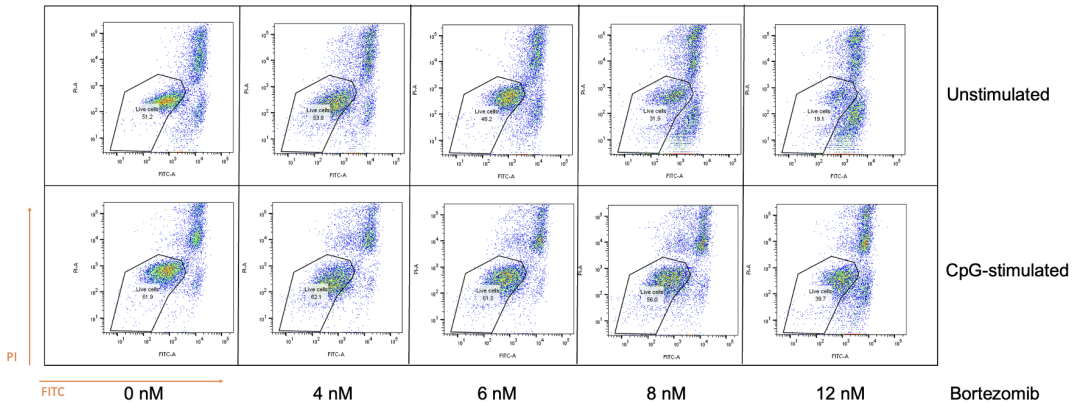

(a) Representative gating of wild-type RPMI8226 cells (WT).

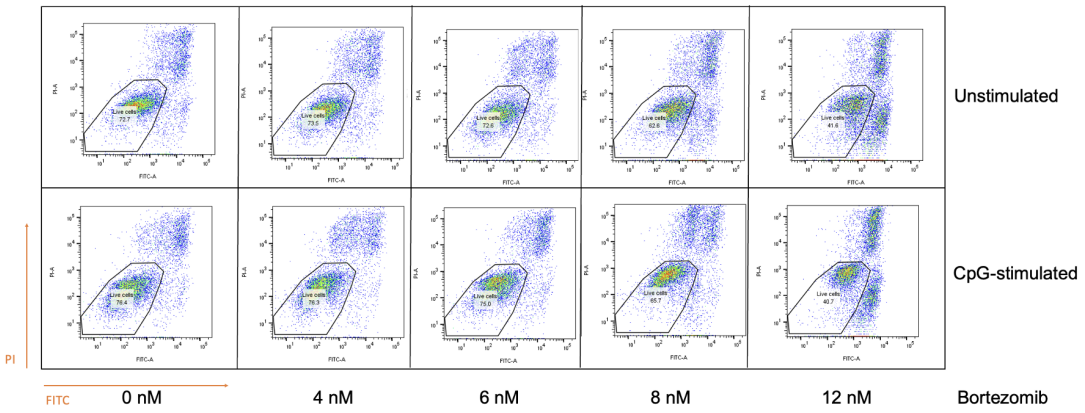

(b) Representative gating of TLR9 knockout RPMI8226 cells (KO).

Figure 4.7 ***(previous page)*****: Representative gating of the MM cell lines RPMI8226 WT and TLR9 KO stimulated with TLR9 agonist CpG, and treated with different concentrations of proteasome inhibitor bortezomib.** Figures **(a)** and **(b)** illustrate the gating of the WT and KO cell lines, respectively, for the different samples: untreated cells (control and CpG-stimulated), and unstimulated and CpG-stimulated cells treated with 4, 6, 8, and 12 nM bortezomib. AnnexinV (FITC) is plotted on the x-axis while PI is plotted on the y-axis.

The percentages of live cells for WT and TLR9 KO upon stimulation are shown in **Figure 4.8a** and **Figure 4.8b**, respectively. The presence of CpG increased the percentage of live cells at all concentrations of bortezomib in the WT cell line, though it reached significance only at 8 nM. TLR9 KO cells on the other hand showed no significant difference or general positive effect of CpG. This indicates that CpG stimulation can reduce drug sensitivity of RPMI8226 cells in a TLR9-dependent manner.

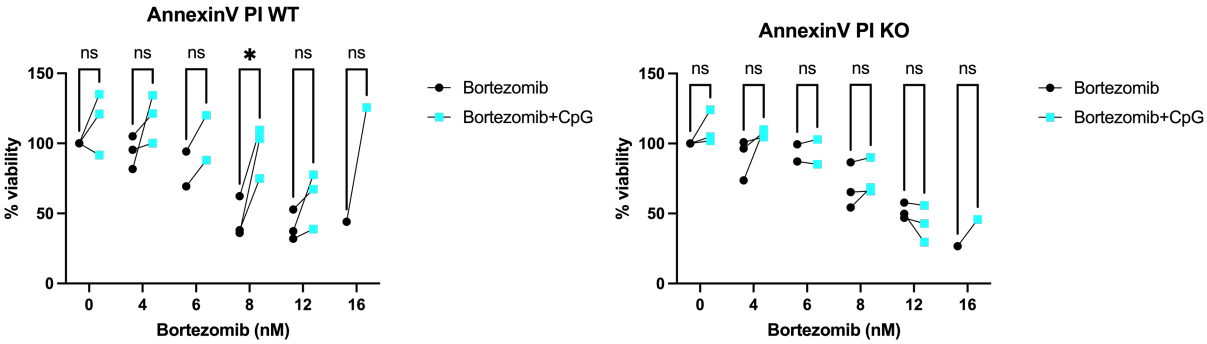

(a) Wild-type RPMI8226 cells (WT).

(b) TLR9 knockout RPMI8226 cells (KO).

Figure 4.8: AnnexinV PI results for MM cell lines RPMI8226 WT and TLR9 KO stimulated with TLR9 agonist CpG, and treated with different concentrations of proteasome inhibitor bortezomib. Figures **(a)** and **(b)** illustrate the viability of unstimulated and CpG-stimulated WT and KO cells as a function of bortezomib concentration, respectively. 3 biological and 1 technical replication were performed. In the first experiment, 16 nM bortezomib was also used as a concentration. * $p < 0.05$ by two-way ANOVA, Tukey's multiple comparisons test.

4.6 Expression of surface protein on MM cell lines RPMI8226 and ANBL-6

Since expression of the cell surface markers BCMA, CD138, and CD38 is important for the response to new immune therapeutic drugs, it was examined if TLR activation could impact the expression of these proteins. Therefore, the MM cell line RPMI8226 was stimulated with LPS and CpG for 24 and 48 hours, stained, and analyzed using flow cytometry. **Figure 4.9** displays the differences in the expression of BCMA, CD138, and CD38 in unstimulated and LPS- and CpG-stimulated RPMI8226 cells. The median fluorescence intensity (MFI) was plotted for each of the surface receptors.

There was a statistically significant decrease in the expression of BCMA for both LPS- and CpG-stimulated cells at 24 hours, while only significant for CpG-stimulated cells at 48 hours. There was a decrease, although not statistically significant, in the expression of CD138 for both LPS- and CpG-stimulated cells, at 24 and 48 hours. The expression of CD38 remained constant for LPS- and CpG-stimulated cells at 24 hours, but decreased slightly at 48 hours.

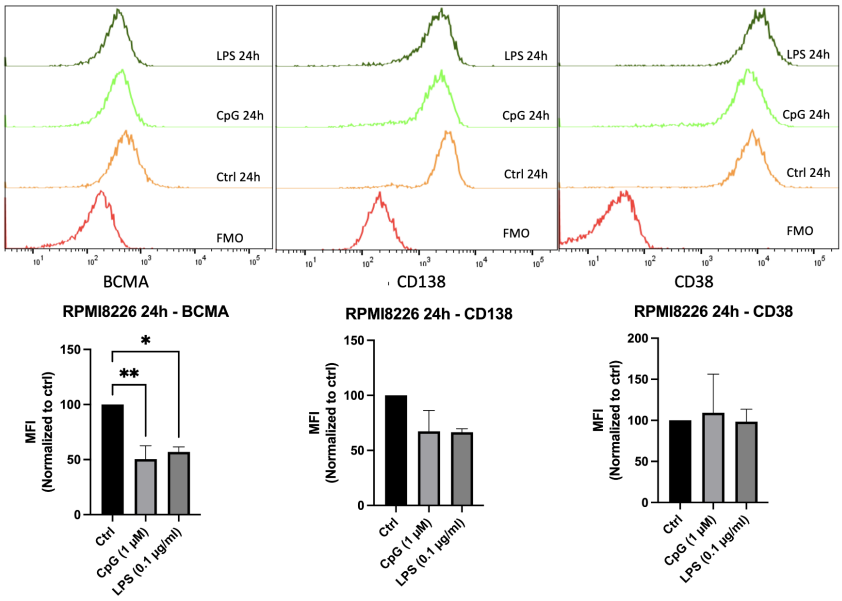

(a) Representative expression of receptors BCMA, CD138, and CD38 on RPMI8226 cells, 24 hours.

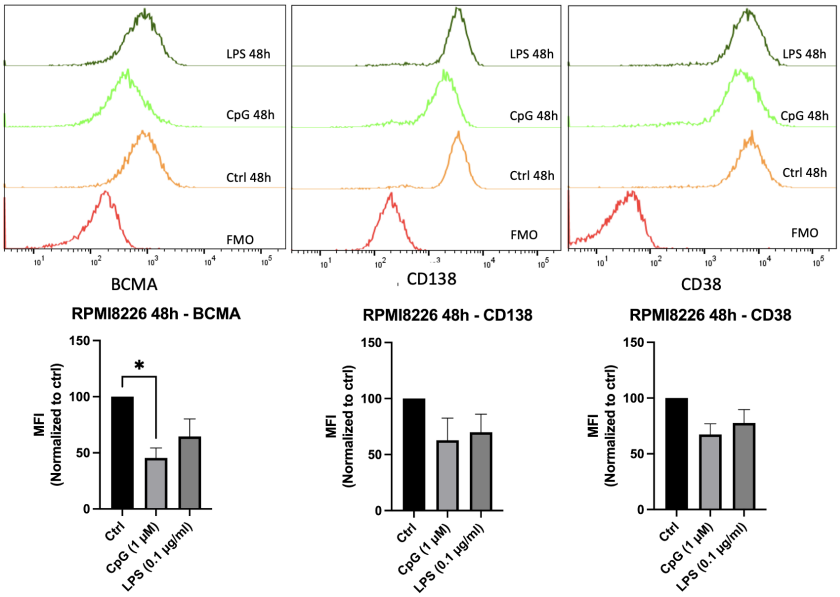

(b) Representative expression of receptors BCMA, CD138, and CD38 on RPMI8226 cells, 48 hours.

Figure 4.9: Flow cytometry results for the expression of receptors BCMA, CD138, and CD38 on MM cell line RPMI8226 stimulated with TLR4 and TLR9 agonists LPS and CpG. Figures **(a)** and **(b)** illustrate the change in expression of surface receptors BCMA, CD138, and CD38 on RPMI8226 when stimulated with LPS and CpG over 24 and 48 hours, respectively. The top figures illustrate representative histograms of the different samples and how they compare to the FMO (fluorescence minus one), while in the plot, the MFI (Median fluorescence intensity) from the histograms is plotted for each of the surface receptors. The mean and SEM with 3 biological and 1 technical replication were calculated. * $p < 0.05$, ** < 0.01 by one-way ANOVA, Dunnett's multiple comparisons test.

Considering the observed downregulation of the biomarkers in RPMI8226, this study further examined if the downregulation with CpG stimulation was TLR9-dependent. The cell lines RPMI8226 TLR9 KO and WT were thus CpG-stimulated. **Figure 4.10** and **Figure 4.11** display the differences in the expression of BCMA, CD138, and CD38 in unstimulated and CpG-stimulated WT and TLR9 KO cells over 24 and 48 hours, respectively. The median fluorescence intensity (MFI) was plotted for each of the surface receptors. Only one biological and technical replicate was performed.

For the TLR9 KO cell line, an increase in BCMA, CD138, and CD38 expression for CpG-stimulated cells at 24 and 48 hours (**Figures 4.10b** and **4.11b**, respectively) was observed. For the WT cell line, a decrease in BCMA expression for CpG-stimulated cells was observed, at 24 and 48 hours (**Figures 4.10a** and **4.11a**, respectively). A small decrease was observed in the expression of CD138 in CpG-stimulated cells at 24 hours, before increasing at 48 hours. The expression of CD38 remained constant for CpG-stimulated cells.

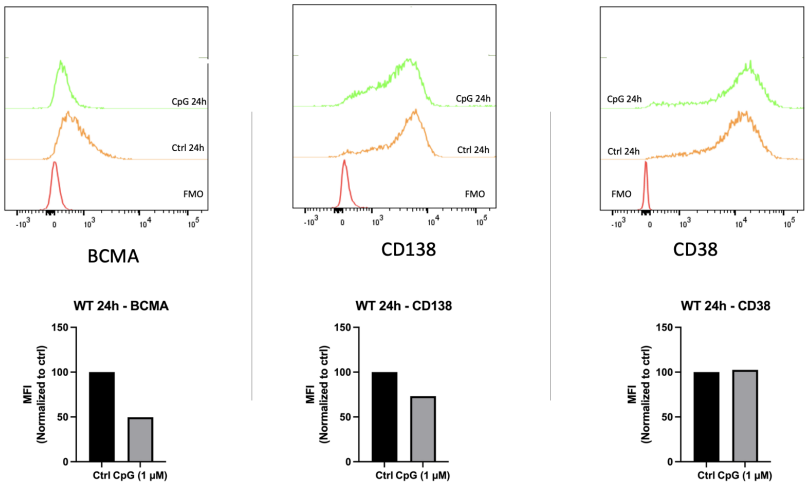

(a) Expression of receptors BCMA, CD138, and CD38 on RPMI8226 WT cells, 24 hours.

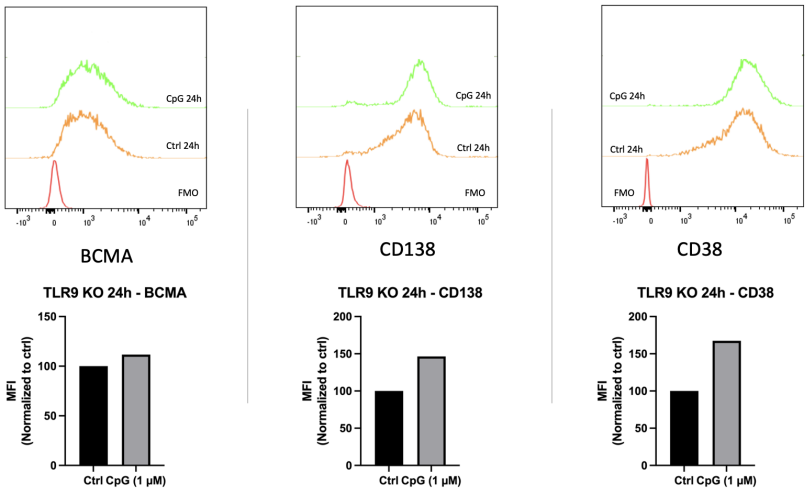

(b) Expression of receptors BCMA, CD138, and CD38 on TLR9 knockout (KO) cells, 24 hours.

Figure 4.10: Flow cytometry results for the expression of receptors BCMA, CD138, and CD38 on MM cell lines RPMI8226 WT and TLR9 KO stimulated with TLR9 agonist CpG. Figures **(a)** and **(b)** illustrate the change in expression of surface receptors BCMA, CD138, and CD38 on WT and TLR9 KO, respectively, when stimulated with CpG over 24 hours. The top figures illustrate the histograms of the different samples and the FMO (fluorescence minus one), while in the plot, the MFI (Median fluorescence intensity) from the histograms is plotted for each of the surface receptors. One biological replication was performed.

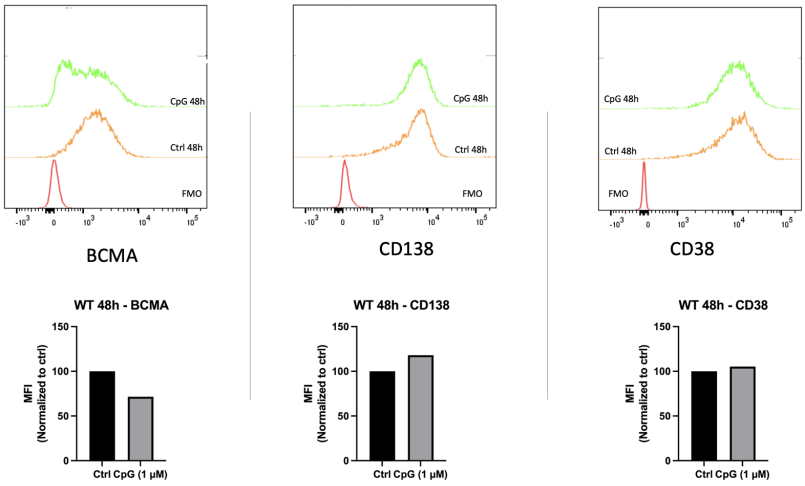

(a) Expression of receptors BCMA, CD138, and CD38 on RPMI8226 WT cells, 48 hours.

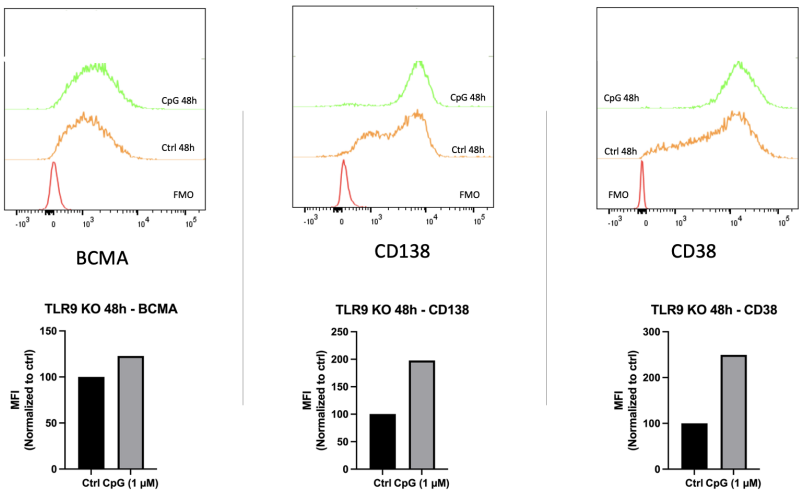

(b) Expression of receptors BCMA, CD138, and CD38 on TLR9 knockout (KO) cells, 48 hours.

Figure 4.11: Flow cytometry results for the expression of receptors BCMA, CD138, and CD38 on MM cell lines RPMI8226 WT and TLR9 KO stimulated with TLR9 agonist CpG. Figures **(a)** and **(b)** illustrate the change in expression of surface receptors BCMA, CD138, and CD38 on WT and TLR9 KO, respectively, when stimulated with CpG over 48 hours. The top figures illustrate the histograms of the different samples and the FMO (fluorescence minus one), while in the plot, the MFI (Median fluorescence intensity) from the histograms is plotted for each of the surface receptors. One biological replication was performed.

Figure 4.12, **Figure 4.13**, and **Figure 4.14** were plotted to compare RPMI8226 WT and TLR9 KO with each other, and show the MFI of WT and TLR9 KO plotted as a function of stimulation for BCMA, CD138, and CD38, respectively. **Figure 4.12a** and **Figure 4.12b** show the difference in the expression of BCMA between TLR9 KO and WT cell lines, over 24 and 48 hours, respectively. For the CpG-stimulated cells, there was a striking difference in the expression level of BCMA between TLR9 KO and WT, with an increase in TLR9 KO and a decrease in WT. This support that the downregulation of BCMA upon CpG stimulation is dependent on TLR9.

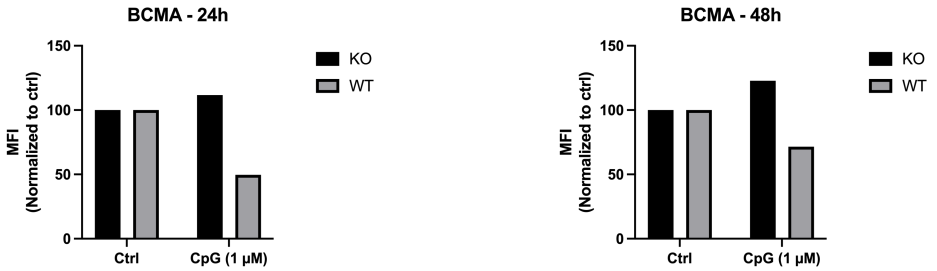

(a) Expression of receptor BCMA on TLR9 KO and WT cells, 24 hours.

(b) Expression of receptor BCMA on TLR9 KO and WT cells, 48 hours.

Figure 4.12: Flow cytometry results for the expression of receptor BCMA on MM cell lines TLR9 KO and WT stimulated with TLR9 agonist CpG. Figures **(a)** and **(b)** illustrate the MFI (Median fluorescence intensity), from the histograms, plotted as a function of stimulation and cell line, over 24 and 48 hours, respectively. One biological replication was performed.

Figure 4.13a and **Figure 4.13b** show the difference in the expression of CD138 between TLR9 KO and WT cell lines, over 24 and 48 hours, respectively. For CpG-stimulated cells, there was a large difference in the expression level of CD138 between TLR9 KO and WT, with an increase in TLR9 KO while the expression decreased at 24 hours before increasing slightly at 48 hours for the WT cell line.

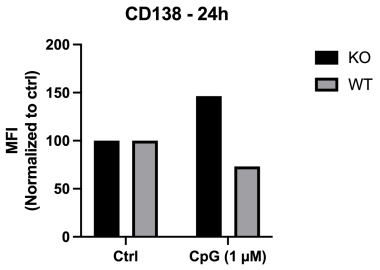

(a) Expression of receptor CD138 on TLR9 KO and WT cells, 24 hours.

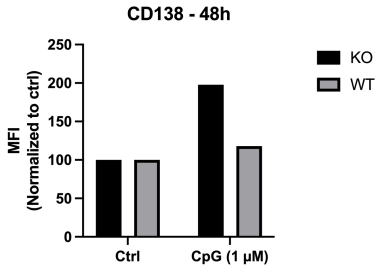

(b) Expression of receptor CD138 on TLR9 KO and WT cells, 48 hours.

Figure 4.13: Flow cytometry results for the expression of receptor CD138 on MM cell lines TLR9 KO and WT stimulated with TLR9 agonist CpG. Figures **(a)** and **(b)** illustrate the MFI (Median fluorescence intensity), from the histograms, plotted as a function of stimulation and cell line, over 24 and 48 hours, respectively. One biological replication was performed.

Figure 4.14a and **Figure 4.14b** show the difference in the expression of CD38 between TLR9 KO and WT cell lines, over 24 and 48 hours, respectively. For CpG-stimulated cells, there was a large difference in the expression of CD38 between TLR9 KO and WT, with an increase in TLR9 KO while the expression remained constant for WT.

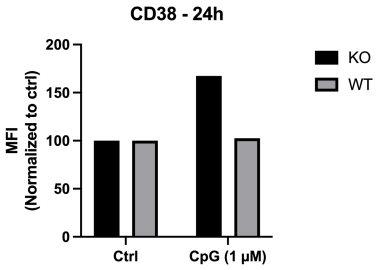

(a) Expression of receptor CD38 on TLR9 KO and WT cells, 24 hours.

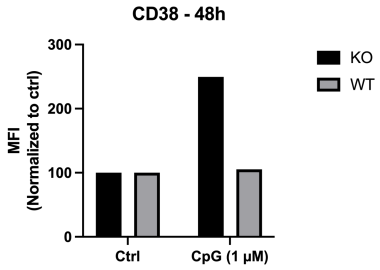

(b) Expression of receptor CD38 on TLR9 KO and WT cells, 48 hours.

Figure 4.14: Flow cytometry results for the expression of receptor CD38 on MM cell lines TLR9 KO and WT stimulated with TLR9 agonist CpG. Figures **(a)** and **(b)** illustrate the MFI (Median fluorescence intensity), from the histograms, plotted as a function of stimulation and cell line, over 24 and 48 hours, respectively. One biological replication was performed.

In the specialization project titled *"The cell survival and proliferation of multiple myeloma cell line ANBL-6 increase in a Toll-like Receptor 4 dependent manner in response to LPS"*, it was observed that the viability of ANBL-6 cells and the expression of pro-survival factors were increased following TLR4 activation [34]. Therefore, potential changes in the expression of BCMA, CD138, and CD38 in the ANBL-6 cell line were also examined after stimulation with LPS. For ANBL-6 (**Figure 4.15**) there was no statistically significant difference in the expression of BCMA, CD138, or CD38 for LPS-stimulated cells. For BCMA, the expression remained constant at both 24 and 48 hours. For both CD138 and CD38, the expression increased at 24 hours before decreasing at 48 hours.

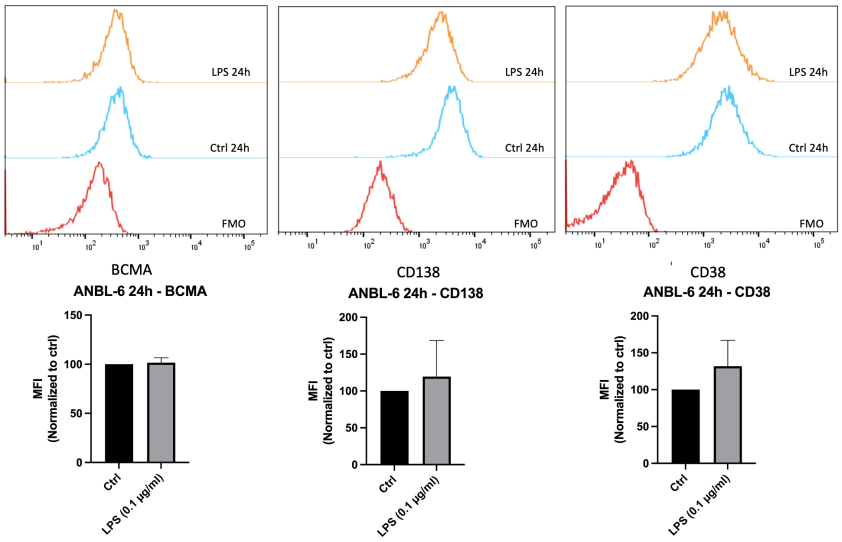

(a) Representative expression of receptors BCMA, CD138, and CD38 on ANBL-6 cells, 24 hours.

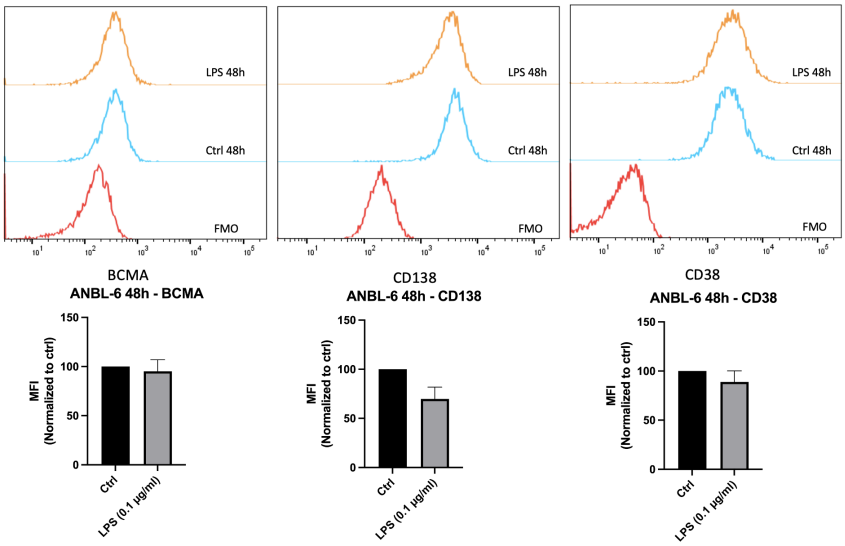

(b) Representative expression of receptors BCMA, CD138, and CD38 on ANBL-6 cells, 48 hours.

Figure 4.15 ***(previous page)*****: Flow cytometry results for the expression of receptors BCMA, CD138, and CD38 on MM cell line ANBL-6 stimulated with TLR4 agonist LPS.** Figures **(a)** and **(b)** illustrate the change in expression of surface receptors BCMA, CD138, and CD38 on ANBL-6 when stimulated with LPS and CpG over 24 and 48 hours, respectively. The top figures illustrate representative histograms of the different samples and the FMO (fluorescence minus one), while in the plot, the MFI (Median fluorescence intensity) from the histograms is plotted as a function of stimulation for each of the surface receptors. The mean and SEM with 3 biological and 1 technical replication were calculated. No statistical significance between the control and LPS-stimulated sample, by unpaired T-test.

4.7 Histone modification in LPS- and CpG-stimulated RPMI8226, TLR9 KO, and WT cells

Considering the observed changes in the expression of plasma cell marker BCMA, and a tendency to decline for CD138 and CD38, this study aimed to further investigate whether these changes could be attributed to epigenetic modifications. Consequently, histone modifications in LPS- and CpG-stimulated RPMI8226 cells, as well as CpG-stimulated TLR9 KO and WT cells, were examined after 48 hours. The protein expression of trimethylated lysine 4, 27, and 36 (H3K4Me3, H3K27Me3, and H3K36Me3), as well as acetylated lysine 9 and 27 (H3K9Ac and H3K27Ac) in histone H3 were analyzed using western blot. **Figure 4.16** shows the results of the analysis. Only one biological replication was performed.

The results indicated a decrease in the expression of both H3K27Me3 and H3K36Me3 for LPS- and CpG-stimulated RPMI8226, and CpG-stimulated TLR9 KO and WT cells (**Figure 4.16a** and **Figure 4.16b**). However, comparing TLR9 KO to both RPMI8226 and WT, there is a smaller decrease in the expression of CpG-stimulated TLR9 KO cells than CpG-stimulated RPMI8226 and WT cells. The expression of H3K4Me3 remained relatively constant for both LPS- and CpG-stimulated RPMI8226 cells, but CpG-stimulated samples decreased in a similar way for both TLR9 KO and WT cells (**Figure 4.16c**). For H3K9Ac (**Figure 4.16d**) the LPS- and CpG-stimulated RPMI8226 and TLR9 KO cells decreased, while the CpG-stimulated WT cells increased minimally. The expression of H3K27Ac (**Figure 4.16e**) also decreased for the LPS- and CpG-stimulated RPMI8226 cells, while the CpG-stimulated samples increased in a similar trend for the TLR9 KO and WT cell lines.

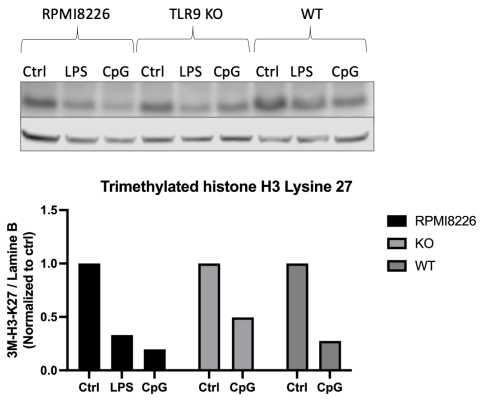

(a) The protein expression of H3K27Me3 relative to Lamin B.

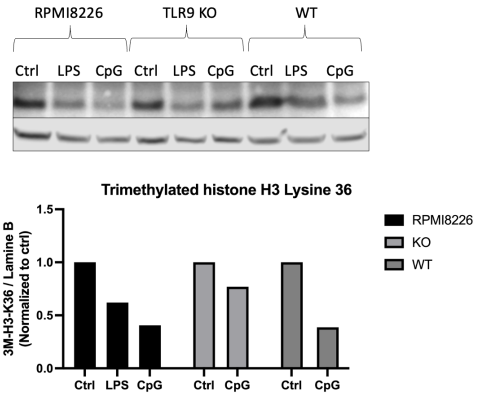

(b) The protein expression of H3K36Me3 relative to Lamin B.

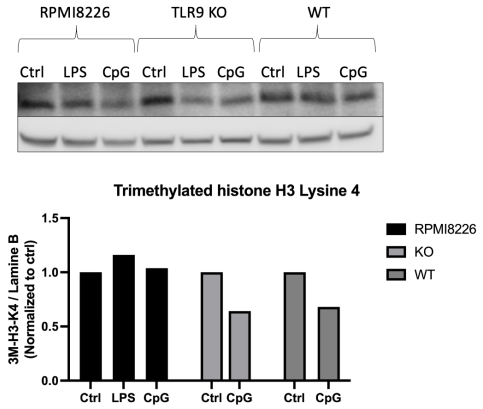

(c) The protein expression of H3K4Me3 relative to Lamin B.

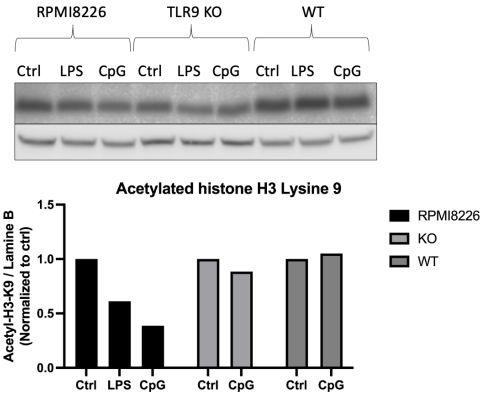

(d) The protein expression of H3K9Ac relative to Lamin B.

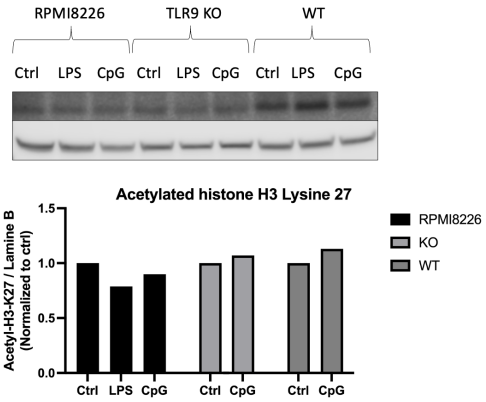

(e) The protein expression of H3K27Ac relative to Lamin B.

Figure 4.16: Western blot results for MM cell lines RPMI8226, RPMI8226 TLR9 KO, and WT stimulated with TLR9 agonist CpG, and TLR4 agonist LPS for RPMI8226, looking at the protein expression of trimethylated lysine 27, lysine 36, and lysine 4 (H3K27Me3, H3K36Me3, and H3K4Me3), and acetylated lysine 9, and lysine 27 (H3K9Ac and H3K27Ac), on histone H3. Figures **(a)**, **(b)**, **(c)**, **(d)**, and **(e)** illustrate the change in H3K27Me3, H3K36Me3, H3K4Me3, H3K9Ac, and H3K27Ac, respectively, of cell lines RPMI8226, RPMI8226 TLR9 KO, and WT over 48 hours when CpG-stimulated. 1 biological replicate was performed.

5 Discussion

TLRs are important in the immune response against infections, but may also play a role in cancer progression and metastases. Elevated expression of TLRs has been observed in multiple myeloma [24]. The aim of this master's thesis was to investigate the potential role of TLR4 and TLR9 activation in the viability and drug resistance of multiple myeloma cells, as well as to explore the underlying mechanisms that contribute to these effects.

5.1 No observed effect of TLR4 or TLR9 activation on the cell viability of MM.1S, AMO-1, and H929 MM cell lines.

Several studies have presented evidence regarding the expression of TLRs in MM cells, with TLR4 and TLR9 being the most prominently expressed receptors [24, 31]. Consequently, the MM cell lines MM.1S, AMO-1, and H929 were screened for TLR4 and TLR9 expression. The expression levels were generally low or absent, with Ct values $\geq$ 30 (**Table 4.1**), and exhibited minimal, statistically insignificant variation in response to LPS and CpG stimulation, as indicated by the fold change values (RQ) lying at around 1 (**Figure 4.1**). However, CpG stimulation led to a decrease, although statistically insignificant, in TLR4 mRNA expression in AMO-1 cells (RQ $\sim$ 0.5), implying a potential downregulation of TLR4 upon CpG stimulation, possibly due to cross-talk. Conversely, CpG stimulation resulted in a statistically insignificant increase in TLR9 mRNA expression in H929 cells (RQ $\sim$ 1.2), suggesting an upregulation of TLR9 upon CpG stimulation. The observed low expressions differ from other studies [46, 47]. However, this may be attributed to differences in cell lines and detection methods.

To determine the possible impact of these subtle changes in expression, the cell lines were subjected to LPS and CpG stimulation, followed by measurement of cell viability. Stimulation with LPS and CpG did not significantly affect the viability of MM.1S cells (**Figure 4.2**). This finding aligns with the moderate to high Ct values obtained for TLR4 (30, 31, and 30 for unstimulated, LPS-stimulated, and CpG-stimulated MM.1S cells, respectively) and TLR9 (35, 36, and 35 for unstimulated, LPS-stimulated, and CpG-stimulated MM.1S cells, respectively) (**Table 4.1**). The consistently moderate values indicate a low basal level of TLR4 and TLR9 mRNA expression in MM.1S cells that remains unaltered by stimulation.

In contrast, AMO-1 cell viability was affected by CpG stimulation at 48 hours (**Figure 4.3**). A significant increase in viability was observed at a concentration of 0.01 µM CpG, while viability remained relatively constant at lower and higher concentrations. This response suggests a dose-dependent effect with a bell-shaped dose-response curve. No significant difference was noted

for LPS-stimulated AMO-1 cells, although a slight increase in viability was observed at 0.01 µg/ml LPS. The Ct values for TLR4 and TLR9 in stimulated AMO-1 cells (36 for TLR4 and 31 for TLR9 in unstimulated, LPS-stimulated, and CpG-stimulated AMO-1 cells) did not differ from those of unstimulated cells. The fold change analysis (**Figure 4.1b**) also revealed no variation in TLR4 expression following LPS stimulation and no change in TLR9 expression following CpG stimulation.

Furthermore, H929 viability was affected by LPS stimulation at 24 hours (**Figure 4.4**). A significant decrease in cell viability was observed at a concentration of 1.0 µg/ml LPS, which was not evident at 48 hours. Similarly, CpG stimulation also led to a decrease in cell viability, albeit not statistically significant. These observations contrast with the Ct values obtained for TLR4 (34, 34, and 33 for unstimulated, LPS-stimulated, and CpG-stimulated H929 cells, respectively) and TLR9 (35, 34, and 34 for unstimulated, LPS-stimulated, and CpG-stimulated H929 cells, respectively) (**Table 4.1**), which did not vary significantly between stimulated and unstimulated samples. The fold change analysis (**Figure 4.1c**) indicated a slight increase in TLR9 expression in CpG-stimulated cells, while TLR4 expression in LPS-stimulated cells remained similar to the control.

Given the lack of substantial changes in cell viability resulting from TLR4 and TLR9 activation, further analysis of the cell lines was not pursued.

5.2 Increased viability of MM cell line RPMI8226 in response to TLR9 activation

In unpublished data from Tryggestad *et al.* it was shown that LPS and CpG stimulation increases the viability of RPMI8226 (**Figure 1.5**) [35]. To investigate if the increase in viability with CpG stimulation was dependent on TLR9 signaling, both wild-type RPMI8226 (WT) and TLR9 knockout (TLR9 KO) cell lines were subjected to stimulation with different concentrations of CpG, and the viability was measured. The viability of the WT cell line exhibited a significant increase as the concentration of CpG increased, while the viability of the TLR9 KO cell line decreased with higher CpG concentrations (**Figure 4.5**). Additionally, the viability of the WT cell line showed a progressive increase over time: +10% at 24 hours and +15% at 48 hours for the 1.0 µM CpG sample. These findings suggest a dose-dependent, time-dependent, and TLR9-dependent increase of viability in RPMI8226 cells in response to CpG stimulation.

5.3 Increased expression of pro-survival/anti-apoptotic factors in MM cell line RPMI8226 in response to TLR4 and TLR9 activation

To shed light on the mechanisms underlying the increased viability observed in TLR-activated RPMI8226 cells, an investigation was conducted into the protein expression of phosphorylated ERK1/2, Mcl-1, and Bcl-xL, which are known to be associated with pro-survival and anti-apoptotic processes, upon TLR activation. The expression levels of phosphorylated ERK1/2 exhibited significant upregulation in both LPS- and CpG-stimulated RPMI8226 cells, and this upregulation was observed to increase over time (**Figure 4.6a**). Activation of ERK1/2 is known to promote cell survival and viability through different mechanisms, including stimulating the expression of Bcl-xL and Mcl-1 [30, 48]. Furthermore, the expression of both Bcl-xL and Mcl-1 were observed to be significantly upregulated in response to LPS and CpG stimulation (**Figure 4.6b** and **Figure 4.6c**, respectively). Notably, a significant difference in expression was observed between the control and LPS- and CpG-stimulated samples for both Bcl-xL and Mcl-1 at 4 hours. At 24 hours, the expression level of stimulated cells remained unchanged while it had increased in the control cells to the level of the stimulated cells, which indicates a negative regulation of the anti-apoptotic signal.

These findings suggest that the observed cell viability in RPMI8226 cells may involve the MAPK signaling pathway, as depicted in **Figure 1.4**. However, further verification is necessary such as assessing the viability of RPMI8226 cells treated with MAPK inhibitors in combination with TLR stimulation.

5.4 TLR9-dependent reduction in bortezomib-sensitivity in RPMI8226 cells

Building upon the observation that the viability of RPMI8226 cells is dependent on TLR9 in response to CpG stimulation, an investigation was conducted to determine whether CpG stimulation could influence the bortezomib-sensitivity of RPMI8226, and if the mediation of drug-sensitivity is attributed to TLR9 signaling. In this experiment, RPMI8226 WT and TLR9 KO cells were pre-stimulated with CpG and subsequently treated with varying concentrations of bortezomib, with the percentage of viable cells measured.

In both unstimulated and CpG-stimulated WT and TLR9 KO cells, there was a decrease in the percentage of viable cells with increasing doses of bortezomib (**Figure 4.8a** and **Figure 4.8b**, respectively). However, a significant difference was observed between the unstimulated and CpG-stimulated WT cells at 8 nM bortezomib, with reduced cell death of the stimulated

cells, and a similar trend was observed for the other doses. In contrast to the WT cell line, no significant difference was found between the CpG-stimulated and unstimulated TLR9 KO cells with the viability decreasing due to bortezomib treatment, supporting that the observed effect was TLR9-dependent.

At a dose of 12 nM bortezomib, the concentration became excessively strong, leading to general cell death. Consequently, no large difference was observed between the unstimulated and CpG-stimulated WT cells at 12 nM. In the initial experiment, a concentration of 16 nM was used instead of 6 nM, resulting in complete cell death. Consequently, gating during data analysis became challenging (**Figure III.1**), which may have contributed to the seemingly significant difference between unstimulated and CpG-stimulated WT cells. At 6 nM, no significant difference was observed. However, conducting a third biological replicate at this concentration could potentially yield a significant difference between the unstimulated and stimulated WT cells, given the visible difference between the two samples.

Collectively, these findings suggest that the activation of TLR9 renders the RPMI8226 cell line less sensitive to bortezomib.

5.5 Altered expression of surface receptors in MM cell line RPMI8226 in response to TLR4 and TLR9 activation

Based on the aforementioned findings, an investigation was conducted to examine whether the activation of TLR4 and TLR9 induces any alterations in the surface expression of plasma cell markers BCMA, CD138, and CD38 in MM cell lines RPMI8226 (including TLR9 KO and WT) and ANBL-6. Subsequently, the cell lines were stimulated with LPS and CpG, and the expression levels of the biomarkers were assessed.

The expression of BCMA in RPMI8226 (**Figure 4.9**) was significantly different between the unstimulated and LPS- and CpG-stimulated samples. Notably, BCMA expression was downregulated in LPS- and CpG-stimulated cells at both 24 and 48 hours (not significant for LPS at 48 hours). Similarly, BCMA expression in the WT cell line (**Figure 4.10a** and **Figure 4.11a**) decreased in CpG-stimulated cells, whereas the TLR9 KO cell line (**Figure 4.10b** and **Figure 4.11b**) demonstrated a small increase in BCMA expression upon CpG stimulation. A comparison of BCMA expression between TLR9 KO and WT is presented in **Figure 4.12**. These results suggest that the activation of TLR9 leads to the downregulation of the BCMA marker in RPMI8226. BCMA is primarily expressed in plasmablasts and plasma cells, and is overexpressed and activated in MM. Thus, BCMA serves as a therapeutic target for MM [12, 17]. The downregulation of BCMA in TLR9-activated RPMI8226 suggests that the BCMA-targeted

treatments may not be effective in MM patients during infections.

The expression of CD138 in RPMI8226 (**Figure 4.9**) decreased in LPS- and CpG-stimulated cells at both 24 and 48 hours, although not with statistical significance. CD138 expression in the CpG-stimulated WT cell line decreased at 24 hours and then unexpectantly increased at 48 hours (**Figure 4.10a** and **Figure 4.11a**, respectively). In contrast, the CpG-stimulated TLR9 KO cell line demonstrated an increase in CD138 expression at both 24 and 48 hours (**Figure 4.10b** and **Figure 4.11b**, respectively). A comparison of CD138 expression between TLR9 KO and WT is presented in **Figure 4.13**. The small increase in CD138 expression in the WT cell line at 48 hours might be inconclusive due to the experiment only having been performed once. Conducting at least three biological replicates could potentially yield results similar to those observed in the RPMI8226 cell line. Overall, these findings suggest that the decrease in CD138 expression observed in CpG-stimulated RPMI8226 cells is dependent on TLR9. CD138 is upregulated during the maturation of plasma cells, serving as a marker for terminally differentiated plasma cells [14, 15]. The observed decrease in CD138 expression may indicate that when MM cells are infected, they become more immature. Studies have observed that more immature MM cells have a higher proliferative potential [15, 16]. Since CD138 is a plasma cell marker considered for novel treatments [15], its efficacy would be compromised if MM cells become immature and lose this marker.

The expression of CD38 exhibited a decrease after 48 hours in both LPS- and CpG-stimulated RPMI8226 cells (**Figure 4.9**). Surprisingly, in CpG-stimulated WT cells, the CD38 expression remained similar to the control (**Figure 4.11a**), while in CpG-stimulated TLR9 KO cells, it increased after 48 hours (**Figure 4.11b**). It was anticipated that the CD38 expression in the CpG-stimulated WT cell line would respond similarly to that of the CpG-stimulated RPMI8226 cells. Further experimentation is required to validate these results.

The viability of the ANBL-6 cell line has been previously observed to increase following LPS stimulation [34]. To investigate the expression of plasma cell markers under LPS stimulation, the levels of BCMA, CD138, and CD38 on ANBL-6 cells were examined (**Figure 4.15**). No significant difference was observed in the expression levels of BCMA, CD138, or CD38 on ANBL-6 cells upon LPS stimulation. BCMA expression remained constant in LPS-stimulated cells, while both CD138 and CD38 exhibited a slight increase at 24 hours before decreasing at 48 hours. Even though increased viability has been observed, no similar changes in BCMA, CD138, or CD38 as in RPMI8226 were observed. This may be due to differences in downstream signaling between the two MM cell lines.

5.6 Decreased expression of trimethylated K27 and K36 on histone H3 in a TLR9-dependent manner

The study further aimed to investigate whether LPS and CpG stimulation resulted in alterations in epigenetic modifications. MM cell line RPMI8226 was subjected to LPS and CpG stimulation, and cell lines TLR9 KO and WT were subjected to CpG stimulation, and the expression of specific histone modifications on histone H3, including trimethylated lysine 4, 27, and 36 (H3K4Me3, H3K27Me3, and H3K36Me3), and acetylated 9 and 27 (H3K9Ac and H3K27Ac), was measured.

The expression of H3K27Me3 and H3K36Me3 (**Figure 4.16a** and **Figure 4.16b**, respectively) exhibited similar patterns in the RPMI8226 and WT cell lines, with a decrease observed in the LPS- and CpG-stimulated RPMI8226 cells, and in the CpG-stimulated WT cells. There was also a decrease in the TLR9 KO cell line, although the decrease in CpG-stimulated cells was less pronounced compared to CpG-stimulated RPMI8226 and WT cells. These findings suggest that CpG stimulation can lead to changes in the trimethylation of H3K27 and H3K36 mediated by TLR9 signaling.

As mentioned in the introduction (see **Section 1.3**), H3K27 is associated with gene silencing, while H3K36 is associated with gene activation. H3K27Me3 recruits a gene silencer called PRC1, which suppresses gene expression by compacting chromatin and rendering the promoter region inaccessible [49]. The demethylation of H3K27 leads to chromatin-opening and accessibility of the promoter region, and has been observed to play a role in the dysregulation of transcriptional tumor suppressor genes [49]. Based on the results in this study, it is possible that CpG stimulation and TLR9 signaling may activate H3K27 demethylases, which could contribute to the observed increase in viability. However, further research is warranted, such as treating CpG-stimulated RPMI8226 cells with H3K27 demethylase inhibitors.

H3K36 is a well-established marker associated with gene activation. The observed decrease in H3K36Me3 expression, coupled with the increased viability resulting from LPS and CpG stimulation in RPMI8226 cells, suggests a potential involvement of H3K36Me3 in the activation of tumor suppressors within these cells. Notably, previous studies have reported the upregulation of H3K36Me3 demethylases in various cancer types, which further supports the notion of H3K36Me3 serving as a tumor suppressor marker [50]. Consequently, the stimulation with LPS and CpG in RPMI8226 cells may lead to the downregulation of the H3K36Me3 modification, subsequently resulting in a reduction in the activation of tumor suppressors. However, further investigation is necessary to elucidate this relationship.

No discernible changes were observed in the expression of 3HK4Me3, 3HK9Ac, and 3HK27Ac

(**Figure 4.16c**, **Figure 4.16d**, and **Figure 4.16e**, respectively). Although further experimentation is required to confirm these findings, it appears that the expression of these markers is unlikely to be dependent on TLR9 activation.

Histone modifications have been implicated in cellular differentiation and the development of cancer. Alterations in these modifications can disrupt gene expression patterns, potentially influencing the onset and progression of cancer [51]. In the current study, TLR stimulation was found to decrease the expression of trimethylated H3K27 and H3K36, accompanied by a decrease in the expression of BCMA and CD138 biomarkers. The observed decrease in 3HK27Me3 (a repressive marker) and 3HK36Me3 (an active marker) may trigger the activation or suppression of specific genes, which could possibly affect the expression of BCMA and CD138, resulting in their downregulation. To further investigate these findings, particularly considering that BCMA and CD138 are targets for anti-myeloma drugs, replication of the experiment is necessary to determine the significance of the observed changes. Additionally, assessing the expression levels of demethylases specific to H3K27 and H3K36 would provide valuable insights into the potential involvement of demethylation in the observed decrease in H3K27Me3 and H3K36Me3 expression. If it is determined that demethylases contribute to the decreased expression, measuring the expression of BCMA and CD138 during TLR stimulation while treating the cells with H3K27Me3 and H3K36Me3 demethylase inhibitors would be informative. Moreover, evaluating the expression of proteins responsible for activating the trimethylation of H3K27 and H3K36 during TLR stimulation would enhance the understanding of the underlying mechanisms governing the changes in histone modifications. These investigations would provide a more comprehensive understanding of the effects of TLR stimulation on histone modifications, gene expression, and the downstream implications for BCMA and CD138 expression.

It is important to note that this experiment was performed with only one biological replication, and therefore, the significance of these differences remains uncertain. Further investigations are necessary to provide more comprehensive insights into the relationship between epigenetic modifications and the observed changes in viability and expression of biomarkers following LPS and CpG stimulation.

6 Conclusion

The objective of this master's thesis was to investigate the impact and underlying mechanisms of TLR4 and TLR9 activation on viability and sensitivity to anti-cancer drugs in multiple myeloma cells. The viability of myeloma cell lines AMO-1, MM.1S, and H929 did not exhibit a significant increase following stimulation with TLR4 agonist LPS or TLR9 agonist CpG. In contrast, previous studies have reported increased viability in the RPMI8226 cell line, which was found in this study to be TLR9-dependent. Stimulation of RPMI8226 cells with LPS and CpG resulted in elevated protein expression levels of phosphorylated ERK1/2, Bcl-xL, and Mcl-1, known pro-survival and anti-apoptotic factors. This suggests that ERK1/2 likely plays a central role in the observed increased viability of RPMI8226 cells. Additionally, the reduced sensitivity of RPMI8226 cells to the anti-cancer drug bortezomib was found to be TLR9-dependent, as demonstrated by the increased viability of the WT cell line compared to the TLR9 KO cell line. Stimulation of RPMI8226 cells with CpG also led to changes in the surface expression of plasma cell biomarkers BCMA and CD138, with a decrease in their expression levels, potentially attributed to TLR9 activation. Finally, a TLR9-dependent reduction in histone modifications, specifically trimethylated lysine 27 and 36 on histone H3, was observed. These findings suggest a potential influence that infection has on the effectiveness of commonly used anti-myeloma drugs and highlight the significance of conducting experiments using patient cells.

Bibliography

1. Kumar S. Multiple Myeloma. Vol. 1. New York: Demos Medical, 2010 :197–9
2. Kreftregisteret. Årsrapport 2021 - Resultater og forbedringstiltak fra Nasjonalt kvalitetsregister for lymfoide maligniteter. [Online]. Available from: https://www.kreftregisteret.no/globalassets/publikasjoner-og-rapporter/arsrapporter/publisert-2022/arsrapport-2021-nasjonalt-kvalitetsregister-for-lymfoide-maligniteter.pdf. [Accessed 14th December 2022]
3. Pinto V, Bergantim R, Caires HR, Seca H, Guimaraes JE and Vasconcelos H. Multiple Myeloma: Available Therapies and Causes of Drug Resistance. Cancers 2020; 12. DOI: 10.3390/cancers12020407
4. Kalambokis GN, Christou L and Tsianos EV. Multiple myeloma presenting with an acute bacterial infection. International journal of laboratory hematology 2009; 31(4):375–83. DOI: 10.1111/j.1751-553X.2009.01154.x
5. Blimark C, Holmberg E, Mellqvist UH, Landgren O, Björkholm M, Hultcrantz M and *et al*. Multiple myeloma and infections: a population-based study on 9253 multiple myeloma patients. Haematologica 2015; 100(1):107–13. DOI: 10.3324/haematol.2014.107714
6. Nucci M and Anaissie E. Infections in patients with multiple myeloma in the era of high-dose therapy and novel agents. Clinical Infectious Diseases 2009; 49(8):1211–25. DOI: 10.1086/605664
7. Child JA, Morgan GJ, Davies FE, Owen RG, Bell SE, Hawkins K and *et al*. High-dose chemotherapy with hematopoietic stem-cell rescue for multiple myeloma. The New England Journal of Medicine 2003; 348(19):1875–83. DOI: 10.1056/NEJMoa022340
8. McBride A and Ryan PY. Proteasome inhibitors in the treatment of multiple myeloma. Expert Review of Anticancer Therapy 2013; 13(3):339–58. DOI: 10.1586/era.13.9
9. Tellier J and Nutt SL. Standing out from the crowd: How to identify plasma cells. European Journal of Immunology 2017; 47. DOI: 10.1002/eji.201747168
10. Flores-Montero J, Tute R, Paiva B, Perez JJ, Böttcher S, Wind H and *et al.* Immunophenotype of normal vs. myeloma plasma cells: Toward antibody panel specifications for MRD detection in multiple myeloma. Cytometry Part B: Clinical Cytometry 2015; 90. DOI: 10.1002/cyto.b.21265
11. Sanz I, Wei C, Jenks SA, Cashman KS, Tipton C, Woodruff MC and *et al.* Challenges and Opportunities for Consistent Classification of Human B Cell and Plasma Cell Populations. Frontiers in Immunology 2019; 10. DOI: 10.3389/fimmu.2019.02458

12. Yu B, Jiang T and Liu D. BCMA-targeted immunotherapy for multiple myelomal. Journal of Hematology Oncology 2020; 13. DOI: 10.1186/s13045-020-00962-7

13. Gozzetti A, Ciofini S, Simoncelli M, Santoni A, Pacelli P, Raspadori D and *et al.* Anti CD38 monoclonal antibodies for multiple myeloma treatment. Human Vaccines and Immunotherapeutics 2022; 18. DOI: 10.1080/21645515.2022.2052658

14. McCarron MJ, Park PW and Fooksman DR. CD138 mediates selection of mature plasma cells by regulating their survival. Blood 2017; 129. DOI: 10.1182/blood-2017-01-761643

15. Kawano Y, Fujiwara S, Wada N, Izaki M, Yuki H, Okuno Y and *et al*. Multiple myeloma cells expressing low levels of CD138 have an immature phenotype and reduced sensitivity to lenalidomide. International Journal of Oncology 2012; 41. DOI: 10.3892/ijo.2012.1545

16. Reid S, Yang S, Brown S, Kabani K, Aklilu E, Ho PJ and *et al.* Characterisation and relevance of CD138-negative plasma cells in plasma cell myeloma. International Journal of Laboratory Hematology 2010; 32. DOI: 10.1111/j.1751-553X.2010.01222.x

17. Yu B, Jiang T and Liu D. B-cell maturation antigen (BCMA) in multiple myeloma: rationale for targeting and current therapeutic approaches. Leukemia 2020; 34. DOI: 10.1038/s41375-020-0734-z

18. Centers for Disease Control and Prevention. What is Epigenetics? [Online]. Available from: https://www.cdc.gov/genomics/disease/epigenetics.htm#:~:text=Epigenetics%20is%20the%20study%20of,body%20reads%20a%20DNA%20sequence.. [Accessed 21st May 2023]

19. Zhang L, Lu Q and Chang C. Epigenetics in Health and Disease. Advances in Experimental Medicine and Biology 2020; 1253. DOI: 10.1007/978-981-15-3449-2_1

20. Zhang Y, Sun Z, Jia J, Du T, Zhang N, Tang Y and *et al.* Overview of Histone Modification. Advances in Experimental Medicine and Biology 2021; 1283. DOI: 10.1007/978-981-15-8104-5_1

21. Stokes BA, Yadav S, Shokal U, Smith LC and Eleftherianos I. Bacterial and fungal pattern recognition receptors in homologous innate signaling pathways of insects and mammals. Frontiers in Microbiology 2015; 6:19. DOI: 10.3389/fmicb.2015.00019

22. Takeuchi O and Akira S. Pattern Recognition Receptors and Inflammation. Cell 2010; 140(6):805–20. DOI: 10.1016/j.cell.2010.01.022

23. Kawasaki T and Kawai T. Toll-Like Receptor Signaling Pathways. Frontiers in Immunology 2014; 5:461. DOI: 10.3389/fimmu.2014.00461

24. Akesolo O, Buey B, Beltrán-Visiedo M, Giraldos D, Marzo I and Latorre E. Toll-like receptors: New targets for multiple myeloma treatment? Biochemical Pharmacology 2022; 199:114992. DOI: 10.1016/j.bcp.2022.114992

25. Park MH and Hong JT. Roles of NF-κB in Cancer and Inflammatory Diseases and Their Therapeutic Approaches. Cells 2016; 5(2):15. DOI: 10.3390/cells5020015

26. Kawai T and Akira S. The role of pattern-recognition receptors in innate immunity: update on Toll-like receptors. Nature Immunology 2010; 11:373–84. DOI: 10.1038/ni.1863

27. O'Neill LAJ, Golenbock D and Bowie AG. The history of Toll-like receptors — redefining innate immunity. Nature Reviews Immunology 2013; 13:453–60. DOI: 10.1038/nri3446

28. Duan T, Du Y, Xing C, Wang HY and Wang RF. Toll-Like Receptor Signaling and Its Role in Cell-Mediated Immunity. Frontiers in Immunology 2022; 13. DOI: 10.3389/fimmu.2022.812774

29. Asl ER, Amini M, Najafi S, Mansoori B, Mokhtarzadeh A, Mohammadi A and *et al.* Interplay between MAPK/ERK signaling pathway and MicroRNAs: A crucial mechanism regulating cancer cell metabolism and tumor progression. Life Sciences 2021; 278. DOI: 10.1016/j.lfs.2021.119499

30. Ullah R, Yin Q, Snell AH and Wan L. RAF-MEK-ERK pathway in cancer evolution and treatment. Seminars in Cancer Biology 2022; 85. DOI: 10.1016/j.semcancer.2021.05.010

31. Bohnhorst J, Rasmussen T, Moen SH, Fløttum M, Knudsen L, Børset M and *et al*. Toll-like receptors mediate proliferation and survival of multiple myeloma cells. Leukemia 2006; 20(6):1138–44. DOI: 10.1038/sj.leu.2404225

32. Xu Y, Zhao Y, Huang H, Chen G, Wu X, Wang Y, Chang W, Zhu Z, Feng Y and Wu D. Expression and function of toll-like receptors in multiple myeloma patients: toll-like receptor ligands promote multiple myeloma cell growth and survival via activation of nuclear factor-B. British journal of Haematology 2010; 150(5):543–53. DOI: 10.1111/j.1365-2141.2010.08284.x

33. Ntoufa S, Vilia MG, Stamatopoulos K, Ghia P and Muzio M. Toll-like receptors signaling: A complex network for NF-κB activation in B-cell lymphoid malignancies. Seminars in Cancer Biology 2016; 39. DOI: 10.1016/j.semcancer.2016.07.001

34. Ørning NEH. The cell survival and proliferation of multiple myeloma cell line ANBL-6 increase in a Toll-Like Receptor 4 dependent manner in response to LPS. Specialization project, NTNU 2022

35. Tryggestad SS and *et al.* [Unpublished data]. NTNU 2022

36. Aass KR, Tryggestad SS, Mjelle R, Kastnes MH, Nedal TMV, Misund K and Standal T. IL-32 is induced by activation of toll-like receptors in multiple myeloma cells. Frontiers in Immunology 2023; 14. DOI: 10.3389/fimmu.2023.1107844

37. Hannah R, Beck M, Moravec R and Riss T. CellTiter-Glo Luminescent Cell Viability Assay: A Sensitive and Rapid Method for Determining Cell Viability. Promega: Cell Notes. 2001; (2).

38. Thermo Fisher Scientific. Overview of Western Blotting. [Online]. Available from: https://www.thermofisher.com/no/en/home/life-science/protein-biology/protein-biology-learning-center/protein-biology-resource-library/pierce-protein-methods/overview-western-blotting.html. [Accessed 10th December 2022]

39. GE Healthcare Life Sciences. Western Blotting - Principles and Methods. [Online]. Available from: https://static.fishersci.eu/content/dam/fishersci/en_EU/promotions/GEHealthcareLifeSciences/Western_Blotting_Handbook.pdf. [Accessed 10th December 2022]

40. Bradford MM. A Rapid and Sensitive Method for the Quantitation of Microgram Quantities of Protein Utilizing the Principle of Protein-Dye Binding. Analytical Biochemistry 1976; 72:248–54. DOI: 10.1006/abio.1976.9999

41. Life Technologies. Real-time PCR handbook. [Online]. Available from: https://www.gene-quantification.de/real-time-pcr-handbook-life-technologies-update-flr.pdf. [Accessed 25th February 2023]

42. Applied Biosystems. Introduction to Gene Expression: GETTING STARTED GUIDE. [Online]. Available from: https://assets.thermofisher.com/TFS-Assets/LSG/manuals/4454239_IntrotoGeneEx_GSG.pdf. [Accessed 25th February 2023]

43. QIAGEN. RNeasy® Mini Handbook. [Online]. Available from: https://www.qiagen.com/us/resources/resourcedetail?id=14e7cf6e-521a-4cf7-8cbc-bf9f6fa33e24&lang=en. [Accessed 20th February 2023]

44. Alizada G, Kiraz Y, Baran Y and Nalbant A. Flow cytometry: basic principles and applications. Critical Reviews in Biotechnology 2017; 37:163–76. DOI: 10.3109/07388551.2015.1128876

45. McKinnon K. Flow Cytometry: An Overview. Critical Reviews in Biotechnology 2018; 120. DOI: 10.1002/cpim.40

46. Bao H, Lu P, Li Y, Wang L, Li H, He D and *et al*. Triggering of toll-like receptor-4 in human multiple myeloma cells promotes proliferation and alters cell responses to immune and chemotherapy drug attack. Cancer Biology and Therapy 2011; 11. DOI: 10.4161/cbt.11.1.13878

47. Abdi J, Mutis T, Garssen J and Redegeld F. Characterization of the Toll-like Receptor Expression Profile in Human Multiple Myeloma Cells. PloS One 2013; 8. DOI: 10.1371/journal.pone.0060671

48. Hideshima T and Anderson K. Signaling Pathway Mediating Myeloma Cell Growth and Survival. Cancers 2021; 13. DOI: 10.3390/cancers13020216

49. Abu-Hanna J, Patel JA, Anastasakis E, Cohen R, Clapp LH, Loizidou M and *et al.* Therapeutic potential of inhibiting histone 3 lysine 27 demethylases: a review of the literature. Clinical Epigenetics 2022; 14. DOI: 10.1186/s13148-022-01305-8

50. Xiao C, Fan T, Tian H, Zheng Y, Zhou Z, Li S and *et al.* H3K36 trimethylation-mediated biological functions in cancer. Clinical Epigenetics 2021; 13. DOI: 10.1186/s13148-021-01187-2

51. Yang Y, Zhang M and Wang Y. The roles of histone modifications in tumorigenesis and associated inhibitors in cancer therapy. Journal of the National Cancer Center 2022; 2. DOI: 10.1016/j.jncc.2022.09.002

Appendix

An example of how the calculations in **Section 3.2** were calculated, the reagent/kit list, gating performed in the AnnexinV PI experiments, and histogram plots of BCMA/CD138/CD38 experiments are found in **Appendix I**, **Appendix II**, **Appendix III**, and **Appendix IV**, respectively.

I Calculations

Feeding and stimulating of all multiple myeloma cells were done under sterile conditions, in a sterile laminar flow hood cleaned with both water and 70% ethanol. All equipment used in the hood was also sterile.

Stimulating MM cells: detailed calculations example

An example of how RPMI8226 multiple myeloma cells were stimulated for a western blot experiment is described in detail, including calculations, in this section.

Wished to stimulate RPMI8226 cells with medium as a control, 0.1 µg/mL LPS, and 1.0 µM CpG in 3 wells, and end up with a total of $1.0 \cdot 10^6$ cells in each well. Each well could contain 3 mL total, so 2.8 mL of cells and 200 µL of LPS and CpG solution were chosen. Since 1:15 (in concentration) of LPS and CpG to cells was chosen, 15X LPS and 15X CpG solutions had to be made.

Transferred 30 mL total of RPMI8226 from culture flask containing $5 \cdot 10^6$ cells to a new 50 mL tube. The tube was then centrifuged at 20°C, 448 RCF, for 5 minutes. The supernatant was discarded, and 1 mL of a new medium (RPMI, 10% FCS) was added to the tube. The cells were then counted by adding 20 µL of cell solution to 10 mL of isotone and measuring using the instrument Coulter Counter. The result was an average of $5.684 \cdot 10^6$ cells/mL. Since $1.0 \cdot 10^6$ cells were wanted per well, and there was 2.8 mL cell solution, one ended up with 357 000 cells/mL. Calculation of needed volume of cells needed to make 2.8 mL for three wells plus extra (10 mL) was then performed:

$$C_1 \cdot V_1 = C_2 \cdot V_2$$

$$5.684 \cdot 10^6 \text{cells/mL} \cdot x = 0.357 \cdot 10^6 \text{cells/mL} \cdot 10\,\text{mL}$$

$$x = \frac{0.357 \cdot 10^6 \text{cells/mL} \cdot 10\,\text{mL}}{5.684 \cdot 10^6 \text{cells/mL}} = 0.628\,\text{mL}$$

$$10\,\text{mL} - 0.628\,\text{mL} = 9.372\,\text{mL}$$

0.628 mL of cell solution was transferred to a new 50 mL tube containing 9.372 mL medium. 2.8 mL of this solution was then pipetted into each of the three wells and incubated at 37°C supplied with 5% CO_2.

Calculations for 0.1 µg/mL (0.2 mL) of LPS were performed, when started with LPS stock solution of 5 mg/mL that was diluted 1:100;

$$\frac{5\,\text{mg/mL}}{100} = 0.05\,\text{mg/mL} = 50\,\mu\text{g/mL}$$

$$1.0\,\mu\text{g/mL} \cdot 15\text{X} = 15\,\mu\text{g/mL}$$

Here, it is multiplied by 15 due to wanting a 15X LPS solution.

$$15\,\mu\text{g/mL} \cdot 0.2\,\text{mL} = 50\,\mu\text{g/mL} \cdot x$$

$$x = \frac{15\,\mu\text{g/mL} \cdot 0.2\,\text{mL}}{50\,\mu\text{g/mL}} = 0.06\,\text{mL} = 60\,\mu\text{L}$$

$$0.2\,\text{mL} - 0.06\,\text{mL} = 0.14\,\text{mL} = 140\,\mu\text{L}$$

Transferred 60 µL of 1:100 LPS solution to a new tube, and combined with 140 µL medium. Then, the solution was mixed. Since a 0.1 µg/mL solution was wanted, and wanted 200 µL total, 20 µL was transferred from the newly made 1.0 µg/mL solution to a new tube containing 180 µL to make a 0.1 µg/mL solution;

$$\frac{200\,\mu\text{L}}{10} = 20\,\mu\text{L}$$

$$200\,\mu\text{L} - 20\,\mu\text{L} = 180\,\mu\text{L}$$

These calculations were performed for 1.0 µM CpG as well, with a stock solution of 500 µM.

The different LPS and CpG concentrations, and medium, were then added separately to the three wells (200 µL). The plates were then incubated for 4 and 24 hours.

II Reagent/kit list

Table II.1 shows all the reagents and kits used in the project, and their manufacturers and catalogue numbers.

Table II.1: Reagents and kits used in this project

Reagent/kit	**Manufacturer**	**Catalogue number**
Cell culture		
RPMI 1640	Sigma Aldrich, St. Louise, MO, USA	R8758
Fetal bovine serum (FCS)	Invitrogen, Carlsbad, CA, USA	10082147
L-Glutamine	Sigma Aldrich, St. Louise, MO, USA	G7513
Recombinant human IL-6	Gibco, Thermo Fisher Scientific, Waltham, USA	PHC0061
2-Mercaptoethanol	Gibco, Thermo Fisher Scientific, Waltham, USA	21985023
Sodium pyruvate	Gibco, Thermo Fisher Scientific, Waltham, USA	11360070
TLR agonists		
LPS-EB Ultrapure	Invivogen, San Diego, CA, USA	tlrl-3-pelps
CpG ODN 2006	TIBMolBiol, Berlin, Germany	1712649
RT-qPCR		
RNeasy® Mini kit	Qiagen, Hilden, Germany	74104
RNeasy® Micro kit	Qiagen, Hilden, Germany	740004
RNase free DNase set	Qiagen, Hilden, Germany	79256
High-capacity RNA-to-cDNA kit	Applied Biosystems, Carlsbad, CA, USA	4387406
TaqMan^{TM} Universal PCR Master Mix	Thermo Fisher Scientific, Waltham, MA, USA	4304437

Continued on next page

Table II.1: Reagents and kits used in this project (Continued)

Reagent/kit	**Manufacturer**	**Catalogue number**
TaqMan® Gene expression assay		
Human TLR4	Thermo Fisher Scientific, Waltham, MA, USA	Hs00152939_m1
Human TLR9	Thermo Fisher Scientific, Waltham, MA, USA	Hs00152973_m1
Human TBP	Thermo Fisher Scientific, Waltham, MA, USA	Hs00427620_m1
Human IL-8	Thermo Fisher Scientific, Waltham, MA, USA	Hs00174103_m1
Western blot		
IGEPAL CA-360 (NP-40)	Sigma Aldrich, St. Louise, MO, USA	I18896
NaCl	Merck, New Jersey, USA	1.06404.1000
Tris-HCl	Sigma Aldrich, St. Louise, MO, USA	T5941
NaF	Sigma Aldrich, St. Louise, MO, USA	201154
Sodium orthovanadate (Na_3VO_4)	Sigma Aldrich, St. Louise, MO, USA	450243
iBlot^{TM}2 Transfer Stacks, nitrocellulose, mini	Invitrogen, Carlsbad, CA, USA	IB23002
iBlot^{TM}2 Transfer Stacks, nitrocellulose, regular size	Invitrogen, Carlsbad, CA, USA	IB23001
Dithiothreitol (DTT)	PanReach AppliChem, Darmstadt, Germany	A3668-0050
Bradford reagent	Sigma Aldrich, St. Louise, MO, USA	B6916
NuPAGE^{TM} 4-12% Bis-Tris Gel 1.0 mm x 10 well	Thermo Fisher Scientific, Waltham, MA, USA	NP0321BOX

Continued on next page

Table II.1: Reagents and kits used in this project (Continued)

Reagent/kit	**Manufacturer**	**Catalogue number**
NuPAGE^{TM} 4-12% Bis-Tris Gel 1.0 mm x 20 well	Thermo Fisher Scientific, Waltham, MA, USA	WG1402BOX
NuPAGE^{TM} LDS Sample Buffer (4X)	Thermo Fisher Scientific, Waltham, MA, USA	NP0007
SeeBluePlus2 Pre-stained Protein Standard	Invitrogen, Carlsbad, CA, USA	LC5925
MagicMark^{TM} XP standard	Invitrogen, Carlsbad, CA, USA	LC5602
NuPAGE^{TM} MES Running Buffer (4X)	Thermo Fisher Scientific, Waltham, MA, USA	NP0002
Bovine serum albumine (BSA)	Thermo Fisher Scientific, Waltham, MA, USA	23209
Super Signal West Femto Maxium Sensitivity	Thermo Fisher Scientific, Waltham, MA, USA	34095
Anti-β-actin	Sigma Aldrich, St. Louise, MO, USA	A2066
Anti-GAPDH	Abcam, Cambridge, UK	ab8245
Anti-Lamin B	Abcam, Cambridge, UK	ab133741
Anti-ERK1/2 (p44/42 MAPK)	Cell Signaling Technology, Danvers, MA, USA	4695s
Anti-p-ERK1/2 (pho-p44/42 MAPK)	Cell Signaling Technology, Danvers, MA, USA	4370
Anti-Mcl-1	Santa Cruz Biotechnology, Dallas, TX, USA	A0815
Anti-Bcl-xL	Cell Signaling Technology, Danvers, MA, USA	2762
Anti-Tri-Methyl-Histone H3 (Lys27)	Cell Signaling Technology, Danvers, MA, USA	9733
Anti-Tri-Methyl-Histone H3 (Lys36)	Cell Signaling Technology, Danvers, MA, USA	4909

Continued on next page

Table II.1: Reagents and kits used in this project (Continued)

Reagent/kit	**Manufacturer**	**Catalogue number**
Anti-Tri-Methyl-Histone H3 (Lys4)	Cell Signaling Technology, Danvers, MA, USA	9751
Anti-Acetyl-Histone H3 (Lys9)	Cell Signaling Technology, Danvers, MA, USA	9649
Anti-Acetyl-Histone H3 (Lys27)	Cell Signaling Technology, Danvers, MA, USA	8173
Polyclonal Goat Anti-rabbit Immunoglobulin/HRP	Dako, Glostrup, Denmark	E0432
CTG assay		
CellTiter-Glo® Luminescent Cell viability assay	Promega, Madison, WI, USA	G7573
Anti-cancer drugs		
Bortezomib	Selleck Chemicals, Houston, TX, USA	PS-341
Flow cytometry		
10X Binding Buffer	Invitrogen, Carlsbad, CA, USA	BB21001
Annexin A5-FITC	Invitrogen, Carlsbad, CA, USA	FI21001
Propidium iodide (PI)	Invitrogen, Carlsbad, CA, USA	P16063
CD38 (HB-7) PE-Cy7	BD Biosciences, Franklin Lakes, New Jersey, USA	335825
FITC Mouse Anti-Human CD138	BD Biosciences, Franklin Lakes, New Jersey, USA	552723
APC anti-human CD269 (BCMA)	BioLegend, San Diego, CA, USA	357506
eBioscience^{TM} Fixable Viability Dye eFluor^{TM} 450	Invitrogen, Carlsbad, CA, USA	65-0863-14
OneComp eBeads	Invitrogen, Carlsbad, CA, USA	01-1111-42
Dulbecco's Phosphate Buffered Saline	Thermo Fisher Scientific, Waltham, MA, USA	D8537

Continued on next page

Table II.1: Reagents and kits used in this project (Continued)

Reagent/kit	**Manufacturer**	**Catalogue number**
Dexamethasone (DMSO)	Sigma Aldrich, St. Louise, MO, USA	D2915

III Flow sheets - AnnexinV PI

Gating for the AnnexinV PI experiments is shown in **Figure III.1** (experiment performed March 8th), **Figure III.2** (experiment performed April 10th), and **Figure III.3** (experiment performed April 12th).

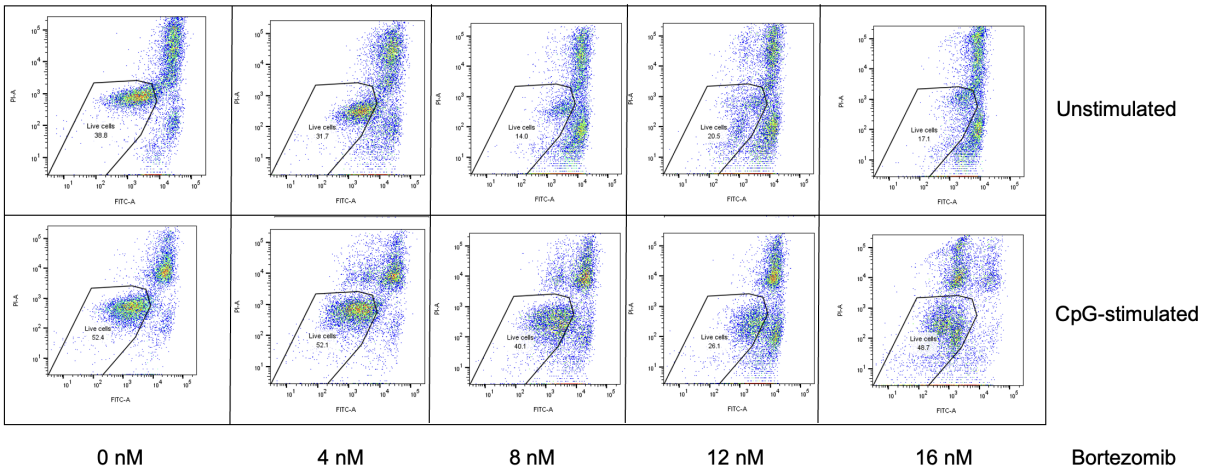

(a) RPMI8226 WT cell line

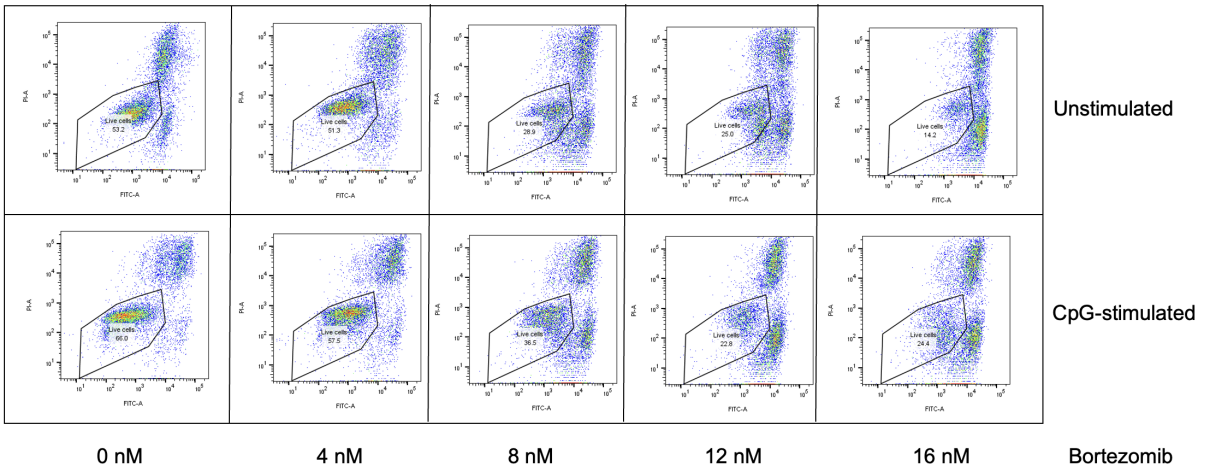

(b) RPMI8226 TLR9 KO cell line

Figure III.1: Gating of the MM cell lines RPMI8226 WT and TLR9 KO stimulated with TLR9 agonist CpG, and treated with different concentrations of proteasome inhibitor bortezomib, for experiment N20230308. Figures **(a)** and **(b)** illustrate the gating of the WT and KO cell lines, respectively, for the different samples: untreated cells (control and CpG-stimulated), and unstimulated and CpG-stimulated cells treated with 4, 6, 8, and 12 nM bortezomib. AnnexinV (FITC) is plotted on the x-axis while PI is plotted on the y-axis.

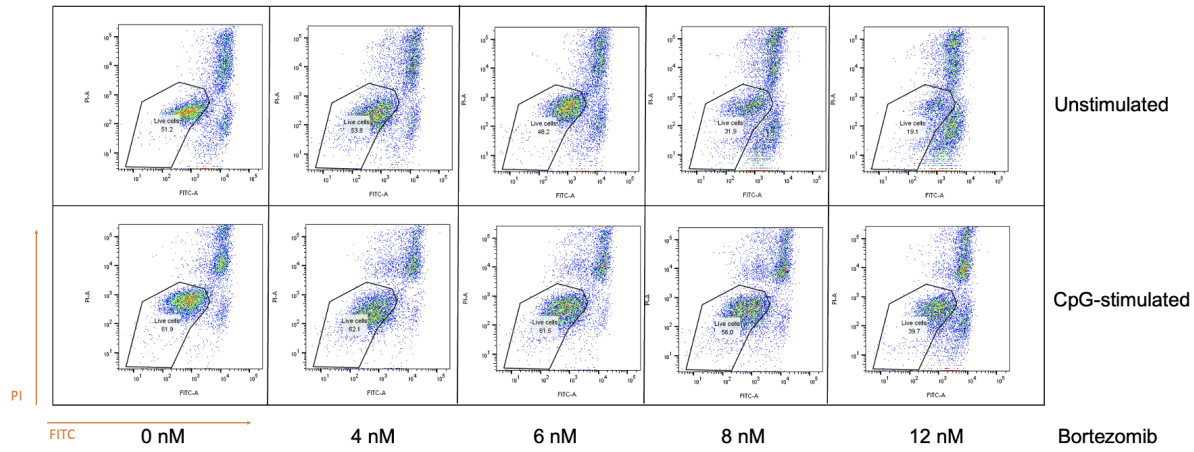

(a) RPMI8226 WT cell line

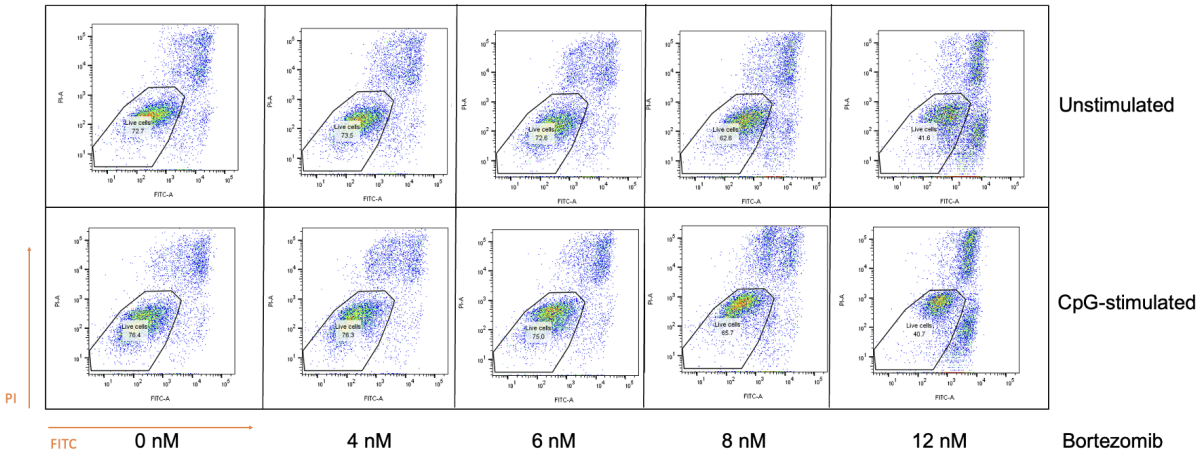

(b) RPMI8226 TLR9 KO cell line

Figure III.2: Gating of the MM cell lines RPMI8226 WT and TLR9 KO stimulated with TLR9 agonist CpG, and treated with different concentrations of proteasome inhibitor bortezomib, for experiment N20230410. Figures **(a)** and **(b)** illustrate the gating of the WT and KO cell lines, respectively, for the different samples: untreated cells (control and CpG-stimulated), and unstimulated and CpG-stimulated cells treated with 4, 6, 8, and 12 nM bortezomib. AnnexinV (FITC) is plotted on the x-axis while PI is plotted on the y-axis.

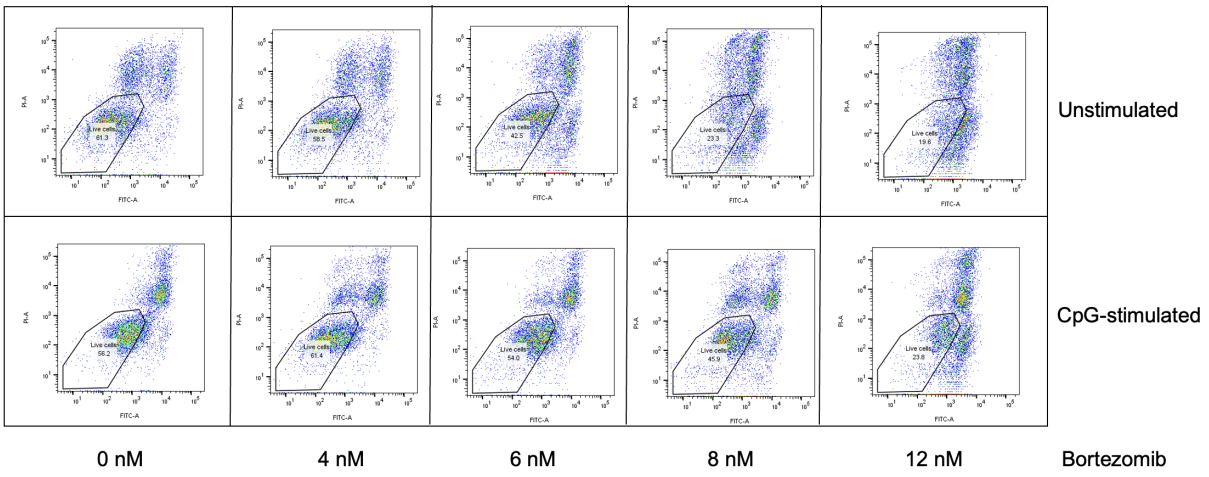

(a) RPMI8226 WT cell line

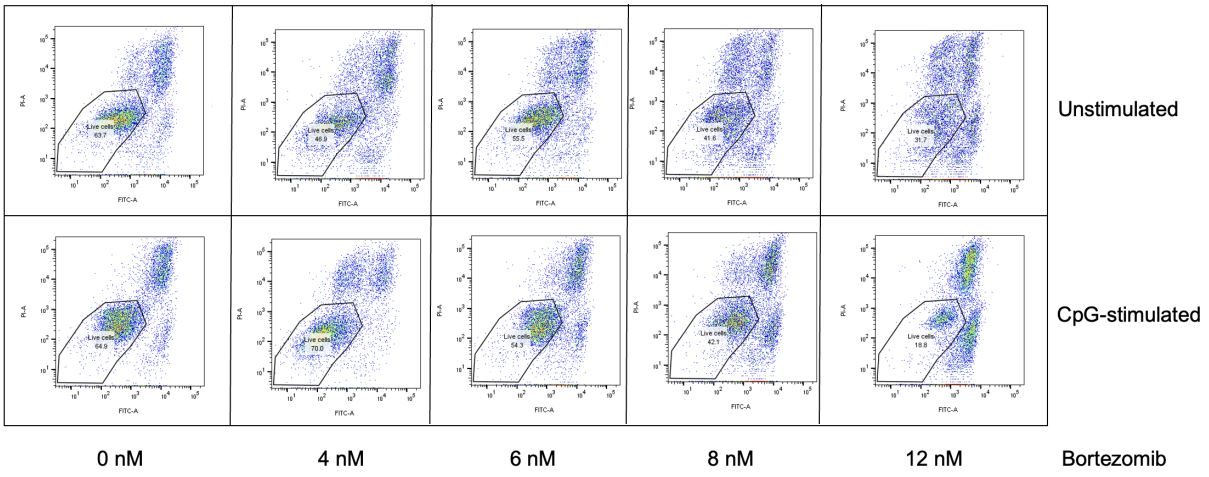

(b) RPMI8226 TLR9 KO cell line

Figure III.3: Gating of the MM cell lines RPMI8226 WT and TLR9 KO stimulated with TLR9 agonist CpG, and treated with different concentrations of proteasome inhibitor bortezomib, for experiment N20230412. Figures **(a)** and **(b)** illustrate the gating of the WT and KO cell lines, respectively, for the different samples: untreated cells (control and CpG-stimulated), and unstimulated and CpG-stimulated cells treated with 4, 6, 8, and 12 nM bortezomib. AnnexinV (FITC) is plotted on the x-axis while PI is plotted on the y-axis.

IV Flow sheets - CD38/CD138/BCMA

Histograms depicting the flow cytometry experiment examining the alteration in the expression of plasma cell biomarkers BCMA, CD138, and CD38, as influenced by LPS and CpG stimulation, are presented in **Figures IV.1-IV.8**. These figures correspond to the following: **Figure IV.1** shows the histogram for the RPMI8226 cell line on March 15, 2023; **Figure IV.2** displays the histogram for the ANBL-6 cell line on March 15, 2023; **Figure IV.3** shows the histogram for the RPMI8226 cell line on April 20, 2023; **Figure IV.4** shows the histogram for the ANBL-6

cell line on April 20, 2023; **Figure IV.5** displays the histogram for the RPMI8226 cell line on April 24, 2023; **Figure IV.6** shows the histogram for the TLR9 KO cell line on April 24, 2023; **Figure IV.7** displays the histogram for the WT cell line on April 24, 2023; and **Figure IV.8** shows the histogram for the ANBL-6 cell line on April 24, 2023.

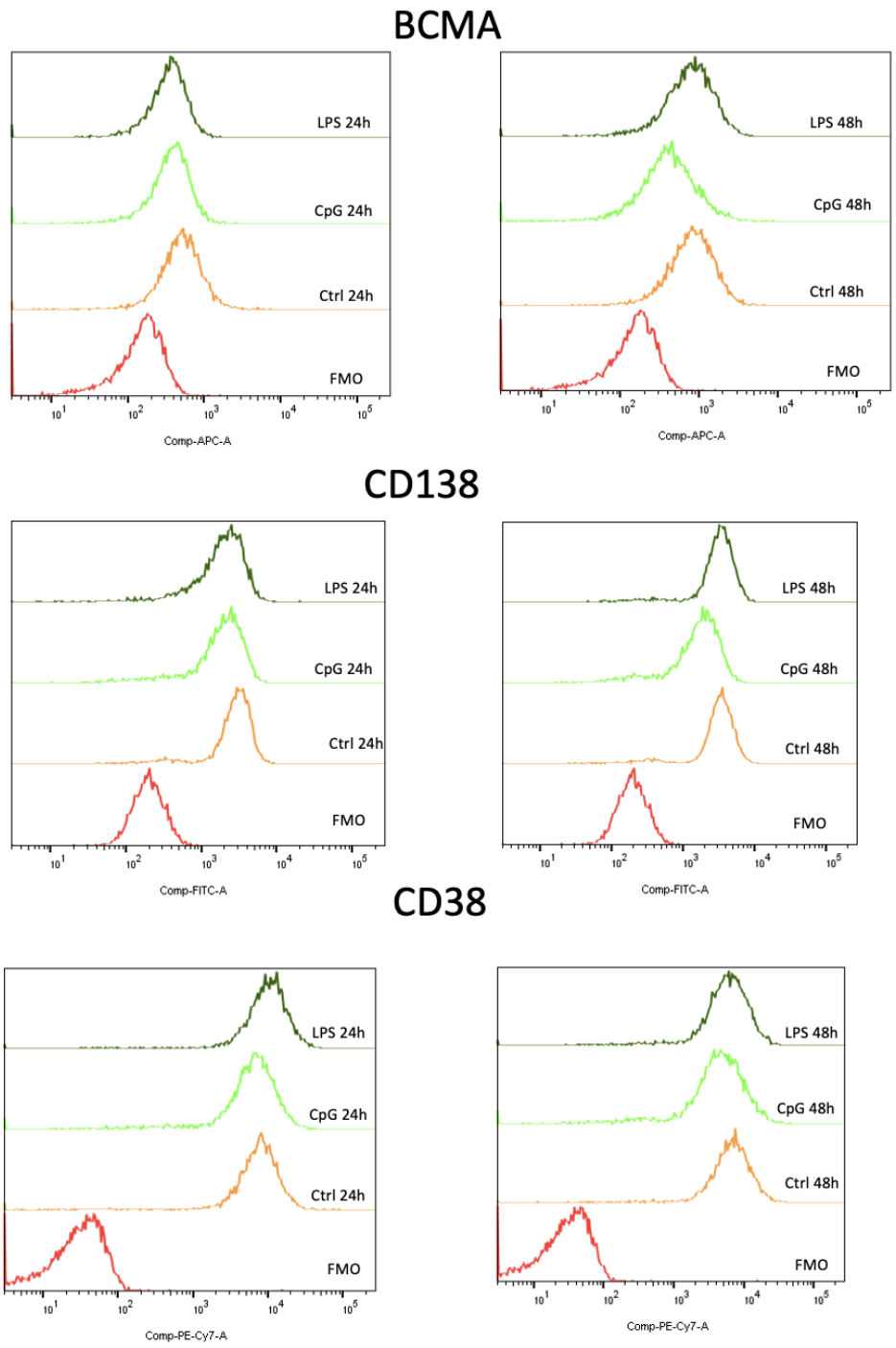

Figure IV.1: The flow cytometry results for experiment N20230315 examined the expression of receptors BCMA, CD138, and CD38 on the MM cell line RPMI8226 following stimulation with TLR4 agonist LPS and TLR9 agonist CpG. The top two figures depict the alterations in the expression of surface receptor BCMA, the middle two figures illustrate CD138 alterations, and the bottom two figures represent CD38 alterations. These figures showcase the changes observed in RPMI8226 cells when stimulated with LPS and CpG over a period of 24 and 48 hours.

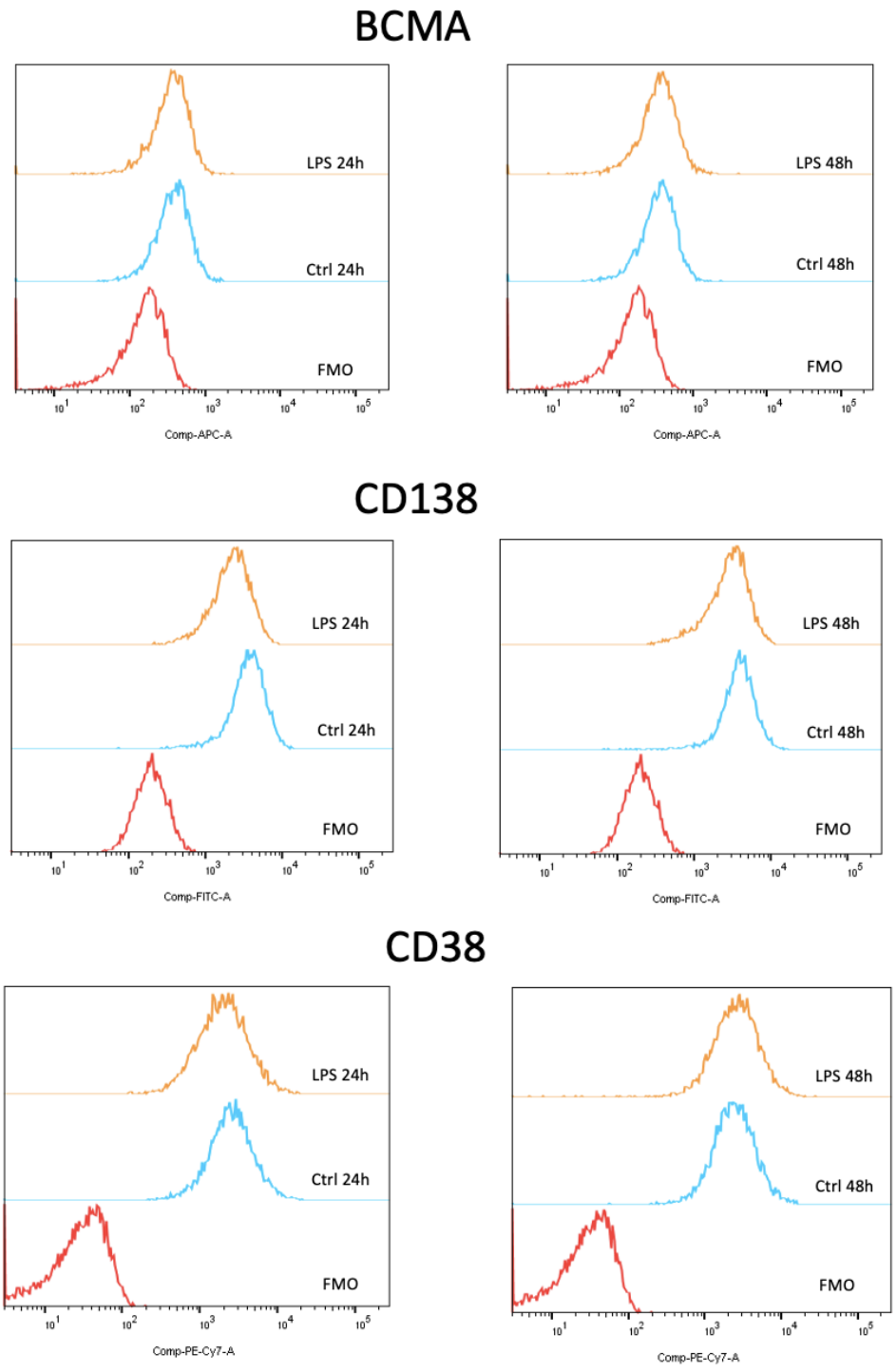

Figure IV.2: The flow cytometry results for experiment N20230315 examined the expression of receptors BCMA, CD138, and CD38 on the MM cell line ANBL-6 following stimulation with TLR4 agonist LPS. The top two figures depict the alterations in the expression of surface receptor BCMA, the middle two figures illustrate CD138 alterations, and the bottom two figures represent CD38 alterations. These figures showcase the changes observed in ANBL-6 cells when stimulated with LPS over a period of 24 and 48 hours.

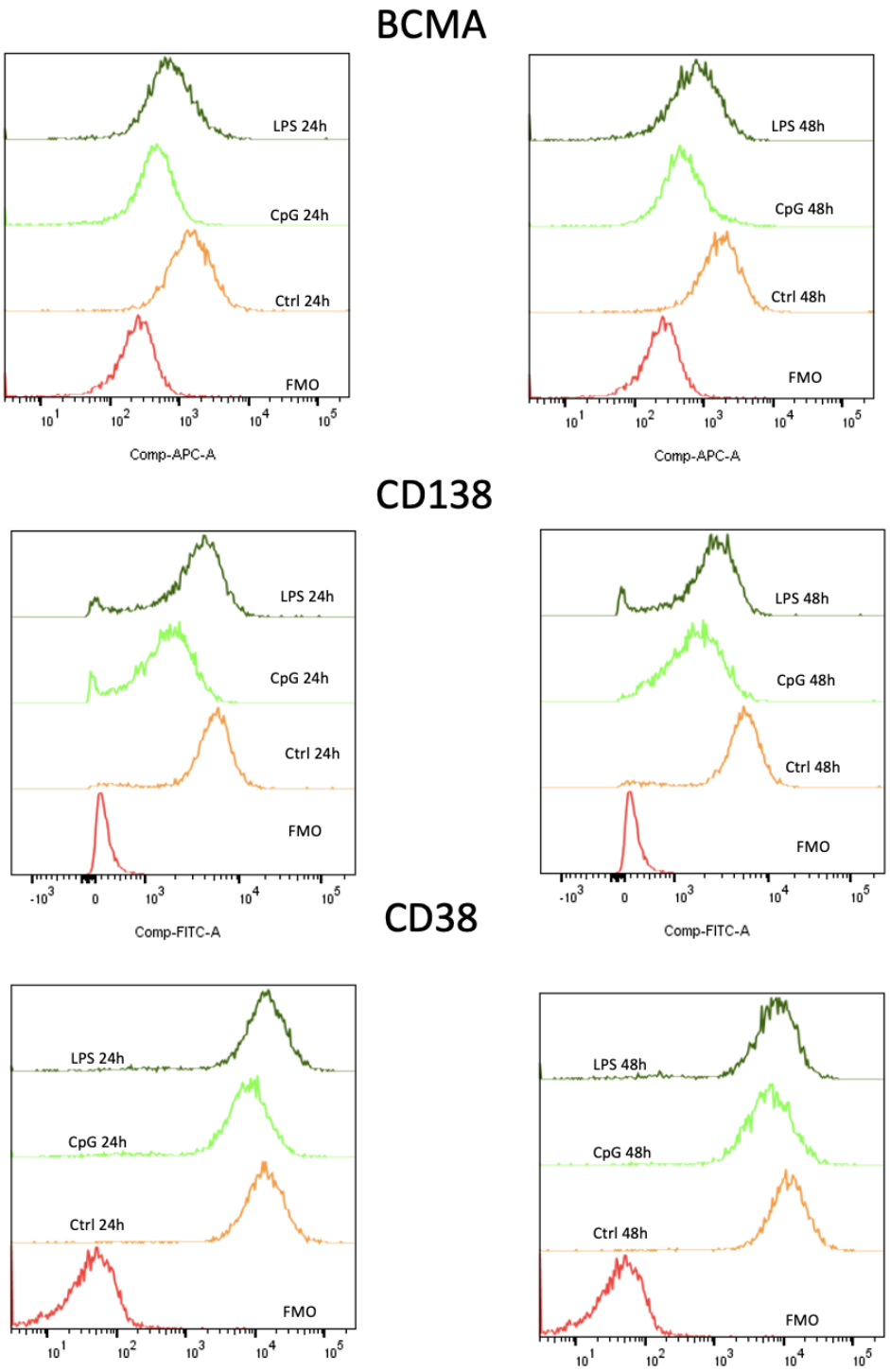

Figure IV.3: The flow cytometry results for experiment N20230420 examined the expression of receptors BCMA, CD138, and CD38 on the MM cell line RPMI8226 following stimulation with TLR4 agonist LPS and TLR9 agonist CpG. The top two figures depict the alterations in the expression of surface receptor BCMA, the middle two figures illustrate CD138 alterations, and the bottom two figures represent CD38 alterations. These figures showcase the changes observed in RPMI8226 cells when stimulated with LPS and CpG over a period of 24 and 48 hours.

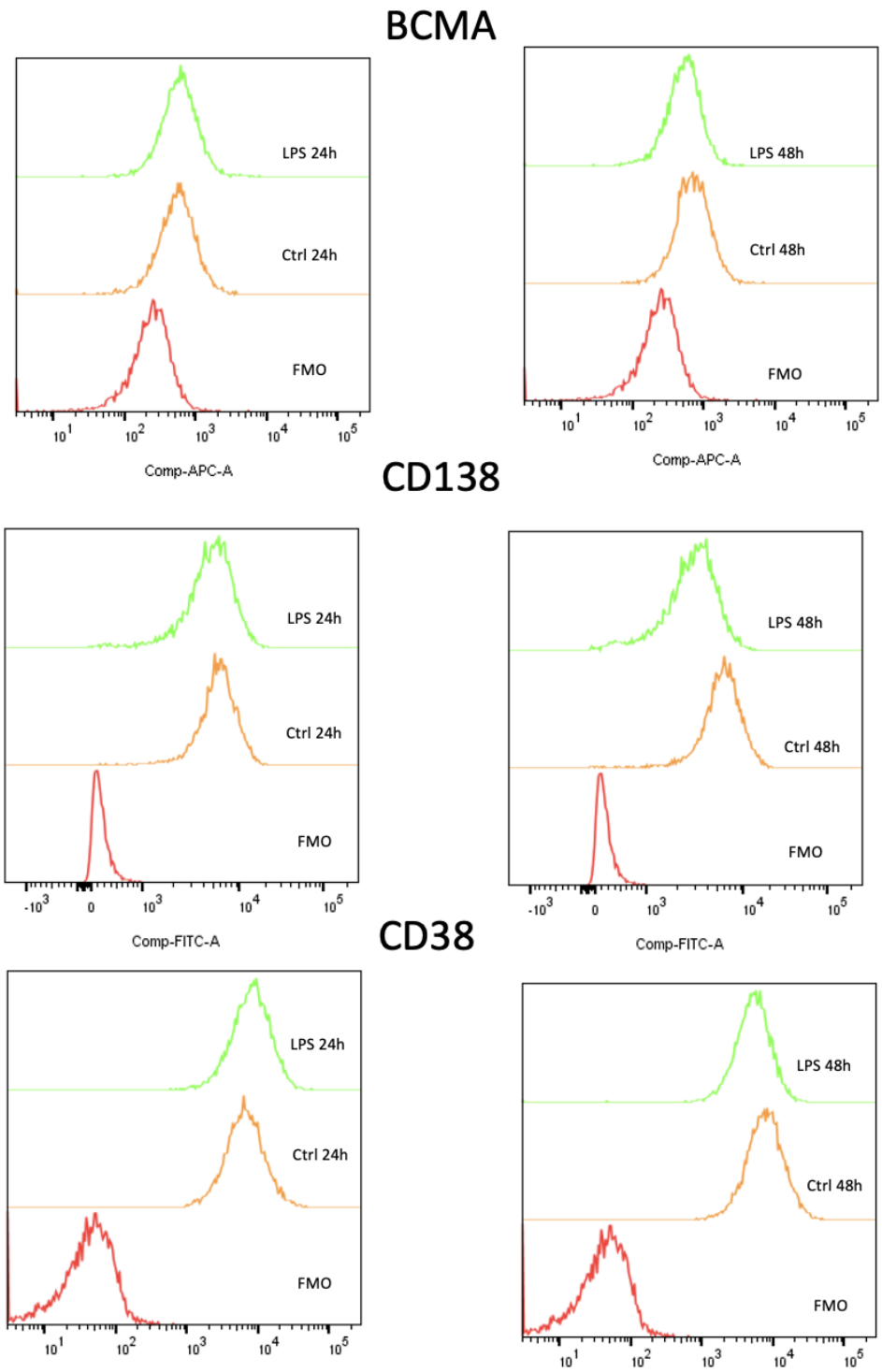

Figure IV.4: The flow cytometry results for experiment N20230420 examined the expression of receptors BCMA, CD138, and CD38 on the MM cell line ANBL-6 following stimulation with TLR4 agonist LPS. The top two figures depict the alterations in the expression of surface receptor BCMA, the middle two figures illustrate CD138 alterations, and the bottom two figures represent CD38 alterations. These figures showcase the changes observed in ANBL-6 cells when stimulated with LPS over a period of 24 and 48 hours.

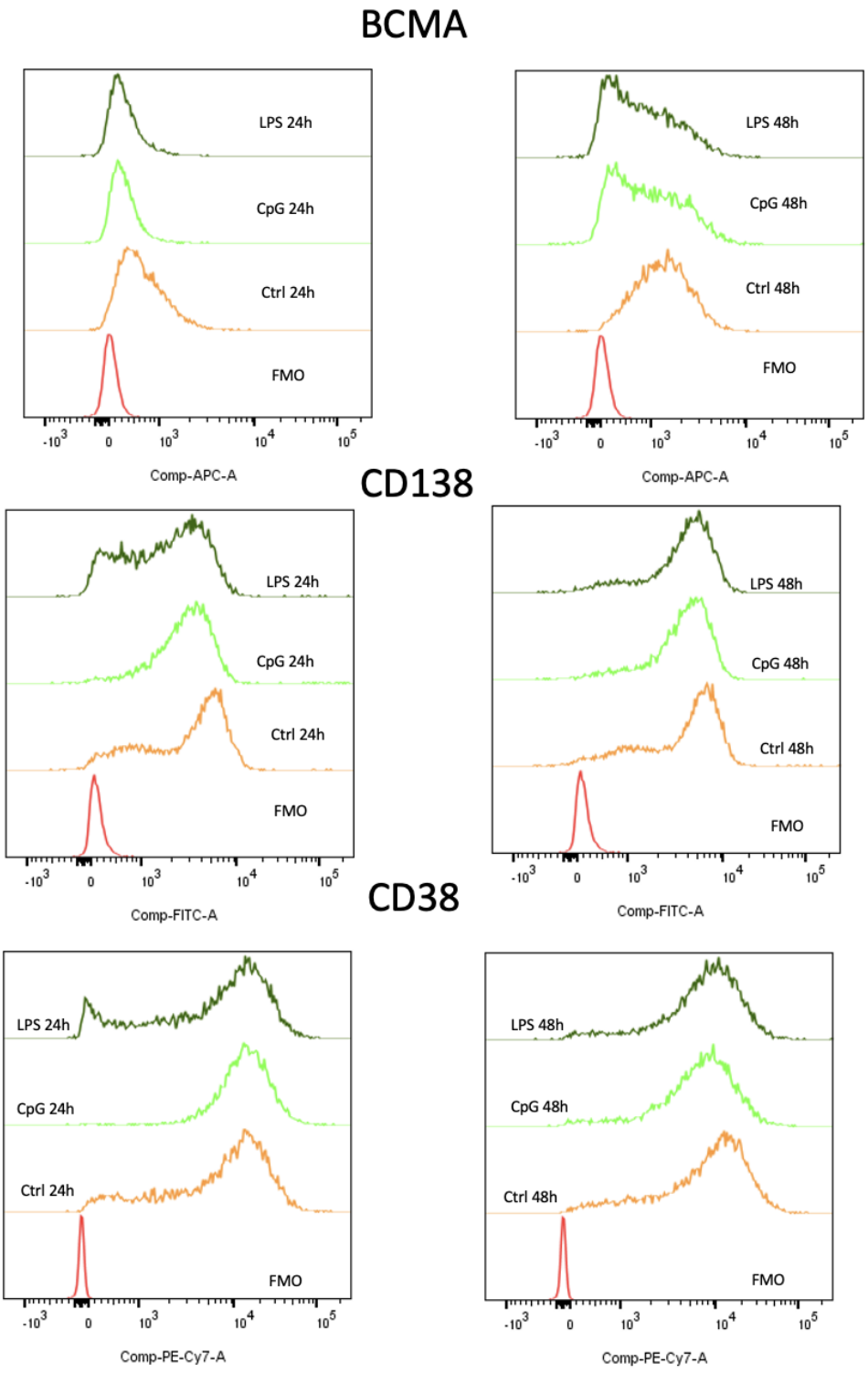

Figure IV.5: The flow cytometry results for experiment N20230424 examined the expression of receptors BCMA, CD138, and CD38 on the MM cell line RPMI8226 following stimulation with TLR4 agonist LPS and TLR9 agonist CpG. The top two figures depict the alterations in the expression of surface receptor BCMA, the middle two figures illustrate CD138 alterations, and the bottom two figures represent CD38 alterations. These figures showcase the changes observed in RPMI8226 cells when stimulated with LPS and CpG over a period of 24 and 48 hours.

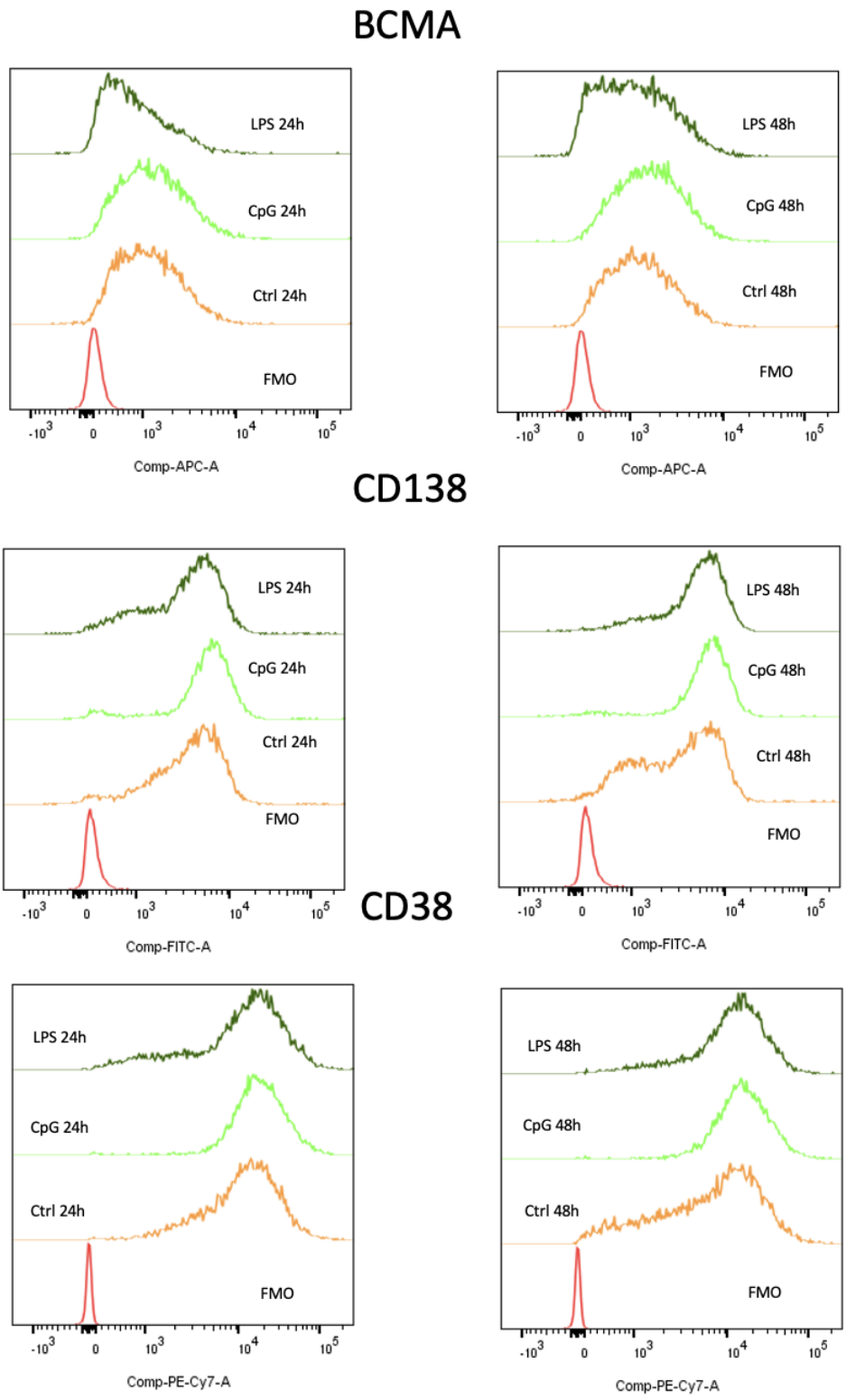

Figure IV.6: The flow cytometry results for experiment N20230424 examined the expression of receptors BCMA, CD138, and CD38 on the MM cell line RPMI8226 TLR9 KO following stimulation with TLR4 agonist LPS and TLR9 agonist CpG. The top two figures depict the alterations in the expression of surface receptor BCMA, the middle two figures illustrate CD138 alterations, and the bottom two figures represent CD38 alterations. These figures showcase the changes observed in TLR9 KO cells when stimulated with LPS and CpG over a period of 24 and 48 hours.

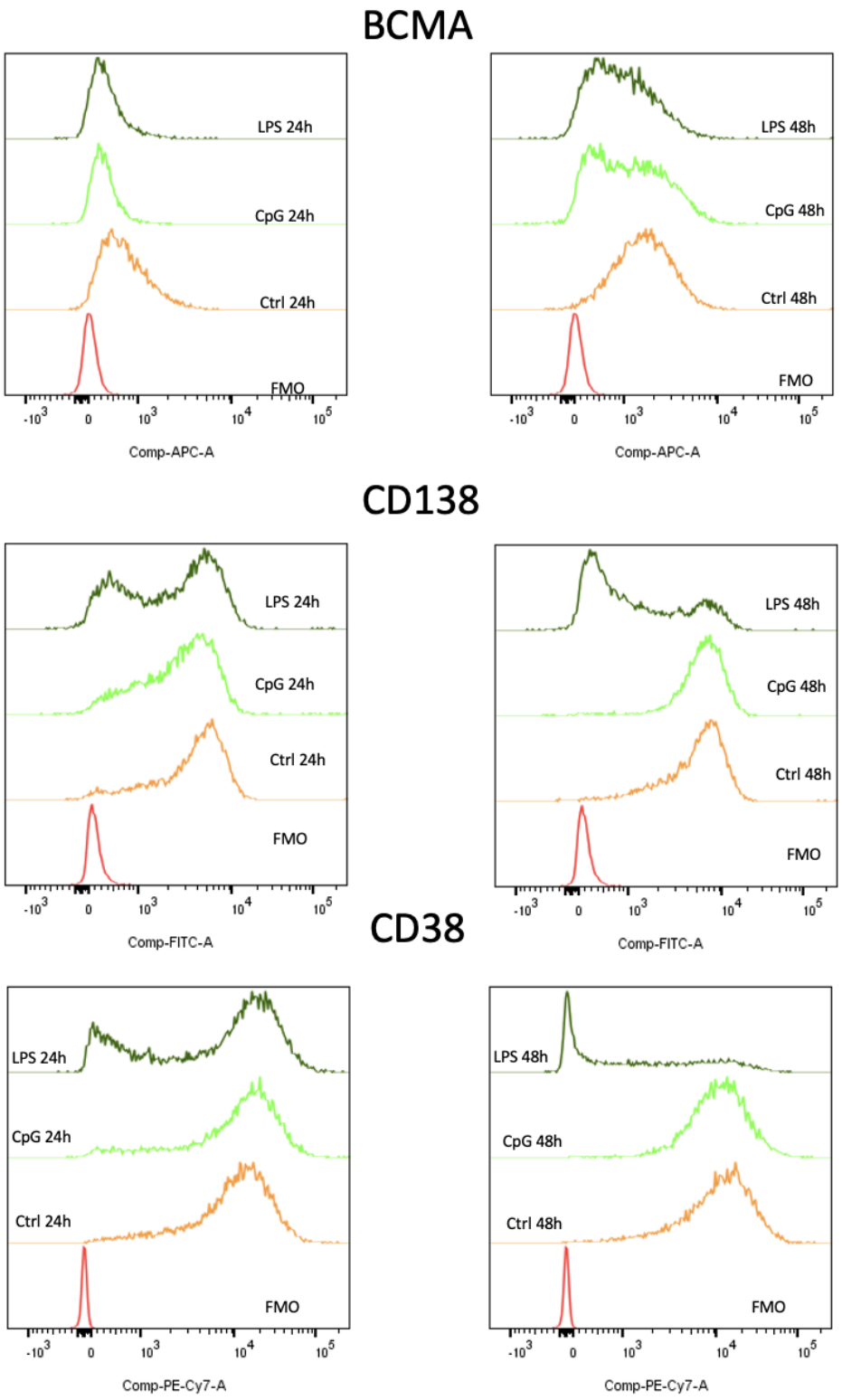

Figure IV.7: The flow cytometry results for experiment N20230424 examined the expression of receptors BCMA, CD138, and CD38 on the MM cell line RPMI8226 WT following stimulation with TLR4 agonist LPS and TLR9 agonist CpG. The top two figures depict the alterations in the expression of surface receptor BCMA, the middle two figures illustrate CD138 alterations, and the bottom two figures represent CD38 alterations. These figures showcase the changes observed in WT cells when stimulated with LPS and CpG over a period of 24 and 48 hours.

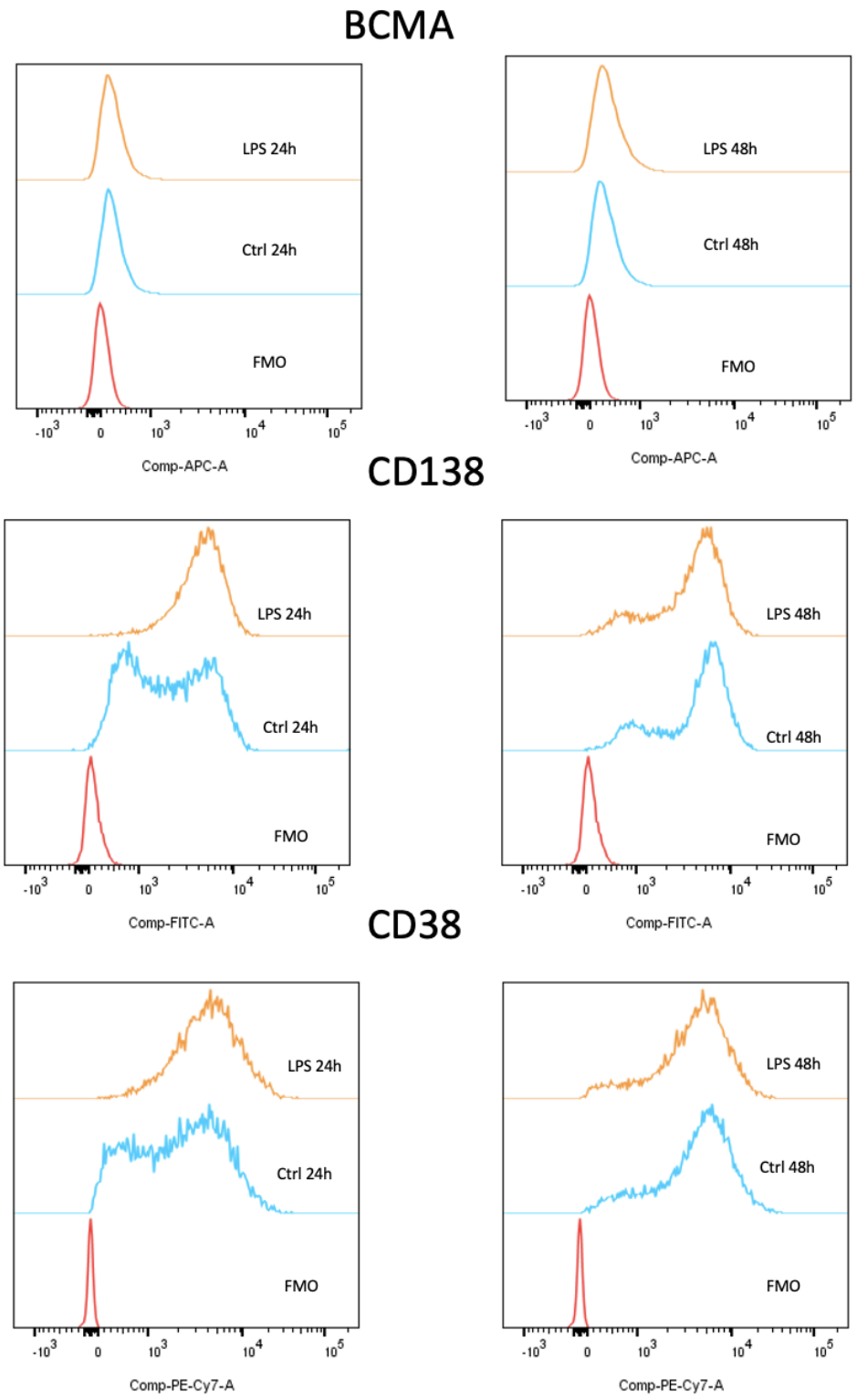

Figure IV.8: The flow cytometry results for experiment N20230424 examined the expression of receptors BCMA, CD138, and CD38 on the MM cell line ANBL-6 following stimulation with TLR4 agonist LPS. The top two figures depict the alterations in the expression of surface receptor BCMA, the middle two figures illustrate CD138 alterations, and the bottom two figures represent CD38 alterations. These figures showcase the changes observed in ANBL-6 cells when stimulated with LPS over a period of 24 and 48 hours.

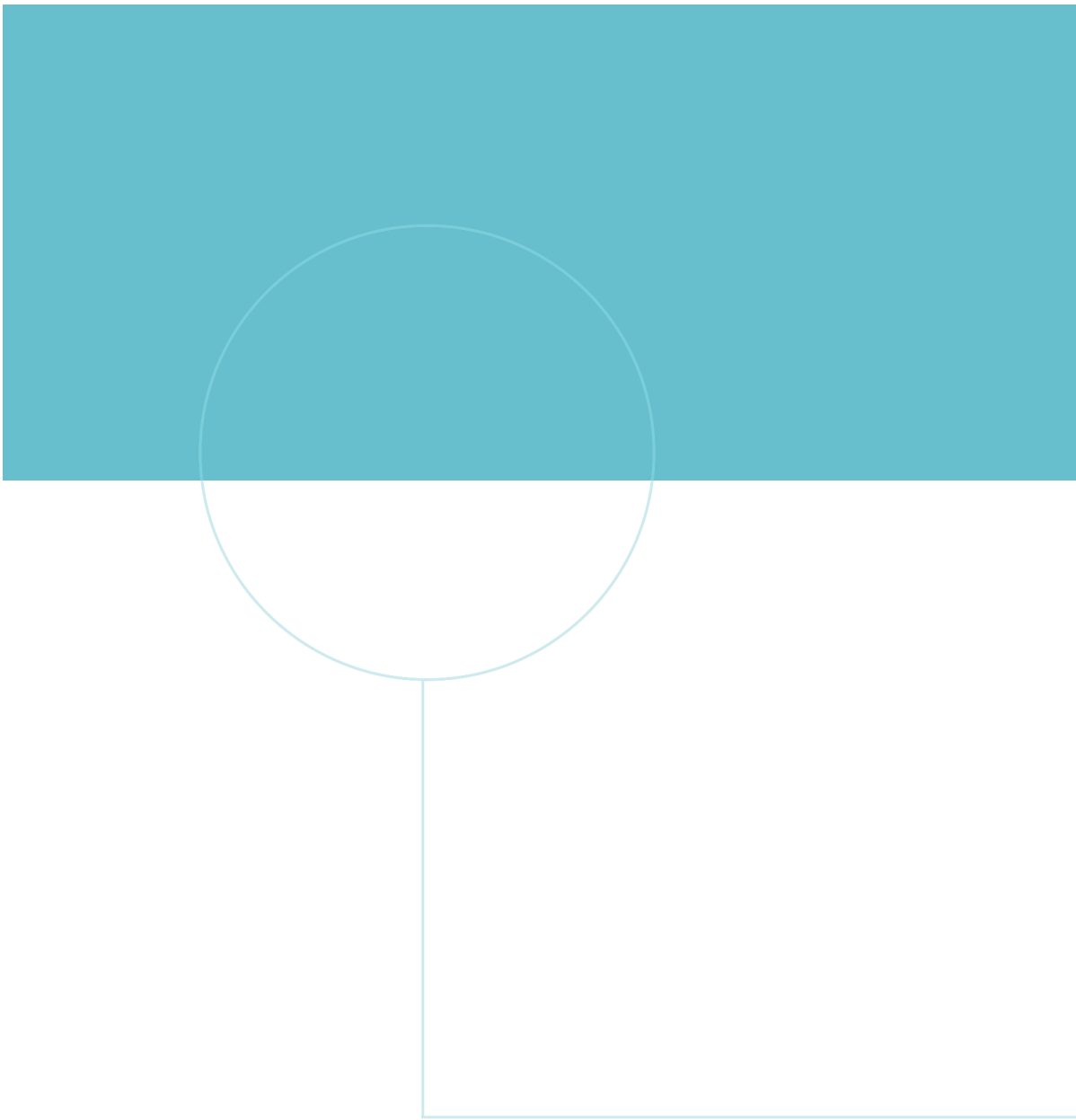

NTNU

Norwegian University of
Science and Technology